2

NTIS HC $8.00

An Experimental and Theoretical Analysis of Increased Thermal Diffusivity Phase Change Devices

CSM-CPR-R472

Chemical and Petroleum-Refining Engineering Department
Colorado School of Mines
Golden, Colorado 80401

128

AN EXPERIMENTAL AND THEORETICAL EVALUATION OF INCREASED THERMAL DIFFUSIVITY PHASE CHANGE DEVICES

by

S. P. White

J. O. Golden

F. J. Stermole

Annual Summary Report No. 1

21 January 1971 - 31 January 1972

Contract NAS 8-30511 Mod 2

for

National Aeronautics and Space Administration

George C. Marshall Space Flight Center

Marshall Space Flight Center, Alabama 35812

School Control No. CSM-CPR-R472

March 2, 1972

PREFACE

This report was prepared by Colorado School of Mines, Golden, Colorado, under Contract NAS 8-30511 Mod 2 "Research in Phase Change Thermal Control Technology" and under Colorado School of Mines Foundation Contracts F-6911 and F-6915. The work was administered under the direction of the Space Sciences Laboratory, George C. Marshall Space Flight Center, with Mr. T. C. Bannister acting as the contracting officers' technical representative.

This report covers work from 21 January 1971 to 31 January 1972.

The work at Colorado School of Mines was carried out by Dr. J. O. Golden, Dr. F. J. Stermole and S. P. White.

ABSTRACT

The goal of this study was to experimentally evaluate and mathematically model the performance of phase change thermal control devices containing high thermal-conductivity metal matrices. Three aluminum honeycomb fillers were evaluated at five different heat flux levels using n-octadecane as the test material. Initially phase change performance was evaluated with no filler in the n-octadecane so that a base line performance for each heat flux level could be established.

The experimental equipment consisted of a test cell, two electric heaters, a watt meter, two ammeters, and a multipoint recorder. The test chamber measured 15.24-by-7.62-by-2.54 centimeters (6-by-3-by-1-inches). The cell was heated by two 7.62-by-7.62 centimeters (3-by-3-inch) electric heaters, which were held at a constant heat flux. The amp and watt meters provided the measurement of the heat flux to the heaters. Temperature responses to the upset were measured by 16 copper-constantan thermocouples located throughout the test cell.

The system was mathematically modeled by approximating the partial differential equations with a three-dimensional-implicit-alternating direction technique. This implicit method was used so that the small time step required by

the presence of the metallic filler in the explicit method could be eliminated. The boundary conditions used in this model were a temperature profile on the copper heating plate and insulated on the other five sides.

The mathematical model predicts the system quite well. All of the phase change times are predicted. The heating of the solid phase is predicted exactly while there is some variation between theoretical and experimental results in the liquid phase. This variation in the liquid phase could be accounted for by the fact that there are some heat losses in the cell and there could be some convection in the experimental system.

TABLE OF CONTENTS

	Page
INTRODUCTION	1
LITERATURE SURVEY	3
THEORY	7
EXPERIMENTAL EQUIPMENT AND PROCEDURE	32
DISCUSSION OF RESULTS	39
RECOMMENDATIONS AND CONCLUSIONS	99
LITERATURE CITED	102
NOMENCLATURE	104
APPENDIX I	107

LIST OF TABLES

Table		Page
1.	Literature values of the physical properties for n-octadecane and aluminum	25
2.	Thermocouple locations	38
3.	Geometry data for the aluminum hexagonal fillers	40

LIST OF FIGURES

Figure		Page
1.	Three-dimensional nodal system	9
2.	One-dimensional nonhomogeneous nodal system	13
3.	Boundary conditions	18
4.	Filler system	26
5.	Experimental nodal system	27
6.	Test cell - exploded view	36
7.	Front and side views of test cell	37
8.	Power input measuring system	38
9.	Theoretical and experimental temperature profiles for filler no. 2 at 40 watts with the literature value for the liquefaction enthalpy	43
10.	Time below a pseudo control temperature as a function of filler weight	44
11.	Experimental and theoretical temperature profiles at 20 watts for pure paraffin	47
12.	Experimental and theoretical temperature profiles at 30 watts for pure paraffin	49
13.	Experimental and theoretical temperature profiles at 40 watts for pure paraffin	51
14.	Experimental and theoretical temperature profiles at 50 watts for pure paraffin	53

Figure | Page

15. Experimental and theoretical temperature profiles at 100 watts for pure paraffin..... 55

16. Hot plate temperature profiles for the pure paraffin runs..... 56

17. Experimental and theoretical temperature profiles at 20 watts for filler no. 1..... 58

18. Experimental and theoretical temperature profiles at 30 watts for filler no. 1..... 60

19. Experimental and theoretical temperature profiles at 40 watts for filler no. 1..... 62

20. Experimental and theoretical temperature profiles at 50 watts for filler no. 1..... 64

21. Experimental and theoretical temperature profiles at 100 watts for filler no. 1..... 66

22. Hot plate temperature profiles for filler no. 1 runs..... 67

23. Experimental and theoretical temperature profiles at 20 watts for filler no. 2..... 70

24. Experimental and theoretical temperature profiles at 30 watts for filler no. 2..... 72

25. Experimental and theoretical temperature profiles at 40 watts for filler no. 2..... 74

26. Experimental and theoretical temperature profiles at 50 watts for filler no. 2..... 76

Figure Page

27. Experimental and theoretical temperature profiles at 100 watts for filler no. 2..... 78

28. Hot plate temperature profiles for filler no. 2..... 79

29. Experimental and theoretical temperature profiles at 20 and 30 watts for filler no. 3..... 82

30. Experimental and theoretical temperature profiles at 40 and 50 watts for filler no. 3..... 84

31. Experimental and theoretical temperature profiles at 100 watts for filler no. 3..... 86

32. Hot plate temperature profiles for filler no. 3..... 87

33. Theoretical temperature profiles for different filler thicknessess..... 89

34. Theoretical temperature profiles in the x-y plane at t=600 sec..... 91

35. Theoretical temperature profiles in the x-y plane at t=1200 sec..... 93

36. Theoretical temperature profiles in the x-y plane at t=1800 sec..... 95

37. Theoretical temperature profiles in the x-y plane at t=2400 sec..... 97

INTRODUCTION

Phase-change phenomena have received wide scientific attention for some time. Phase change is of significant importance in many technical problems such as solidification of an asphalt layer, melting and solidification of metals and alloys and general crystal growth. In recent years solid-liquid phase change has been used for thermal control devices in space vehicles. In concept, such materials would be used in passive systems that employ the process of melting or solidification to remove or add thermal energy from or to a system.

In a study by Northrop Corporation (1), the properties that phase-change materials must have in order to control the temperature of electronic equipment were found. The phase-change material should be nontoxic, chemically inert, stable and noncorrosive. The material should also have small density variations with a high latent heat of fusion. The material should also melt in 283 to 338°K (50-to 150°F) range. N-paraffins with an even number of carbon atoms are the most promising phase-change materials. N-octadecane was used in this study.

Virtually all of the currently used phase-change materials have a low thermal diffusivity. Therefore, their use in phase-change thermal control units is hampered

by their inability to conduct heat. Their thermal conductivities are on the same order of magnitude as thermal conductivities of some of the best insulating materials. A method to improve heat transfer rate of the phase-change material is to surround the phase-change material with a high thermally conductive metal matrix. The metal would conduct the heat and the phase-change material would absorb the heat load.

Bentilla, Sterrett and Karre (1) evaluated a number of metallic fillers in a phase-change environment. They evaluated aluminum foam, aluminum wool, aluminum honeycomb and copper foam. Their work showed that the most advantageous type of filler was the aluminum honeycomb. Hale, Hoover and O'Neill (2) developed a method using an overall energy balance to predict the performance of thermal control phase-change devices. In their study they found that by neglecting three-dimensional heat transfer significant errors were introduced. The goal of this study was to increase the understanding of increased thermal diffusivity phase-change devices by experimentally evaluating and mathematically modeling them. With the aid of the three-dimensional mathematical model developed in this study engineers will be able to design phase-change thermal control units more efficiently.

LITERATURE SURVEY

There has been a large amount of literature published on the subject of phase-change phenomena. This literature survey deals with only a small portion of the published material. One of the first studies of phase change was made by Carslaw and Jaeger (3). In their study they developed an approximate mathematical model for semi-infinite bodies. They discussed the problem of modeling a system with a moving interface. No exact solutions were given for the mathematical modeling of finite bodies with phase change.

At this institution two studies have been completed which are concerned with the one-dimensional interface equation given by Arpaci (4). In the first study Pujado, Stermole and Golden (5) developed a theoretical model for the one-dimensional melting of a finite paraffin slab. Finite difference methods were used to solve the partial differential equations governing the physical system. This model solved the two-phase one-dimensional heat-transfer equations with phase change and variable thermal properties. In their theoretical analysis Pujado, Stermole and Golden neglected free convection in the liquid phase. The results from the study were in agreement with those of an earlier study by Northrop Corporation. The second study

by Ukanawa, Stermole and Golden (6) was the investigation of the solidification of a finite amount of liquid paraffin. A mathematical model was developed to solve the two-phase heat-transfer equation with phase change. This model used constant thermal properties for each phase and moveable boundary conditions. The model neglected convection, supercooling and nucleation effects. The comparison was good between theoretical and experimental results.

There have been three studies at this institution which concern the two-dimensional phase-change problem. Shah (7) investigated the solidification of n-octadecane using microphotographic equipment and a temperature recorder. In this study a two-dimensional mathematical model was developed to predict the temperature profiles in the freezing paraffin and the average interfacial height during the solidification process. The model neglected convection. An approximate method was used to calculate the phase change. A presentation of the various types of phase-change calculations is given by Dusinberre (8). Reasonably good agreement was obtained between the experimental and theoretical results. The second study by Bain, Stermole and Golden (9) was an investigation of the gravity-induced free convection in the melting of a finite paraffin slab. Temperature profiles were measured when the test cell was inclined at different angles to produce the free convection. In this study a two-dimensional pure-conduction model was

presented. Finite difference methods were used to solve the governing partial differential equations while the method of excess degrees was used to calculate the phase change. Since the model neglected convection there were significant differences between the theoretical and experimental results. This study showed that gravity-induced free convection can be important in the melting process. The third investigation by Ukanawa (10) studied the effect of gravity-induced free convection upon the solidification of a finite paraffin slab. A two-dimensional heat-transfer model was developed in this study. The model used an important velocity profile and a limiting velocity in the convection calculation. A pseudo heat-capacity was used to calculate the phase change.

Other papers have also been published which deal with the melting of finite slabs. Chi-Tien and Yin-Chao Ten (11) presented an approximate solution for the temperature distributions and melting rate. The heat transfer was by natural convection caused by buoyancy forces. Goodman and Shea (12) developed a series solution to solve the one-dimensional problem of the melting of a finite slab.

Crank and Nicholson (13), Douglas and Rachford (14), Peaceman and Rachford (15) and Brian (16) all developed three-dimensional finite difference techniques to solve the unsteady state heat-conduction partial differential equation. The three-dimensional alternating direction

technique developed by Brian was used in this study. Brian showed this technique is unconditionally stable and has the accuracy of the Crank-Nicholson method.

Grodzka (17) suggested two methods to increase the thermal diffusivities of phase-change materials and thus the heat-transfer rate into the thermal control unit. One was to put metallic panels in with the phase-change material. The other was to mix the phase-change material with a compatable but higher thermal diffusivity material. She pursued the second method and suggested several possible materials that could be mixed with the phase-change material. In their recommendation for the improvements of thermal control phase-change packages, Shlosinger and Bentilla (18) recommended that a metallic filler be added to increase the heat transfer rate. Bentilla, Sterrett and Karre (1) evaluated a number of metallic fillers in a phase-change environment. These fillers included aluminum wool, aluminum foam, aluminum honeycomb and copper foam. Their work showed that the aluminum honeycomb was the most advantageous geometry for a high thermal diffusivity filler material. Hale, Hoover and O'Neill (2) developed a method by which the ratio of the phase-change material to the filler material may be optimized. They used an overall energy balance to optimize the ratio of the filler material area to phase-change material area as a function of the hot plate temperature.

THEORY

The finite difference equation which can be used to mathematically model a nonhomogeneous system with phase change will be developed in this section. The test cell was heated from the top to minimize convection, however, presence of the metal matrix is likely to cause convection. The paraffin closer to the metal matrix will heat up faster due to the high rate of heat transfer through the metal and this situation will cause some convection. The convection caused in this way will be considered negligible. Since the assumption was made that convection currents have no significant effect on the heat transfer in the test chamber, this development will neglect convection. For a discussion of mathematically modeling a phase-change system with convection see reference 10. The general three-dimensional heat-conduction model will be developed first, then the three-dimensional alternating direction technique of Brian (16) will be discussed. Finally, the general heat-conduction equation and the three-dimensional alternating direction technique will be applied to the non-homogeneous phase-change problem in this study.

General Three-Dimensional Equation

The general heat-conduction equation may be derived by making an energy balance on a three-dimensional non-

homogeneous nodal system. Making an energy balance on node i,j,k in figure 1 yields

Energy in - energy out + energy generated
= energy accumulated (1)

or,

$$\frac{(\rho C_p V)_{eff}}{\Delta t}\,(T^*(i,j,k)-T(i,j,k)) = (q_x A_x)_{in}-(q_x A_x)_{out} + (q_y A_y)_{in}-(q_y A_y)_{out} + (q_z A_z)_{in}-(q_z A_z)_{out} + GV' \quad (2)$$

where

q_x = the heat flux in the x-direction

q_y = the heat flux in the y-direction

q_z = the heat flux in the z-direction

A_x = the cross sectional area of the node i,j,k perpendicular to the x-direction

A_y = the cross sectional area of the node i,j,k perpendicular to the y-direction

A_z = the cross sectional area of the node i,j,k perpendicular to the z-direction

G = energy generated per volume

V' = volume of the material generating energy

T* = the temperature at time $t+\Delta t$

T = the temperature at time t

t = time

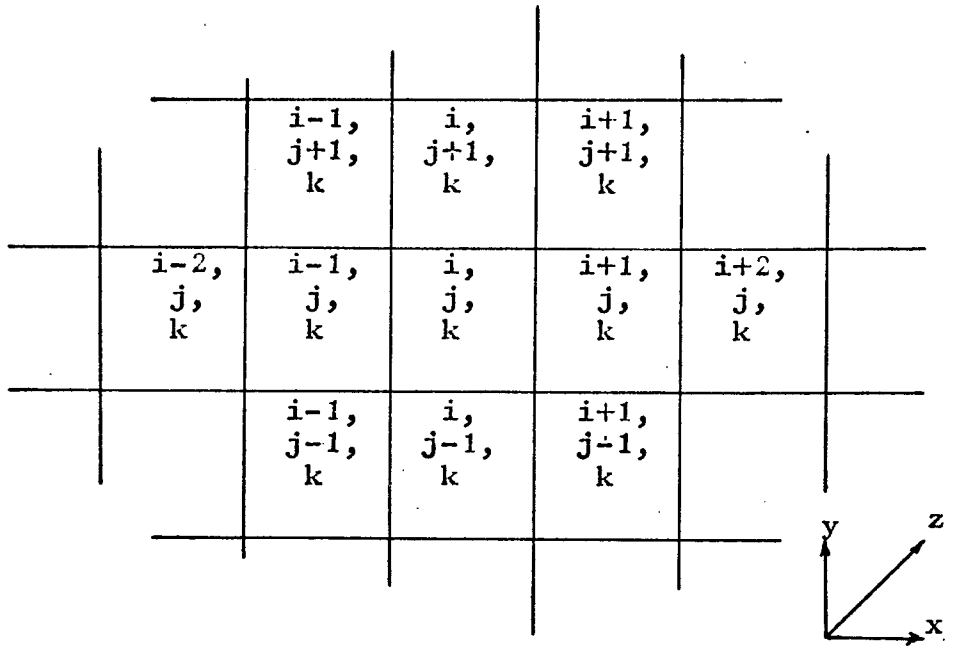

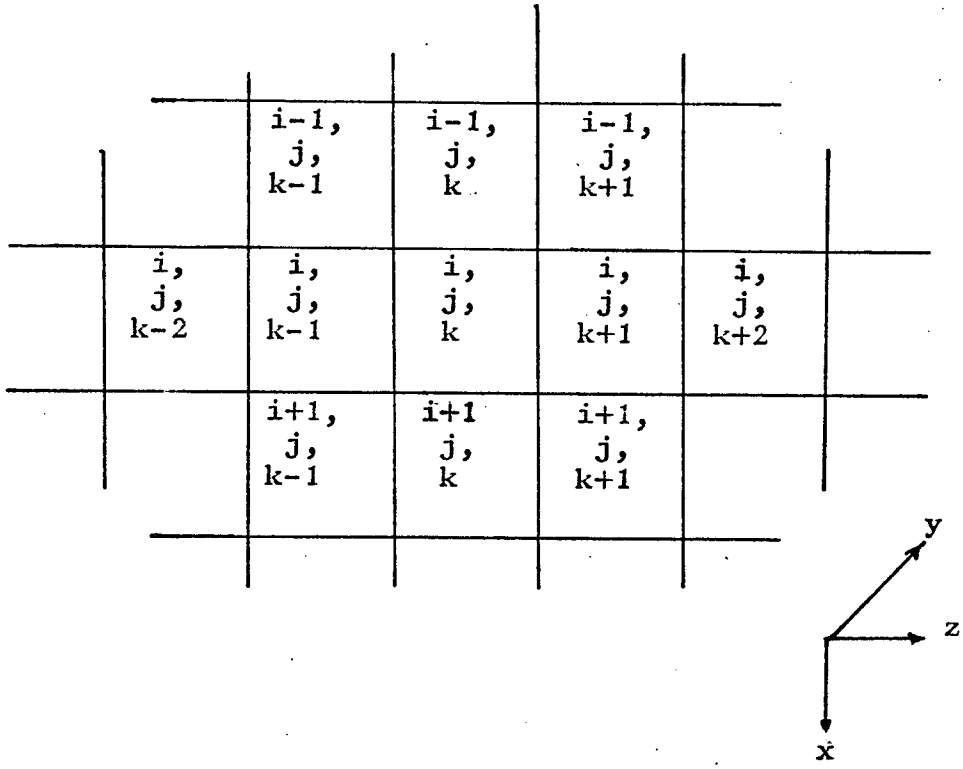

Figure 1

Three-Dimensional Nodal System

Δt = time increment

$(\rho C_p V)_{eff}$ = the effective $(\rho C_p V)$ for a nonhomogeneous system

The heat flux may be found in terms of the temperature difference of the nodal system from Fourier's law. From Fourier's law one obtains

$$(q_x)_{in} = K(T(i-1,j,k)-T(i,j,k))/\Delta x \qquad (3)$$

where

K = the thermal conductivity of the material

Δx = the incremental distance between nodes in the x-direction

Writing a similar equation for each of the other heat flux terms in equation (1) and substituting back into equation (1) yields

$$\frac{(\rho C_p V)_{eff}}{\Delta t} (T^*(i,j,k)-T(i,j,k)) =$$

$$((KA)_x)_{eff} (T(i-1,j,k)-T(i,j,k))/\Delta x -$$

$$((KA)_x)_{eff} (T(i,j,k)-T(i+1,j,k))/\Delta x +$$

$$((KA)_y)_{eff} (T(i,j-1,k)-T(i,j,k))/\Delta y -$$

$$((KA)_y)_{eff} (T(i,j,k)-T(i,j+1,k))/\Delta y +$$

$$((KA)_z)_{eff} (T(i,j,k-1)-T(i,j,k))/\Delta z -$$

$$((KA)_z)_{eff} (T(i,j,k)-T(i,j,k+1))/\Delta z + GV' \qquad (4)$$

where

$((KA)_x)_{eff}$ = the effective thermal conductivity times the effective area in the x-direction for a nonhomogeneous system

$((KA)_y)_{eff}$ = the effective thermal conductivity times the effective area in the y-direction for a nonhomogeneous system

$((KA)_z)_{eff}$ = the effective thermal conductivity times the effective area in the z-direction for a nonhomogeneous system

Δy = the incremental distance in the y-direction

Δz = the incremental distance in the z-direction

Equation (4) is the general three-dimensional heat-conduction equation written in an explicit finite difference form. To use this equation one must define and evaluate the effective $\rho C_p V$ and the effective KA terms. The effective $\rho C_p V$ will be defined as the sum of the $\rho C_p V$ terms representing each material present in the node or,

$$(\rho C_p V)_{eff} = \sum^{N} \rho_n C_{pn} V_n \qquad (5)$$

where

N = the number of different materials present in the node

This is just the sum of the heat capacitance of each of the different materials. An expression for the effective

KA term can be found by looking at the one-dimensional steady state energy balance on a nonhomogeneous node. A three-dimensional system could be used to derive this expression, but the analysis is simpler in one-dimension while the same result is obtained. An energy balance on node m in figure 2 yields

$$(qA)_{in}-(qA)_{out} = 0 \tag{6}$$

The heat flux into node m is the sum of the heat which flows through each of the different materials, or

$$(qA)_{in} = A_1q_1 + A_2q_2 + A_3q_3 \tag{7}$$

where

q_1 = the heat flux through material 1

q_2 = the heat flux through material 2

q_3 = the heat flux through material 3

A_1 = the area of material 1 perpendicular to the heat flux

A_2 = the area of material 2 perpendicular to the heat flux

A_3 = the area of material 3 perpendicular to the heat flux

From Fourier's law the heat flux terms may be evaluated as follows:

$$(qA)_{in} = (KA)_{eff}\ (T_1-T_m)/\Delta x \tag{8}$$

$$A_1q_1 = (KA)_1\ (T_{11}-T_{1m})/\Delta x \tag{9}$$

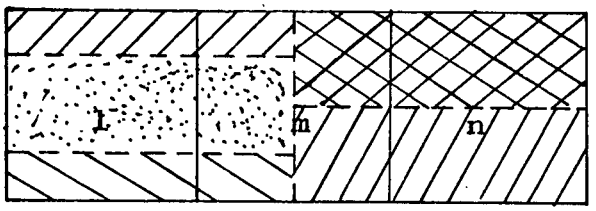

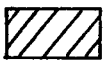
Material no. 1


Material no. 2


Material no. 3


Material no. 4


Material no. 5

Figure 2

One-Dimensional Nonhomogeneous Nodal System

$$A_2q_2 = (KA)_2\ (T_{21}-T_{2m})/\Delta x \tag{10}$$

$$A_3q_3 = (KA)_3\ (T_{31}-T_{3m})/\Delta x \tag{11}$$

Substituting equations (8) through (11) into equation (7) yields

$$(KA)_{eff}\ (T_1-T_m) = (KA)_1(T_{11}-T_{1m}) + (KA)_2(T_{21}-T_{2m}) + (KA)_3(T_{31}-T_{3m}) \tag{12}$$

Since there is assumed to be no gradients in a node in a finite difference network the following is true.

$$T_1 = T_{11} = T_{21} = T_{31} \tag{13}$$

$$T_m = T_{1m} = T_{2m} = T_{3m} \tag{14}$$

The effective KA may be found by substituting equations (13) and (14) into equation (12) and dividing by T_1-T_m. This procedure yields

$$(KA)_{eff} = (KA)_1 + (KA)_2 + (KA)_3 \tag{15}$$

or more generally

$$(KA)_{eff} = \sum^{N} K_nA_n \tag{16}$$

For the nonhomogeneous system we must define an effective ρC_pV for each node and an effective KA for each of the six sides for each node. Equation (4) may now be rewritten in terms of the above relations as

$$T^*(i,j,k)-T(i,j,k) = \frac{\Delta t(KA(i,j,k)_x)_{eff}\ (T(i-1,j,k)-T(i,j,k))}{\Delta x(\rho C_pV(i,j,k))_{eff}}$$

$$- \frac{\Delta t(KA(i+1,j,k)_x)_{eff}}{\Delta x(\rho C_p V(i,j,k))_{eff}} (T(i,j,k)-T(i+1,j,k))$$

$$+ \frac{\Delta t(KA(i,j,k)_y)_{eff}}{\Delta y(\rho C_p V(i,j,k))_{eff}} (T(i,j-1,k)-T(i,j,k))$$

$$- \frac{\Delta t(KA(i,j+1,k)_y)_{eff}}{\Delta y(\rho C_p V(i,j,k))_{eff}} (T(i,j,k)-T(i,j+1,k))$$

$$+ \frac{\Delta t(KA(i,j,k)_z)_{eff}}{\Delta z(\rho C_p V(i,j,k))_{eff}} (T(i,j,k-1)-T(i,j,k))$$

$$- \frac{\Delta t(KA(i,j,k+1)_z)_{eff}}{\Delta z(\rho C_p V(i,j,k))_{eff}} (T(i,j,k)-T(i,j,k+1))$$

$$+ \frac{GV' \Delta t}{C_p V(i,j,k)_{eff}} \qquad (17)$$

where

$(KA(i,j,k)_x)_{eff}$ = the effective KA term perpendicular to the x-direction on the left side of the node

$(KA(i+1,j,k)_x)_{eff}$ = the effective KA term perpendicular to the x-direction on the right side of the node

$(KA(i,j,k)_y)_{eff}$ = the effective KA term perpendicular to the y-direction on the left side of the node

$(KA(i,j+1,k)_y)_{eff}$ = the effective KA term perpendicular to the y-direction on the right side of the node

$(KA(i,j,k)_z)_{eff}$ = the effective KA term perpendicular to the z-direction on the left side of the node

$(KA(i,j,k+1)_z)_{eff}$ = the effective KA term perpendicular to the z-direction on the right side of the node

$\rho C_p V(i,j,k)_{eff}$ = the effective $\rho C_p V$ term for the node

A simpler form of equation (17) can be written in terms of variable constants in place of the effective terms.

$$T^*(i,j,k)-T(i,j,k) = C_{11}(T(i-1,j,k)-T(i,j,k))\Delta t$$
$$- C_{12}(T(i,j,k)-T(i+1,j,k))\Delta t$$
$$+ C_{21}(T(i,j+1,k)-T(i,j,k))\Delta t$$
$$- C_{22}(T(i,j,k)-T(i,j+1,k))\Delta t$$
$$+ C_{31}(T(i,j,k-1)-T(i,j,k))\Delta t$$
$$- C_{32}(T(i,j,k)-T(i,j,k+1))\Delta t + GC_4\Delta t \qquad (18)$$

where the constants are defined as follows and are evaluated for each node as indicated.

$$C_{11} = \frac{(KA(i,j,k)_x)_{eff}}{\rho C_p V(i,j,k)_{eff}\Delta x} = \frac{\sum KA(i,j,k,n)_x}{\Delta x \sum \rho C_p V(i,j,k,n)} \qquad (19)$$

$$C_{12} = \frac{(KA(i+1,j,k)_x)_{eff}}{\rho C_p V(i,j,k)_{eff}\Delta x} = \frac{\sum KA(i+1,j,k,n)_x}{\Delta x \sum \rho C_p V(i,j,k,n)} \qquad (20)$$

$$C_{21} = \frac{(KA(i,j,k)_y)_{eff}}{\rho C_p V(i,j,k)_{eff}\Delta y} = \frac{\sum KA(i,j,k,n)_y}{\Delta y \sum \rho C_p V(i,j,k,n)} \qquad (21)$$

$$C_{22} = \frac{(KA(i,j+1,k)_y)_{eff}}{\rho C_p V(i,j,k)_{eff}\Delta y} = \frac{\sum KA(i,j+1,k,n)_y}{\Delta y \sum \rho C_p V(i,j,k,n)} \quad (22)$$

$$C_{31} = \frac{(KA(i,j,k)_z)_{eff}}{\rho C_p V(i,j,k)_{eff}\Delta z} = \frac{\sum KA(i,j,k,n)_z}{\Delta z \sum \rho C_p V(i,j,k,n)} \quad (23)$$

$$C_{32} = \frac{(KA(i,j,k+1)_z)_{eff}}{\rho C_p V(i,j,k)_{eff}\Delta z} = \frac{\sum KA(i,j,k+1,n)_z}{\Delta z \sum \rho C_p V(i,j,k,n)} \quad (24)$$

$$C_4 = V'/(\rho C_p V(i,j,k)_{eff} = \frac{V'}{\rho C_p V(i,j,k,n)} \quad (25)$$

Equation (18) may be used over the entire nodal system by just varying the above constants in order to define the effective terms for each node. By redefining the constants in equation (18) it may be used on the boundaries also. To see how this may be done look at the one-dimensional form of equation (18). Again a three-dimensional analysis will give the same result, but the one-dimensional analysis is simpler.

$$\begin{aligned} T^*(i,j,k)-T(i,j,k) = {} & C_{11}\,(T(i-1,j,k)-T(i,j,k))\Delta t \\ & + C_{12}\,(T(i,j,k)-T(i+1,j,k))\Delta t \\ & + GC_4\Delta t \end{aligned} \quad (26)$$

Figure 3 shows the four types of boundary conditions that can be used. Each type will be described in the following section.

Type I: This boundary condition represents a system in which there is heat transfer to a fluid. An energy balance on node 2 of this nodal system yields

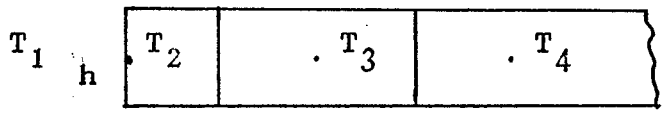

Type I

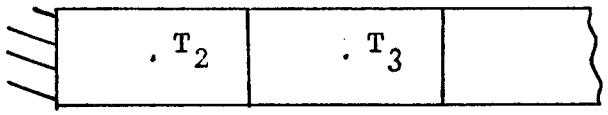

Type II

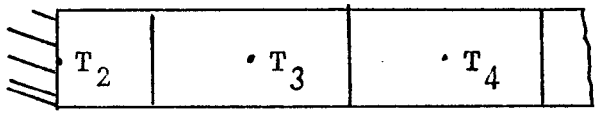

Type III

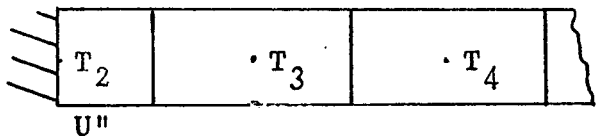

Type IV

Figure 3
Boundary Conditions

$$T^*_2 - T_2 = \frac{\Delta t\ hA(T_1-T_2)}{\rho C_p V(1)_{eff}} - \frac{\Delta t\ KA(2)_{eff}(T_2-T_3)}{\Delta x\, \rho C_p V(1)_{eff}} \tag{27}$$

Comparison of equation (27) to equation (26) shows that

$$C_{11} = \frac{hA}{\rho C_p V(1)_{eff}} \tag{28}$$

$$C_4 = 0; \text{ since there is no generation of energy in this node} \tag{29}$$

C_{12} is defined by equation (20).

Types II and III: These are two types of insulated boundary conditions. An energy balance on node 2 of these two systems yields

$$T^*_2 - T_2 = \frac{-\Delta t\ KA(2)_{eff}(T_2-T_3)}{\Delta x \rho C_p V(1)_{eff}} \tag{30}$$

Comparing equation (30) with equation (26) indicates that

$$C_{11} = 0 \tag{31}$$

$$G = 0 \tag{32}$$

Type IV: This type of boundary is insulated and energy is being generated in the boundary node. An energy balance on this system yields

$$T^*_2 - T_2 = \frac{-\Delta t\ KA(2)_{eff}(T_2-T_3)}{\Delta x\, \rho C_p V(1)_{eff}} + \frac{\dot{U}''\ V'\Delta t}{\rho C_p V(1)_{eff}} \tag{33}$$

A comparison of this equation with equation (26) yields

$$C_{11} = 0 \tag{34}$$

$$G = U'' \tag{35}$$

By setting G equal to the energy source in any node in the system, there may be a generation term in any node or boundary equation.

Three-Dimensional Alternating Direction Technique

The time step required by the stability criteria in the explicit solution of equation (18) is extremely small due to the presence of the metallic matrix. The required time step is such that the computer time required to model an experimental run exceeds the actual experimental run time. Therefore, an implicit technique was used to eliminate the stability requirement on the size of the time step. The implicit method used in this study is the three-dimensional alternating direction technique developed by Brian (16). This method is a variation of the Douglas-Rachford method that has the accuracy of the Crank-Nicholson method and has been shown to be unconditionally stable.

The three-dimensional technique of Brian solves for three intermediate half-time-step temperatures and then uses these to solve for the new full-time-step temperature. The equations that demonstrate this method are as follows:

$$\Delta_x^2(CT^*(i,j,k)) + \Delta_y^2(CT(i,j,k)) + \Delta_z^2(CT(i,j,k)) = \frac{T^*(i,j,k)-T(i,j,k)}{\Delta t/2} \qquad (36)$$

$$\Delta_x^2(CT^*(i,j,k)) + \Delta_y^2(CT^{**}(i,j,k)) + \Delta_z^2(CT(i,j,k)) = \frac{T^{**}(i,j,k)-T(i,j,k)}{\Delta t/2} \tag{37}$$

$$\Delta_x^2(CT^*(i,j,k)) + \Delta_y^2(CT^{**}(i,j,k)) + \Delta_z^2(CT^{***}(i,j,k)) = \frac{T^{***}(i,j,k)-T(i,j,k)}{\Delta t/2} \tag{38}$$

$$\Delta_x^2(CT^*(i,j,k)) + \Delta_y^2(CT^{**}(i,j,k)) + \Delta_z^2(CT^{***}(i,j,k)) = \frac{T'(i,j,k)-T(i,j,k)}{\Delta t} \tag{39}$$

where

$$\Delta_x^2(CT(i,j,k)) = C_{11}T(i-1,j,k)-(C_{11}+C_{12})T(i,j,k) + C_{12}T(i+1,j,k) \tag{40}$$

$$\Delta_y^2(CT(i,j,k)) = C_{21}T(i,j-1,k)-(C_{21}+C_{22})T(i,j,k) + C_{22}T(i,j+1,k) \tag{41}$$

$$\Delta_z^2(CT(i,j,k)) = C_{31}T(i,j,k-1)-(C_{31}+C_{32})T(i,j,k) + C_{32}T(i,j,k+1) \tag{42}$$

T = the temperature at time t

T' = the temperature at the new full time step $t+\Delta t$

T^*, T^{**}, T^{***} = the intermediate half-time-step temperatures

C_{11}, C_{12}, C_{21}, C_{31} and C_{32} are evaluated for each node and are defined by equations (19) through (24). For stability it is imperative that T* be used in the x-direction difference, T** be used in the y-direction difference and T*** be used in the z-direction difference.

A simpler form of the equations (36) through (39) were used to solve the problem presented in this thesis. When T*** is eliminated from equations (36) through (39), the following set of equations results.

$$\Delta_x^2(CT^*(i,j,k)) + \Delta_y^2(CT(i,j,k)) + \Delta_z^2(CT(i,j,k)) = \frac{T^*(i,j,k)-T(i,j,k)}{\Delta t/2} \tag{43}$$

$$\Delta_y^2(CT^{**}(i,j,k)) - \Delta_y^2(CT(i,j,k)) = \frac{T^{**}(i,j,k)-T^*(i,j,k)}{\Delta t/2} \tag{44}$$

$$\Delta_z^2(CT'(i,j,k)) - \Delta_z^2(CT(i,j,k)) = \frac{T'(i,j,k)+T(i,j,k)-2T^{**}(i,j,k)}{\Delta t/2} \tag{45}$$

Equation (44) is the difference between equations (36) and (37), while equation (45) is found by eliminating T*** from the difference of equations (37) and (38) and the difference of equations (38) and (39). Equation (43) relates the unknown T* values along a row parallel to the x-axis. When equation (43) is solved for the unknown T* values a system of simultaneous equations results:

$$
\begin{aligned}
b_1T_1^* + c_1T_2^* &= d_1 \\
a_2T_1^* + b_2T_2^* + c_2T_3^* &= d_2 \\
a_3T_2^* + b_3T_3^* + c_3T_4^* &= d_3 \\
&\cdots\cdots\cdots\cdots \\
a_{n-2}T^*_{n-3} + b_{n-2}T^*_{n-2} + c_{n-2}T^*_{n-1} &= d_{n-2} \\
a_{n-1}T^*_{n-2} + b_{n-1}T^*_{n-1} &= d_{n-1}
\end{aligned}
\tag{46}
$$

The values of the coefficient a_i, b_i and c_i are the coefficients of the unknown T* temperatures and d_i is the sum of the remaining terms. It is supposed that the grid points are designated by 0, 1, 2, 3, . . . n-1, n and that T_0 and T_n are determined from the boundary conditions.

The matrix of the coefficients a, b, and c is tridiagonal. There is a very efficient method of the solution for the tridiagonal system. The value of T_i^* in equation (46) can be found by following procedure:

$$T^*_{n-1} = F_{n-1} \tag{47}$$

$$T^*_i = F_i - c_i T^*_{n+1}/w_i \tag{48}$$

where W_i and F_i are determined by the following recursion formula

$$w_i = b_i - \frac{a_i c_{i-1}}{w_{i-1}} \quad \text{with } w_1 = b_1 \tag{49}$$

$$F_i = d_i - \frac{a_i F_{i-1}}{b_i} \quad \text{with } F_i = d_1/b_1 \tag{50}$$

Equation (44) is then solved in a similar manner, but this time the simultaneous equations relate T** values along a row parallel to the y-axis. The solution of equation (45) is then found in a similar manner with sets of tridiagonal simultaneous equations relating T*** values along a row parallel to the z-axis.

Nonhomogeneous Phase-Change Problem

The system in this study consists of a hexagonal aluminum matrix in n-octadecane. The physical properties of aluminum and n-octadecane are given in reference 19 and 20 and are tabulated in table 1. Due to the symmetry of the system only a small portion of the test cell must be modelled. Figure 4a shows how the test cell can be broken down by lines of symmetry in the two horizontal directions. Using these lines of symmetry the filler system can be broken down into the system shown in figure 4b. The sides in the x and y directions are considered insulated from lines of symmetry. The bottom of the cell will be considered insulated in this analysis. Actually this may not be the case but fairly good agreement between theoretical and experimental data results if the bottom is considered insulated in the theoretical analysis. The nodal system will be defined as shown in figures 5a and 5b. The x-direction is indicated by i, j indicates the y-direction and k represents

Table 1

Literature values of the physical properties for n-octadecane and aluminum.

N-OCTADECANE

Density

ρ(solid) = (-0.0003336)T + 1.0918; g/cc

ρ(liquid) = (-0.0012505)T + 1.1316; g/cc

Heat Capacity

C_p (solid) = 2.164; watt-sec/gm/^oK

C_p (liquid) = (0.008213)T - 0.14237; watt-sec/gm/^oK

Conductivity

K (solid) = $(-0.50054 \times 10^{-5})$T + 0.002914; watt/cm/$^oK$

K (liquid) = $(-0.50054 \times 10^{-5})$T + 0.002914; watt/cm/$^oK$

Melt point = 300.60 ^oK

H_f (liquefaction enthalpy) = 243.9; watt-sec/gm

ALUMINUM

ρ = 2.685 gm/cc

C_p = 0.9792 watt-sec/gm/^oK

K = 0.1282 watt/cm/^oK

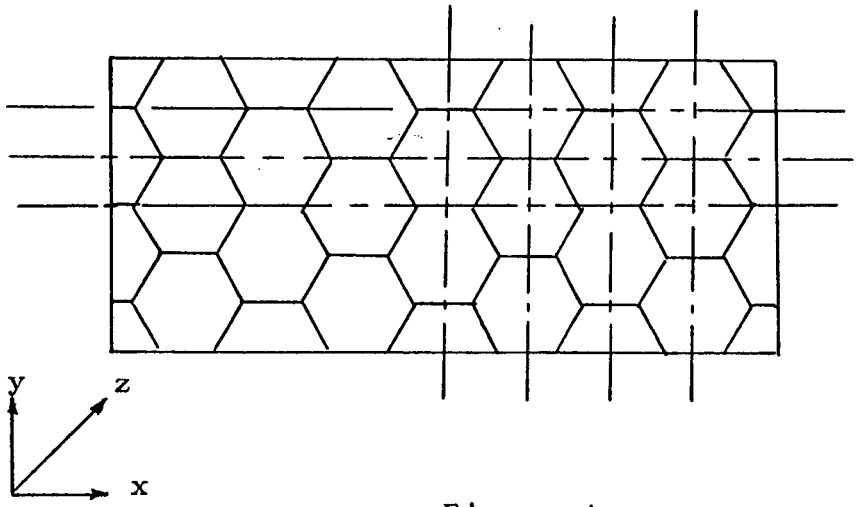

Figure 4a

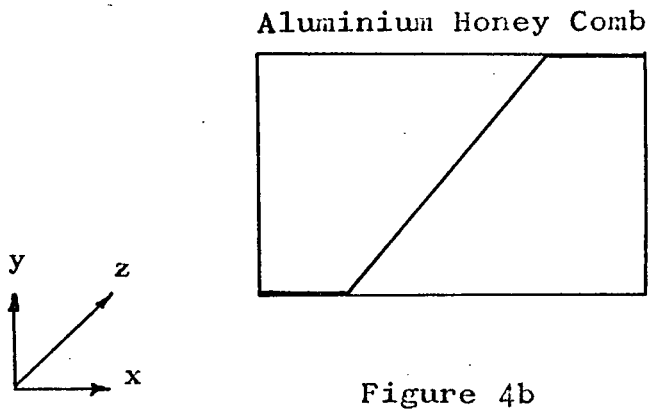

Figure 4b

Figure 4

Filler System

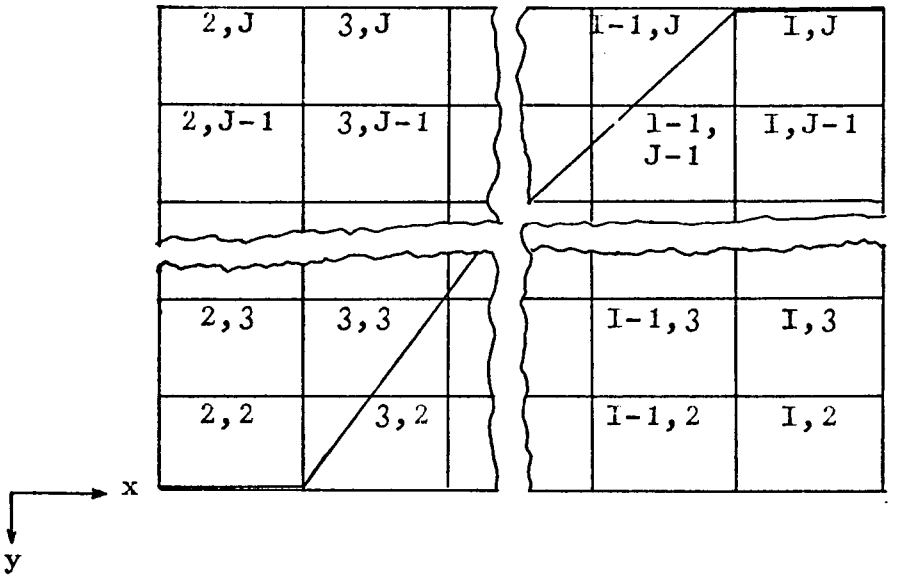

Figure 5a

X-Y Plane of Nodal System

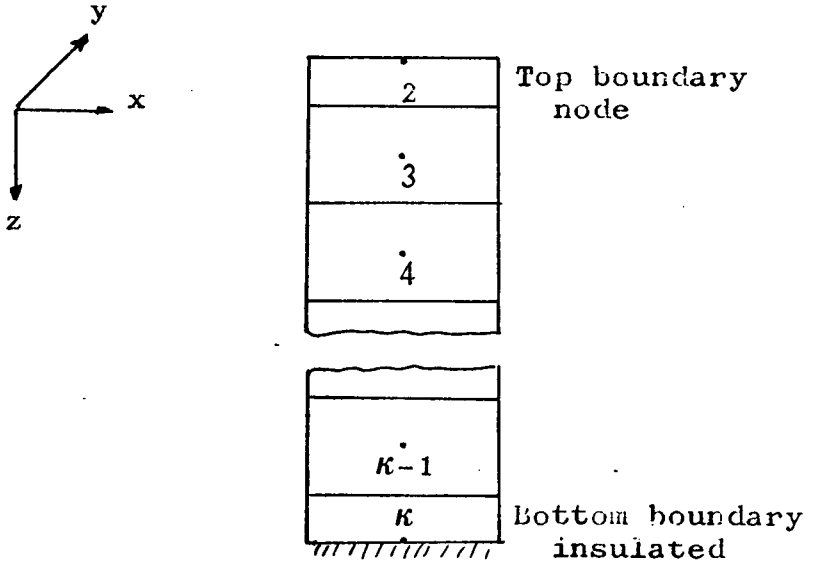

Figure 5b

One Nodal Column Parallel to the z-axis

Figure 5

Experimental Nodal System

the z-direction. When the system of equations (43) through (44) is applied to equation (18) the following systems of equations results, where $\Delta t = \Delta t/2$

For all i, j and k the a_i, b_i, c_i and d_i are defined as follows for equation (43).

$$a_i = -C_{11}\Delta t \tag{51}$$

$$b_i = 1 + (C_{11} + C_{12})\Delta t \tag{52}$$

$$c_i = -C_{12}\Delta t \tag{53}$$

$$d_i = T(i,j,k) + (\Delta_y^2(CT(i,j,k)) + \Delta_z^2(CT(i,j,k)))\Delta t \tag{54}$$

C_{11}, C_{12}, C_{21}, C_{31} and C_{32} are calculated for each node according to equations (19) and (24). If there is no filler in the node the volume and area of the filler in these calculations is set equal to zero. The insulated boundary conditions are evaluated as follows:

when i and/or j = 2 for $3<k<\kappa$

$$C_{11} = 0$$
$$C_{21} = 0 \tag{55}$$

when i = I and/or j = J for $3<k<\kappa$

$$C_{12} = 0$$
$$C_{22} = 0 \tag{56}$$

when $k = \kappa$ for $2<j<J$ and $2<i<I$

$$C_{32} = 0 \tag{57}$$

A temperature boundary condition was used on the copper heating plate in this study. This condition is taken care of by setting T(i,j,2) equal to the heating plate temperature.

For all i, j and k the a_j, b_j, c_j and d_j are defined as follows for equation (44),

$$a_j = -C_{21}\Delta t \tag{58}$$

$$b_j = 1 + (C_{21} + C_{22})\Delta t \tag{59}$$

$$c_j = -C_{22}\Delta t \tag{60}$$

$$d_j = T^*(i,j,k)-(\Delta_y^2(CT(i,j,k)))\Delta t \tag{61}$$

The boundary condition coefficients are calculated by equations (55) through (57).

For all i, j and k the a_k, b_k, c_k and d_k are defined as follows for equation (45).

$$a_k = -C_{31}\Delta t \tag{62}$$

$$b_k = 1 + (C_{31} + C_{32})\Delta t \tag{63}$$

$$c_k = -C_{32}\Delta t \tag{64}$$

$$d_k = 2T^{**}(i,j,k)-T(i,j,k)-(\Delta_z^2(CT(i,j,k)) + E)\Delta t \tag{65}$$

where

$$E = 0 \text{ for } 2<i<I;\ 2<j<J;\ 4<k<K \tag{66}$$

$$E = C_{31}\ T(i,j,2) \text{ for } 2<i<I;\ 2<j<J;\ k=3 \tag{67}$$

$$c_k = 0 \text{ for } 2<i<I;\ 2<j<J;\ k=3 \tag{68}$$

A summary of the various phase-change calculation techniques is given by Dusinberre (8). A modification of the method of excess degrees was used in this study. Since the n-octadecane used in this study was not a pure material (practical grade) it was allowed to melt over a 1.76°K (3°F) temperature range. Since the heat capacity of n-octadecane is the same above and below the melting point, a term which has the units of degrees results when the latent heat is divided by the heat capacity. This term is called the excess degrees, which is the number of degrees the node would have risen if the phase change had not occurred. The following procedure is used to calculate the phase change.

$$T(i,j,k).R.T_m \tag{69}$$

If $$T(i,j,k) < T_{mo} \tag{70}$$

the node is still solid.

If $$T(i,j,k) > T_{mo} \tag{71}$$

the node is in the process of melting.

If equation (71) holds then the following procedure is followed.

$$T_e(i,j,k) = (T(i,j,k)-T_{mo}).R.H_f/C_p \tag{72}$$

If $$T_e(i,j,k) < H_f/C_p \tag{73}$$

the node is partially melted and its temperature is defined by

$$T(i,j,k) = T_{mo} + T_e(i,j,k) \ *C_p \ *1.76/ \ H_f \tag{74}$$

But if

$$T_e(i,j,k) > H_f/C_p \tag{75}$$

the node has melted and the temperature of the now liquid node is given by

$$T(i,j,k) = T_{mo}(i,j,k) + 1.76 + (T_e(i,j,k)*C_p - H_f)/C_p \tag{76}$$

Each new full-time-step temperature is corrected by the above phase-change calculation.

A computer program was written using the above procedure to solve the nonhomogeneous heat-transfer problem with phase-change presented in the study. The results are shown and described in the discussion of results.

EXPERIMENTAL EQUIPMENT AND PROCEDURE

A description of the experimental equipment and the experimental procedure are given in this section.

Equipment

The equipment used in this study can be seperated into three sections which are the test cell, the power input measuring system and the temperature recording system. These sections are discussed below.

Test Cell: The test cell (figures 6 and 7) consisted of a rectangular test chamber and a heating plate. The test chamber, 7.62-by-15.24-by-2.54 centimeters (3-by-6-by-1-inches) was milled out of a block of plexiglass to minimize the sources of leaks. The heating plate was a 10.16-by-17.78-by-0.625 centimeter (4-by-7-by-0.25-inch) copper plate upon which two 7.62-by-7.62 centimeter (3-by-3-inch) electric heaters were epoxied. The electric heaters were obtained from Electrofilm Incorporated of North Hollywood California. The cell was sealed by compressing the O-ring. During the run the cell was encased in approximately 3.81 centimeters (1.5 inches) of styrofoam.

Power Input Measuring System: This system, shown in figure 8, consisted of a seven and one half ampere powerstat, a Hickok watt meter and two Welch A.C. ammeters. The powerstat provided a variable source of power

to the electric heaters. This power was measured by the watt meter. The output of the watt meter is a direct measure of the heat flux liberated by the electric heaters. The function of the ammeters was to insure that each heater received the same current and thus provide even heating.

Temperature Recording System: Sixteen copper-constatan thermocouples and a Bristol multipoint recorder comprised the temperature recording system. The recorder was able to record each point every two seconds with an accuracy of $\pm$ 0.4267°K ($\pm$ 0.75°F). The thermocouple wires in the test cell were encased in glass probes. The glass probes served two purposes. One was to insulate the thermocouple wire from the metallic filler, the other was to keep the thermocouple at a constant height. The thermocouple locations are given in table 2, where coordinate 0, 0, 0 is the left front upper corner of the test chamber.

Experimental Procedure

Experimental runs were made using the following procedure.

1. The cell was filled with n-octadecane after the filler material had been put into the test chamber. The cell was then bolted down to seal it.
2. The cell was leveled to help minimize convection.
3. The recorder was turned on to record the initial

temperature of the cell.

4. When the test chamber had reached a constant initial temperature the powerstat was turned on to start the run.

5. The run was allowed to continue until the hot plate reached a temperature of 338.61°K (150°F). At this temperature the plexiglass began to deform around the copper plate.

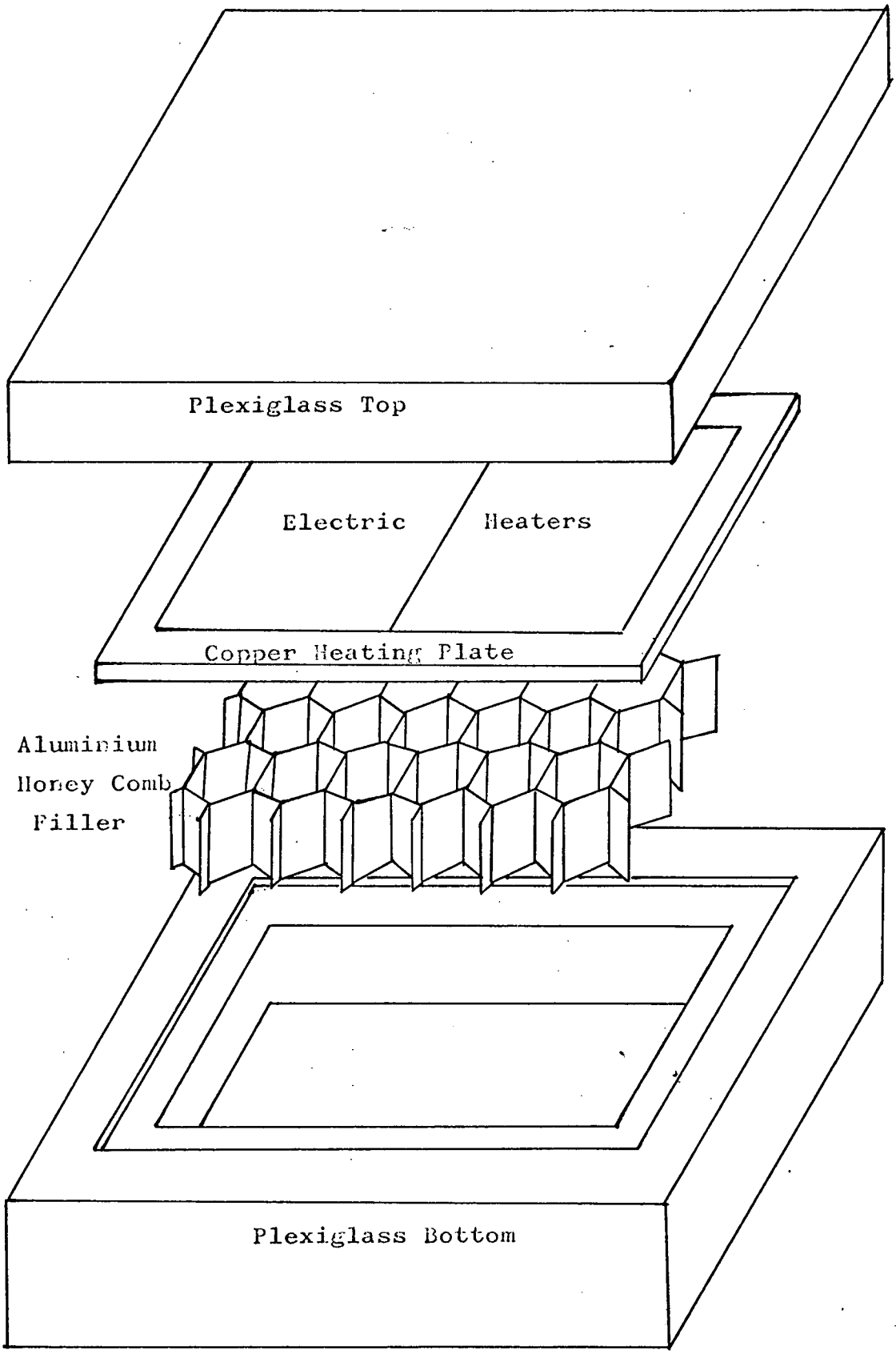

Figure 6

Test Cell - Exploded View

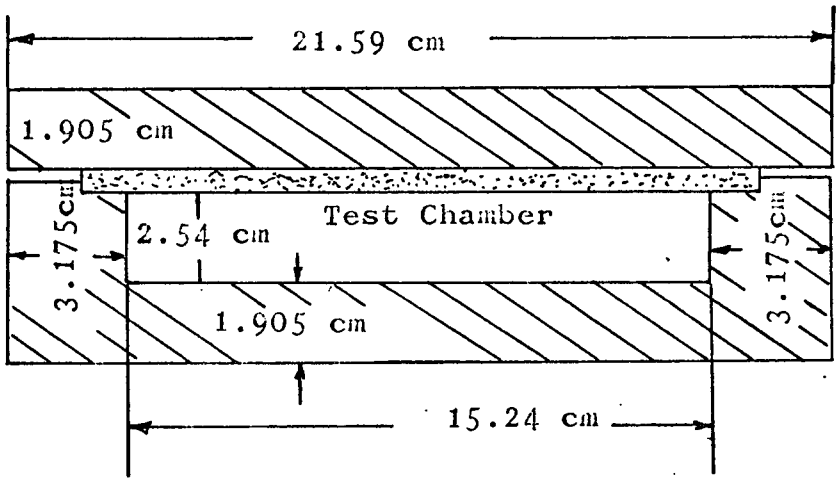

Front View of Test Cell
1/2 Scale

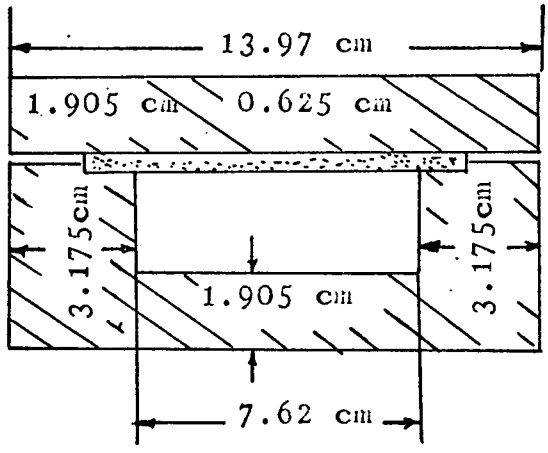

Side View of Test Cell
1/2 Scale

Figure 7

Frount and Side Views of Test Cell

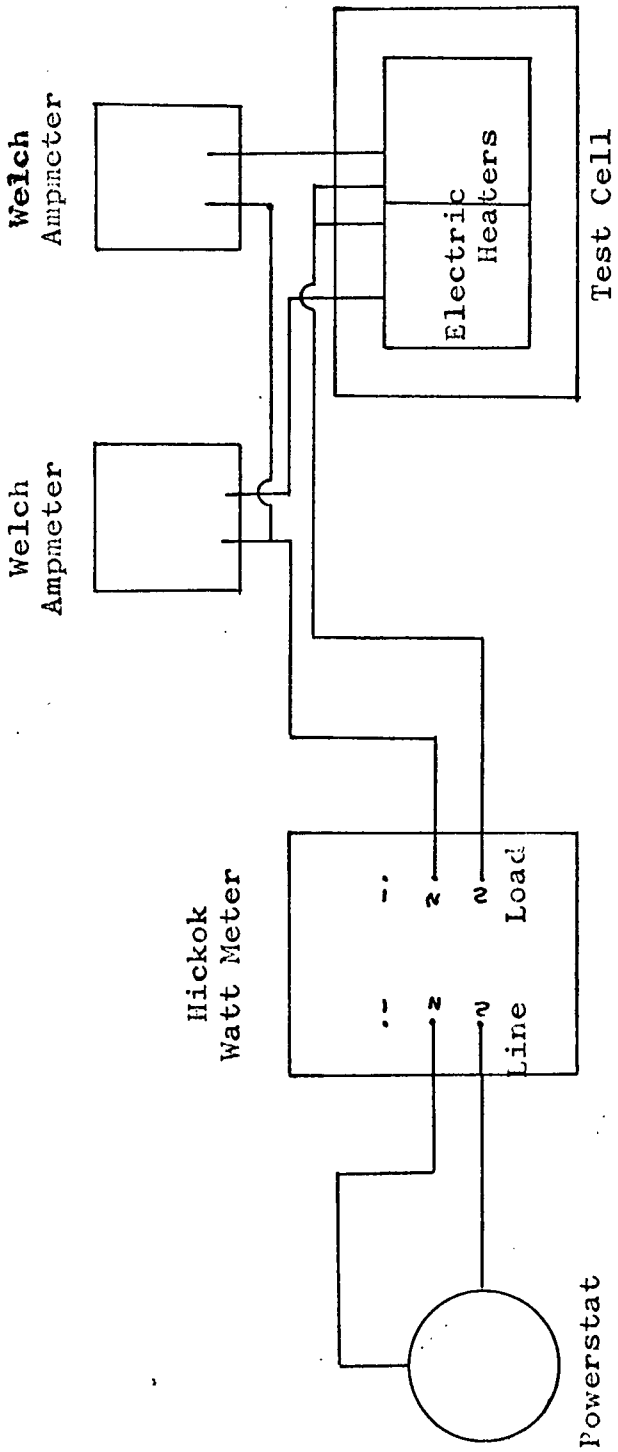

Figure 8

Power Input Measuring System

Table 2

THERMOCOUPLE LOCATIONS

The location of the coordinate 0,0,0 is the left front upper corner of the test chamber. The x-axis is along the 15.24 cm side of the test chamber, the y-direction is along the 7.62 cm side while the z-direction is along the vertical 2.54 cm.

Thermocouple No.	x cm	y cm	z cm
1	1.905	.9525	0.635
2	5.715	.9525	0.635
3	9.525	.9525	0.635
4	13.335	.9525	0.635
5	1.905	2.8575	1.27
6	5.715	2.8575	1.27
7	9.235	2.8575	1.27
8	13.335	2.8575	1.27
9	1.905	4.7625	1.905
10	5.715	4.7625	1.905
11	9.235	4.7625	1.905
12	13.335	4.7625	1.905
13	5.715	6.6675	2.54
14	9.235	6.6675	2.54
15	13.335	6.6675	2.54
16	7.62	3.81	0.0

DISCUSSION OF RESULTS

Three types of fillers were evaluated in this study at five different levels of heat flux. A set of runs was made without a filler to set a performance base line for each power level. The three fillers that were tested are presented in table 3. The thickness given in the table is the wall thickness of the filler, while the depth is the length of the filler in the z-direction. In the theoretical analysis, average physical properties were used for n-octadecane, while the literature values, given in table 1, were used for the aluminum filler. The average physical properties that were used are as follows:

Density

ρ(solid) = 0.8969 gm/cc

ρ(liquid) = 0.8545 gm/cc

Heat Capacity

C_p (solid) = 2.164 watt-sec/gm/^oK

C_p (liquid) = 2.406 watt-sec/gm/^oK

Thermal Conductivity

K (solid) = 0.001521 watt/cm/^oK

K (liquid) = 0.00735 watt/cm/^oK

When the literature value of the latent heat of fusion was used in the mathematical model, the phase-change times were not predicted. This can be seen by

Table 3

GEOMETRY DATA FOR THE ALUMINUM HEXAGONAL FILLERS

The thickness is the wall thickness of the filler, the cell size is the distance across one cell of the filler, while the depth is the distance in the z-direction.

Filler No.	Thickness cm	Cell Size cm	Depth cm
1.	0.00889	1.905	2.54
2.	0.011938	0.635	2.54
3.	0.05969	0.635	1.7

comparing figures 9 a-d and 25 a-d. Therefore, a reduced value of the latent heat of fusion was used. When this value was used it predicted the phase-change times more accurately. The latent heat of fusion for n-octadecane used in this study is given by Bain (21) and is as follows.

H_f = 182.83 watt-sec/gm

If the addition of fillers increases the heat-transfer rate into the phase-change material, the hot plate temperature should remain below a given control temperature for a longer period of time as the amount of filler is increased. In figure 10 the ratio of filler weight to n-octadecane weight is plotted against a pseudo control temperature. This pseudo control temperature is the hot plate control temperature minus the initial temperature. This figure is not intended to be used for design, but rather to show that the experimental data is consistant. However, if the control temperature minus the initial temperature should be 22°K, this figure could be used for approximate design purposes. This graph should not be extrapolated beyond the experimental data.

Figures 11 through 34 represent the theoretically predicted temperature profiles compared with the corresponding experimental data. The thermocouple locations are given in table 2. Response data from only one thermocouple will be plotted for each height since there

Figure 9

Theoretical and experimental temperature profiles for filler no. 2 at 40 watts with the literature value for the liquefaction enthalpy

Figure

9a 0.635 cm from the heating plate

9b 1.27 cm from the heating plate

9c 1.905 cm from the heating plate

9d 2.54 cm from the heating plate

Legend

△ F2-40-1

○ F2-40-2

—— Theoretical

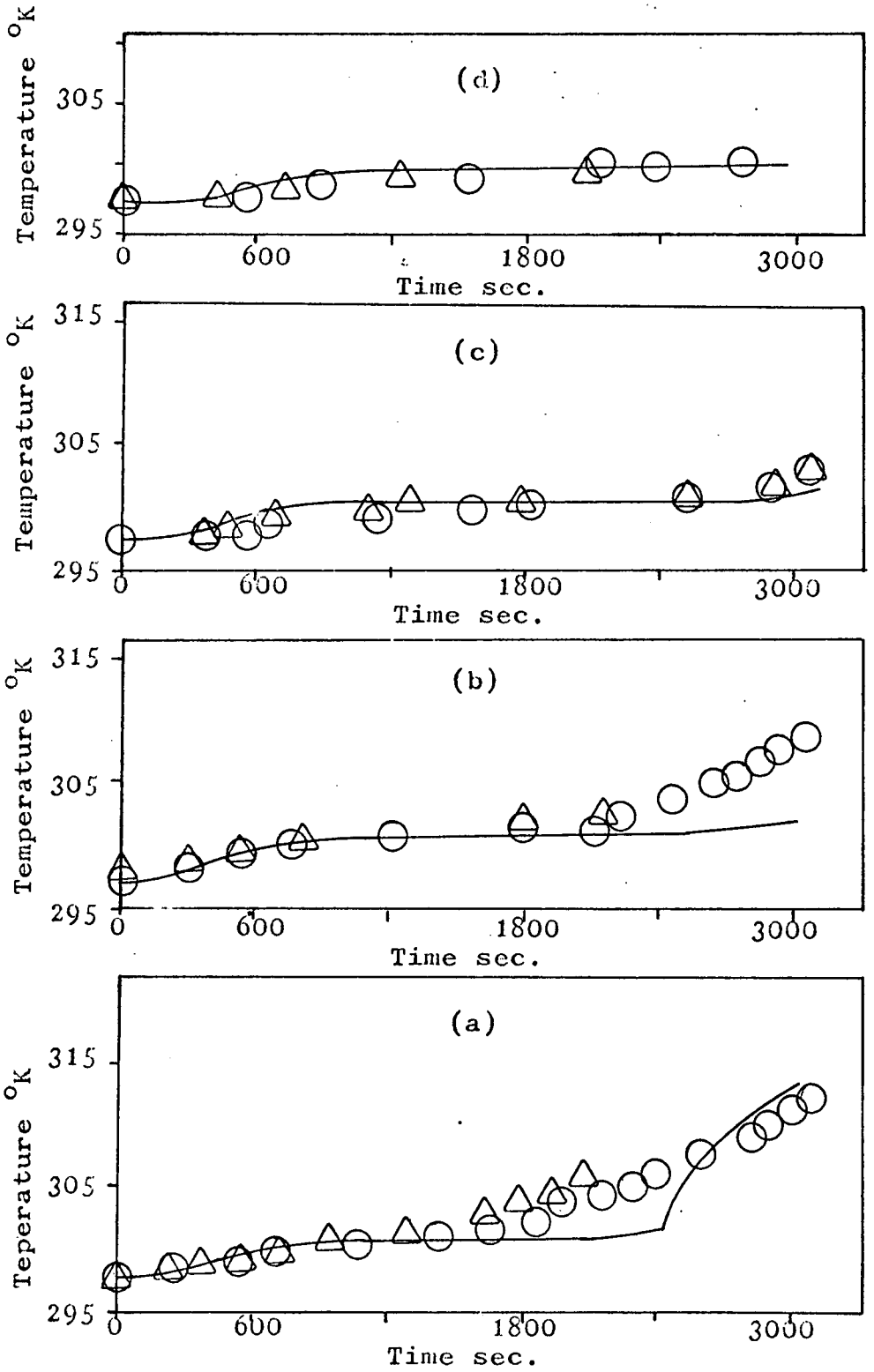
(d)
Temperature °K
305
295
0
600
1800
3000
Time sec.
(c)
Temperature °K
315
305
295
0
600
1800
3000
Time sec.
(b)
Temperature °K
315
305
295
0
600
1800
3000
Time sec.
(a)
Teperature °K
315
305
295
0
600
1800
3000
Time sec.

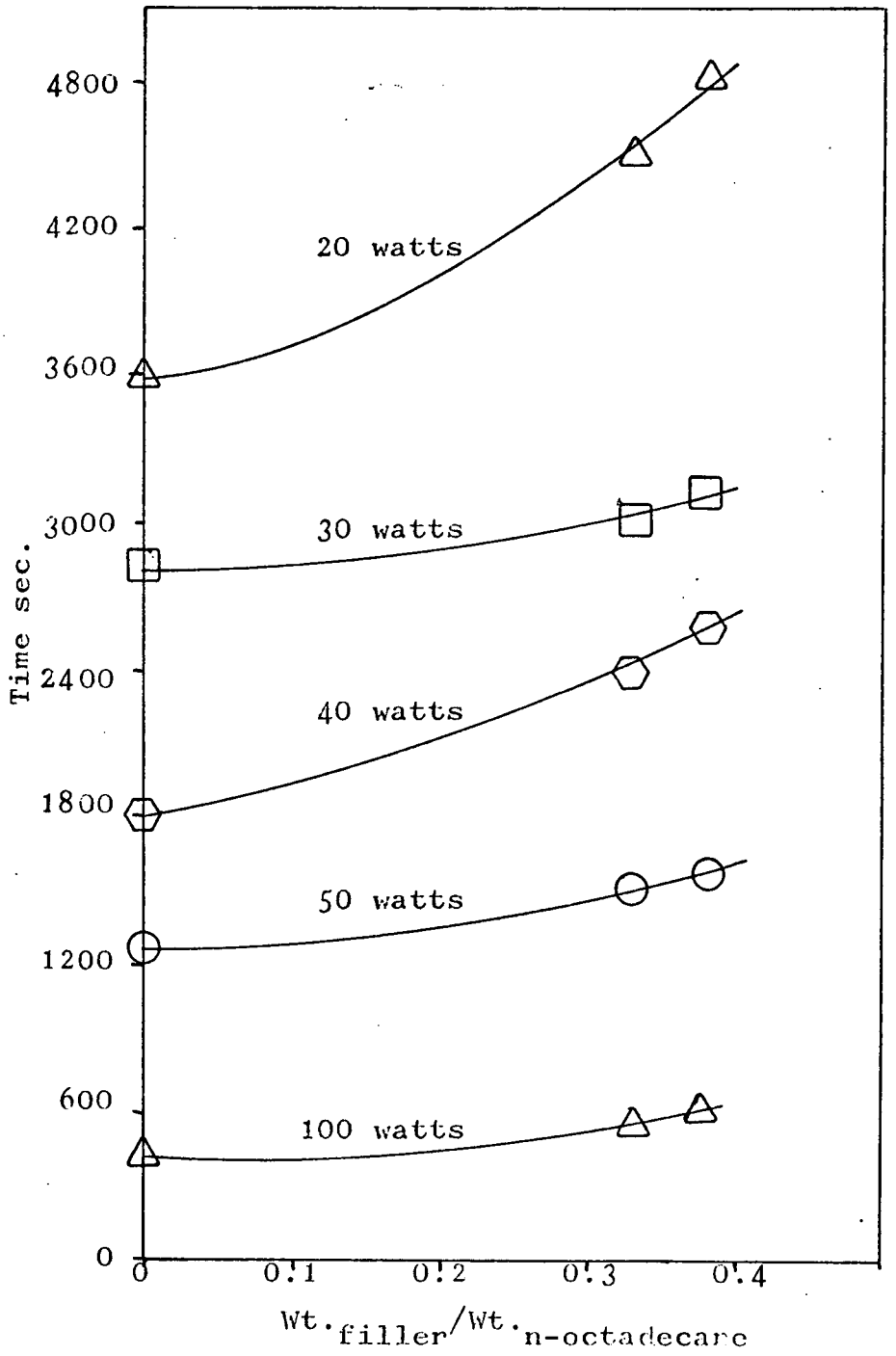

Figure 10

Time Below a Pseudo Control Temperature

is little difference between the temperature profiles recorded by each thermocouple for a given height.

In figures 11 through 16 the theoretical and experimental data from the pure paraffin or no filler runs are plotted. Due to the low heat-transfer rate of n-octadecane and the hot plate temperature limitation discussed earlier only a small portion of the n-octadecane melted during these runs. In these figures the paraffin at 0.635 cm has melted and the temperature of the liquid is rapidly rising for all power levels. At 1.27 cm the paraffin has just melted in the 20 and 30 watt runs while it has just reached the melt point in the 40 watt run. It is still below the melt temperature in the 50 and 100 watt runs. In the 20 and 30 watt runs the paraffin is in the process of melting at 2.905 and 2.54 cm. In the 40, 50 and 100 watt runs the paraffin at 1.905 and 2.54 cm is still heating up to the melt temperature. The hot plate temperature profiles for the pure paraffin runs are presented in figure 16.

The filler runs are presented in figures 17 through 34. The fillers will be discussed in the order in which they are presented in table 3, and referred to by the number indicated in the table. In figures 17 to 22 the theoretical and experimental data for filler number 1 are plotted. In these runs more of the n-octadecane has

Figure 11

Theoretical and experimental temperature profiles at 20 watts for pure n-octadecane

Figure

11a 0.635 cm from the heating plate

11b 1.27 cm form the heating plate

11c 1.905 cm from the heating plate

11d 2.54 cm from the heating plate

Legend

△ P-20-1

○ p-20-2

—— Theoretical

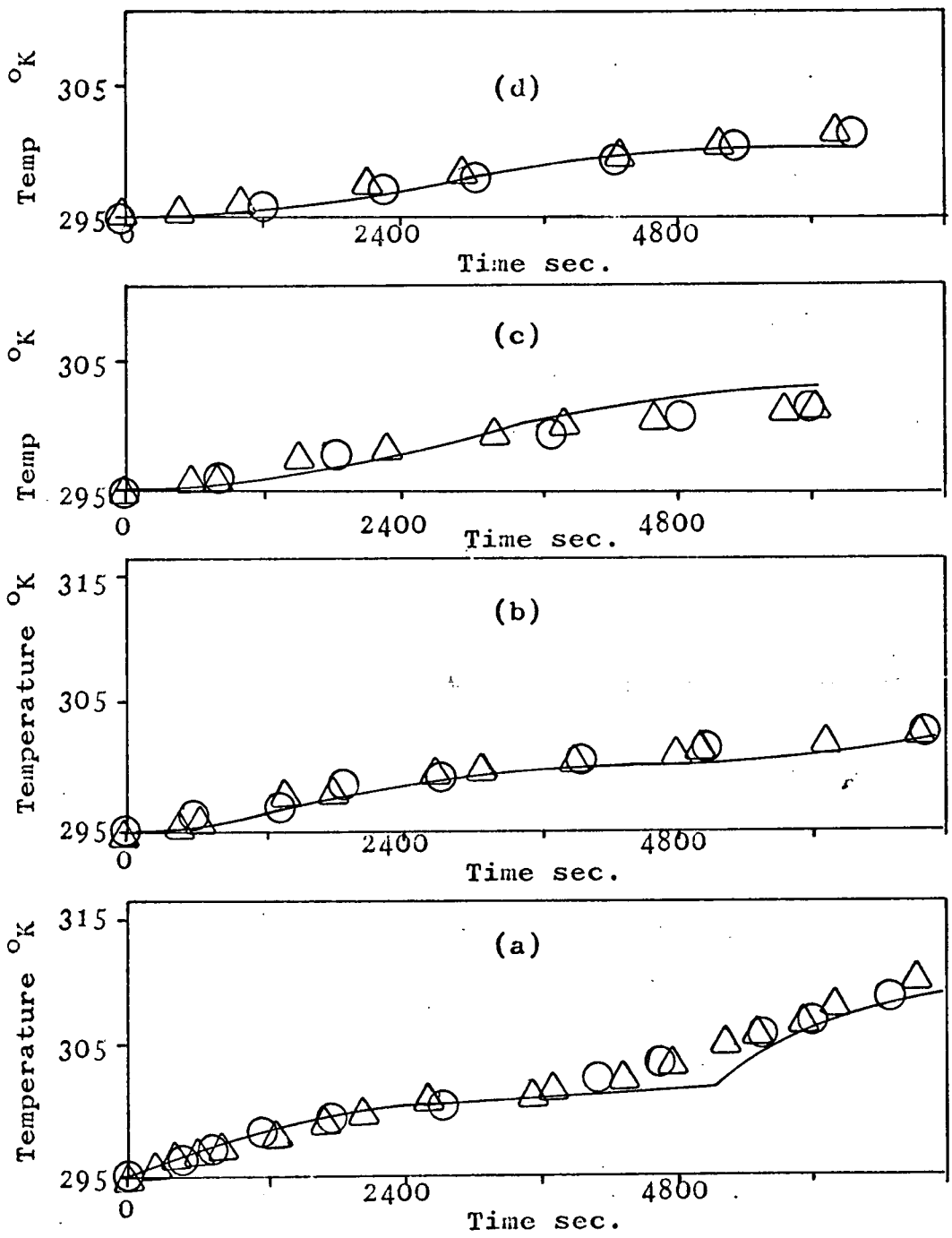
(d)
Temp °K
305
295
0
2400
4800
Time sec.
(c)
Temp °K
305
295
0
2400
4800
Time sec.
(b)
Temperature °K
315
305
295
0
2400
4800
Time sec.
(a)
Temperature °K
315
305
295
0
2400
4800
Time sec.

Figure 12

Experimental and theoretical temperature profiles at 30 watts for pure n-octadecane

Figure

12a 0.635 cm from the heating plate

12b 1.27 cm from the heating plate

12c 1.905 cm from the heating plate

12d 2.54 cm from the heating plate

Legend

△ P-30-1

○ P-30-2

—— Theoretical

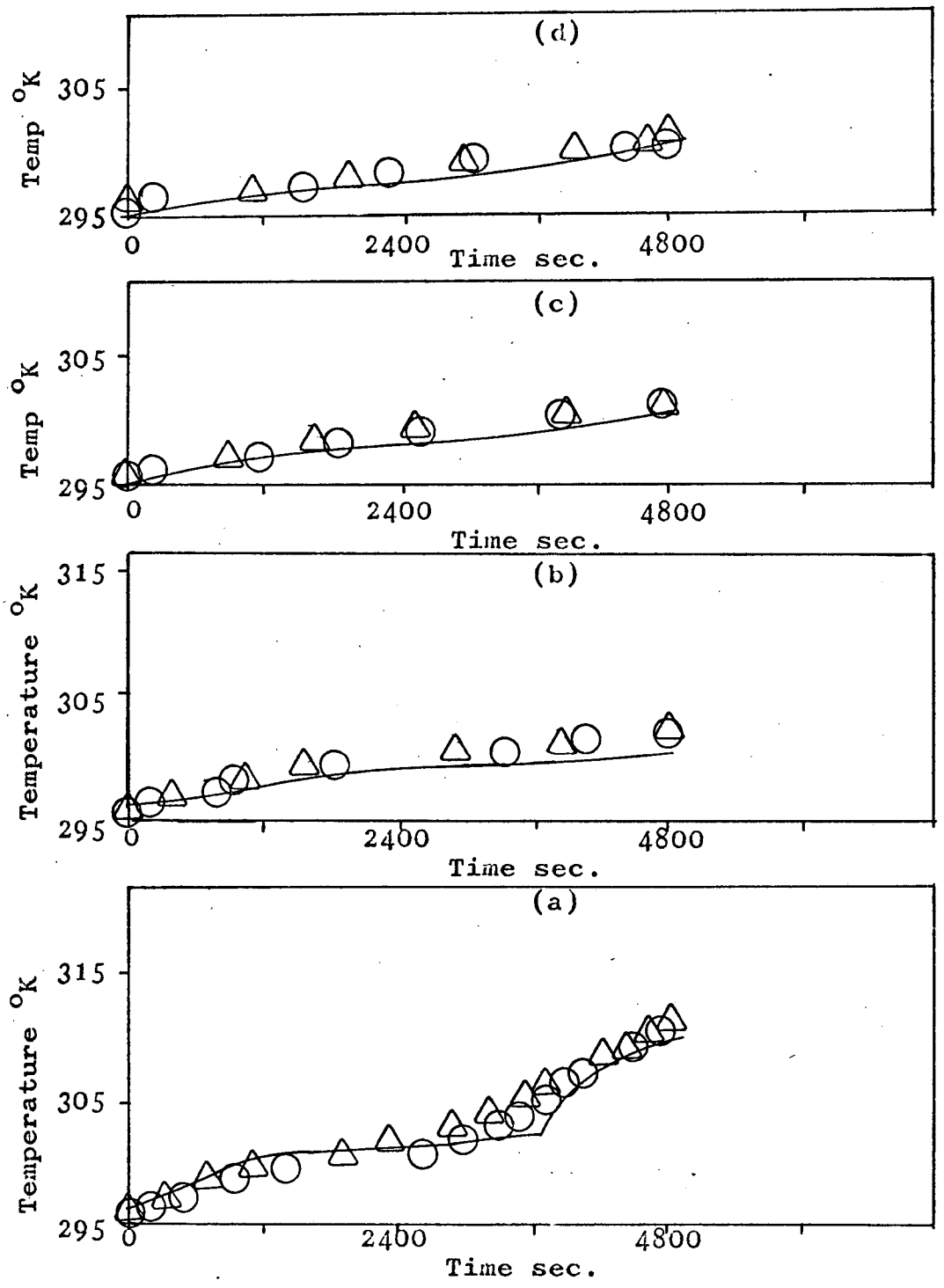
(d)
Temp °K
305
295
0
2400
4800
Time sec.
(c)
Temp °K
305
295
0
2400
4800
Time sec.
(b)
Temperature °K
315
305
295
0
2400
4800
Time sec.
(a)
Temperature °K
315
305
295
0
2400
4800
Time sec.

Figure 13

Experimental and theoretical temperature profiles at 40 watts for pure n-octadecane

Figure

13a 0.635 cm from the heating plate

13b 1.27 cm from the heating plate

13c 1.905 cm from the heating plate

13d 2.54 cm from the heating plate

Legend

△ P-40-1

○ P-40-2

—— Theoretical

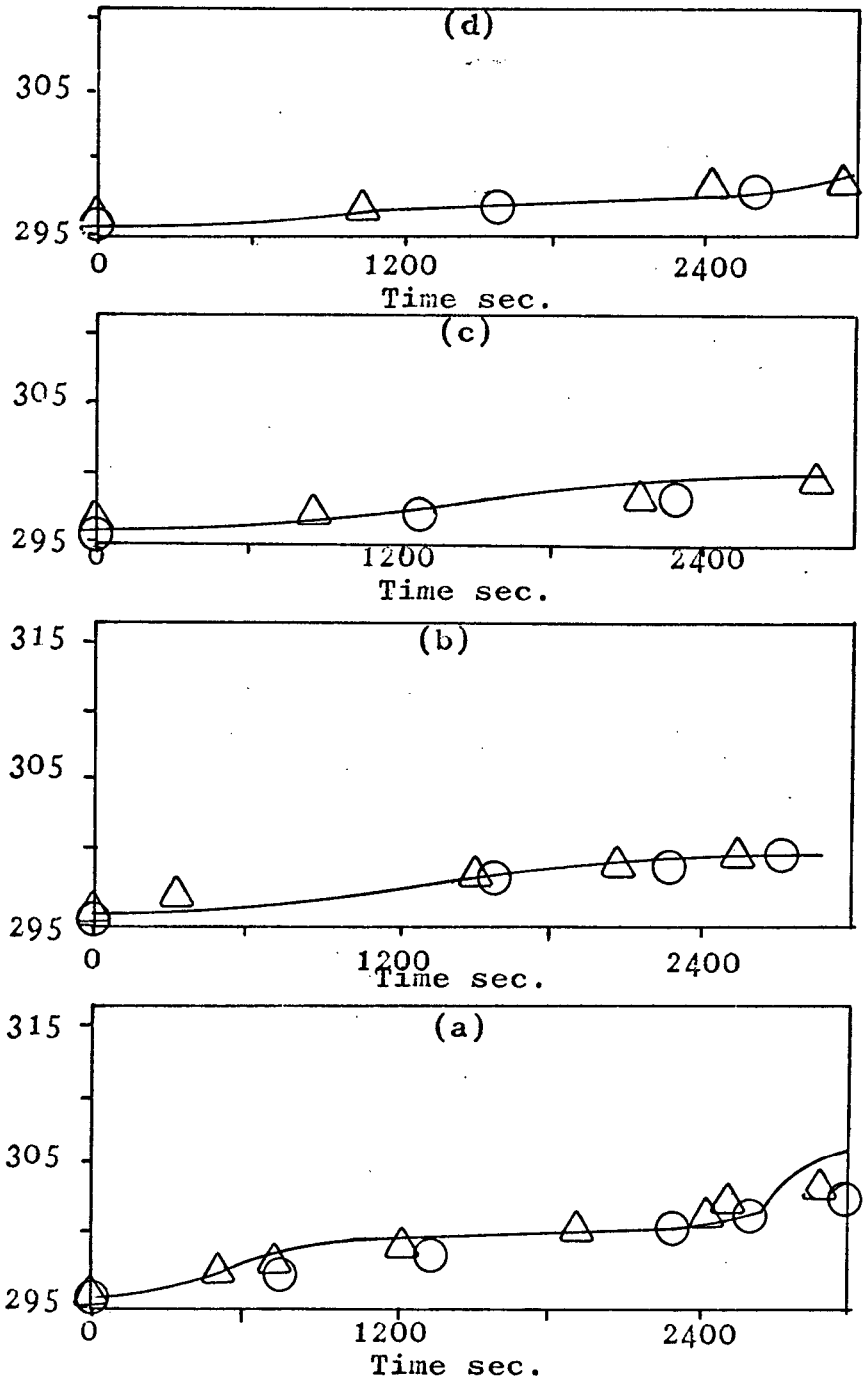
(d)
305
295
0
1200
2400
Time sec.
(c)
305
295
0
1200
2400
Time sec.
315
(b)
305
295
0
1200
2400
Time sec.
315
(a)
305
295
0
1200
2400
Time sec.

Figure 14

Experimental and theoretical temperature profiles at 50 watts for pure n-octadecane

Figure

14a 0.635 cm from the heating plate

14b 1.27 cm from the heating plate

14c 1.905 cm from the heating plate

14d 2.54 cm from the heating plate

legend

△ P-50-1

○ P-50-2

—— Theoretical

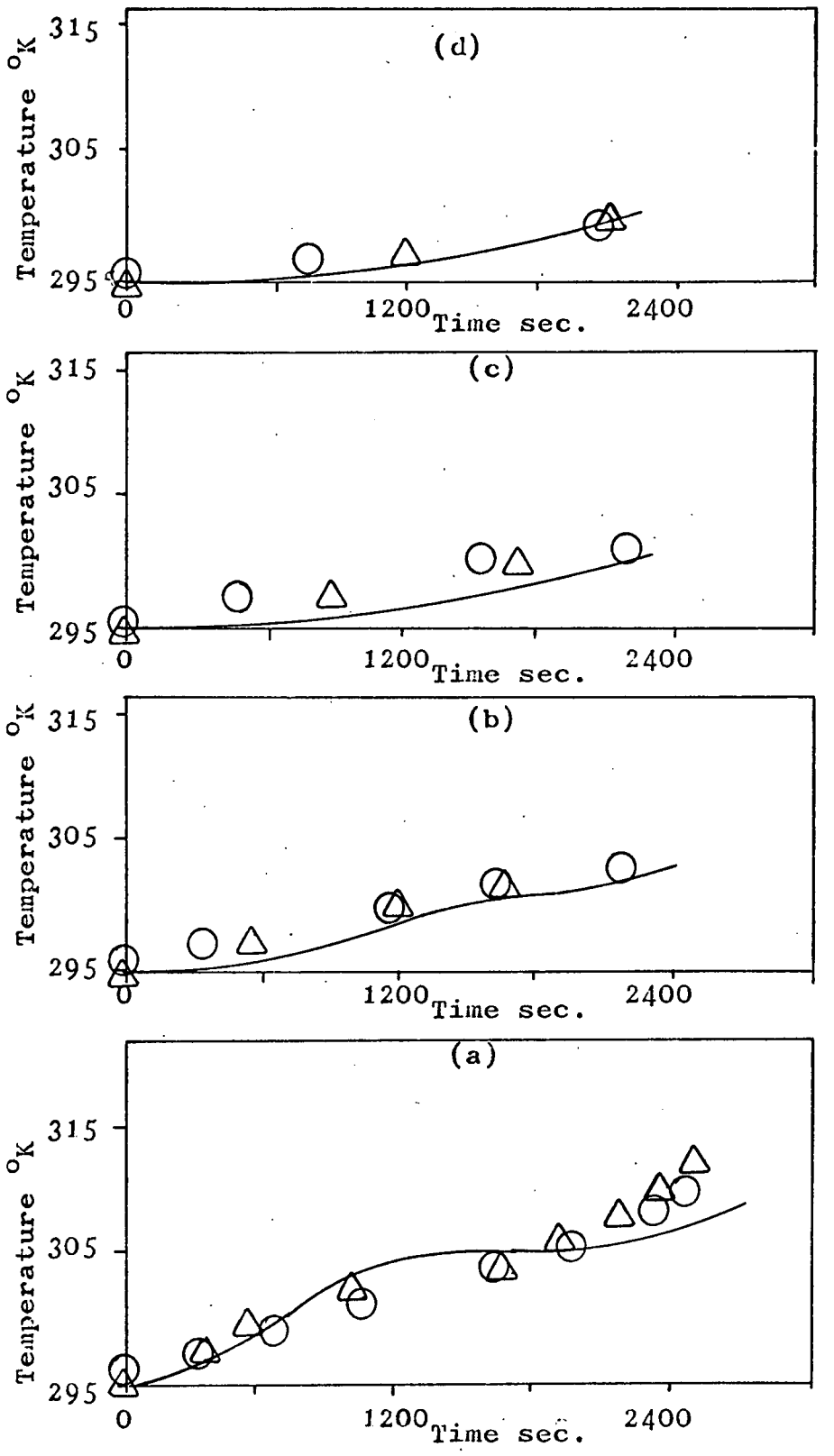
(d)
Temperature °K
315
305
295
0
1200
2400
Time sec.
(c)
Temperature °K
315
305
295
0
1200
2400
Time sec.
(b)
Temperature °K
315
305
295
0
1200
2400
Time sec.
(a)
Temperature °K
315
305
295
0
1200
2400
Time sec.

Figure 15

Experimental and theoretical temperature profiles at 100 watts for pure n-octadecane

Figure

15a 0.635 cm from the heating plate

15b 1.27 cm from the heating plate

15c 1.905 cm from the heating plate

15d 2.54 cm from the heating plate

Legend

△ P-100-1

○ P-100-2

—— Theoretical

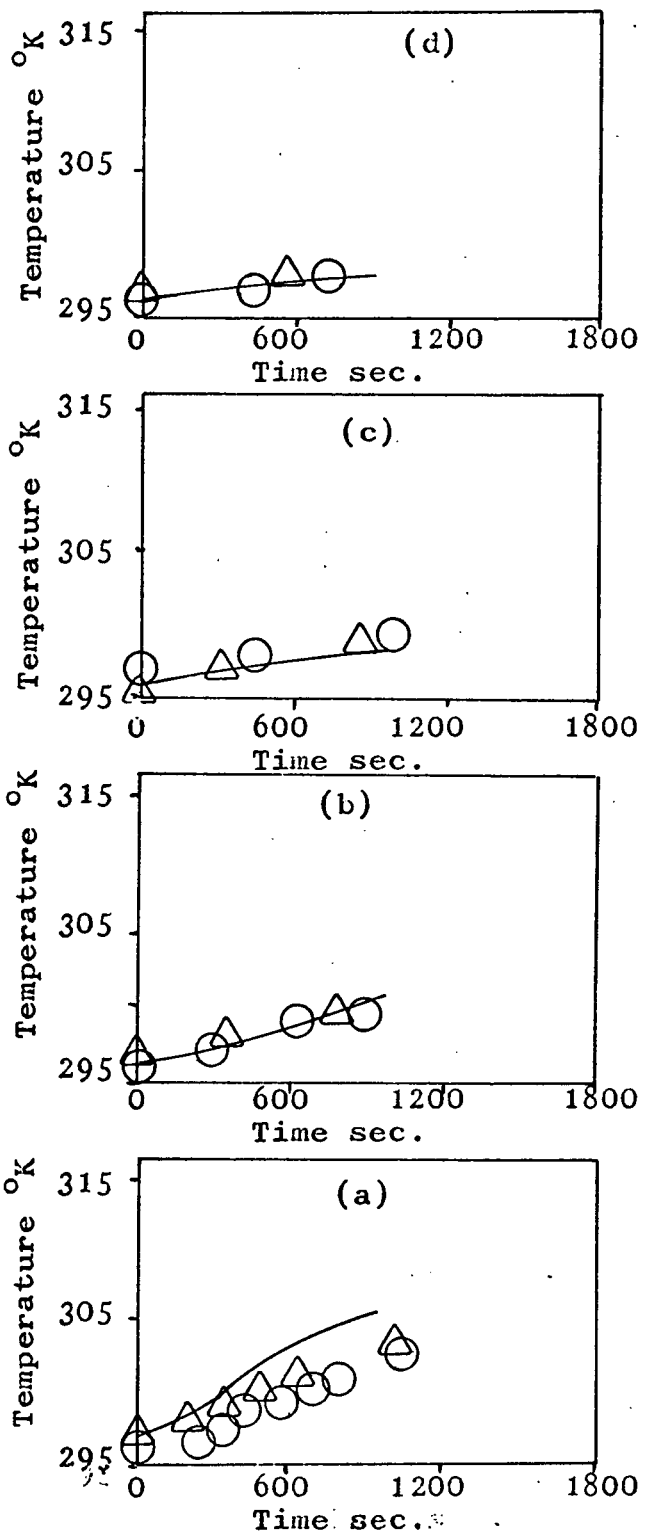
(d)
(c)
(b)
(a)
Temperature °K
315
305
295
0
600
1200
1800
Time sec.

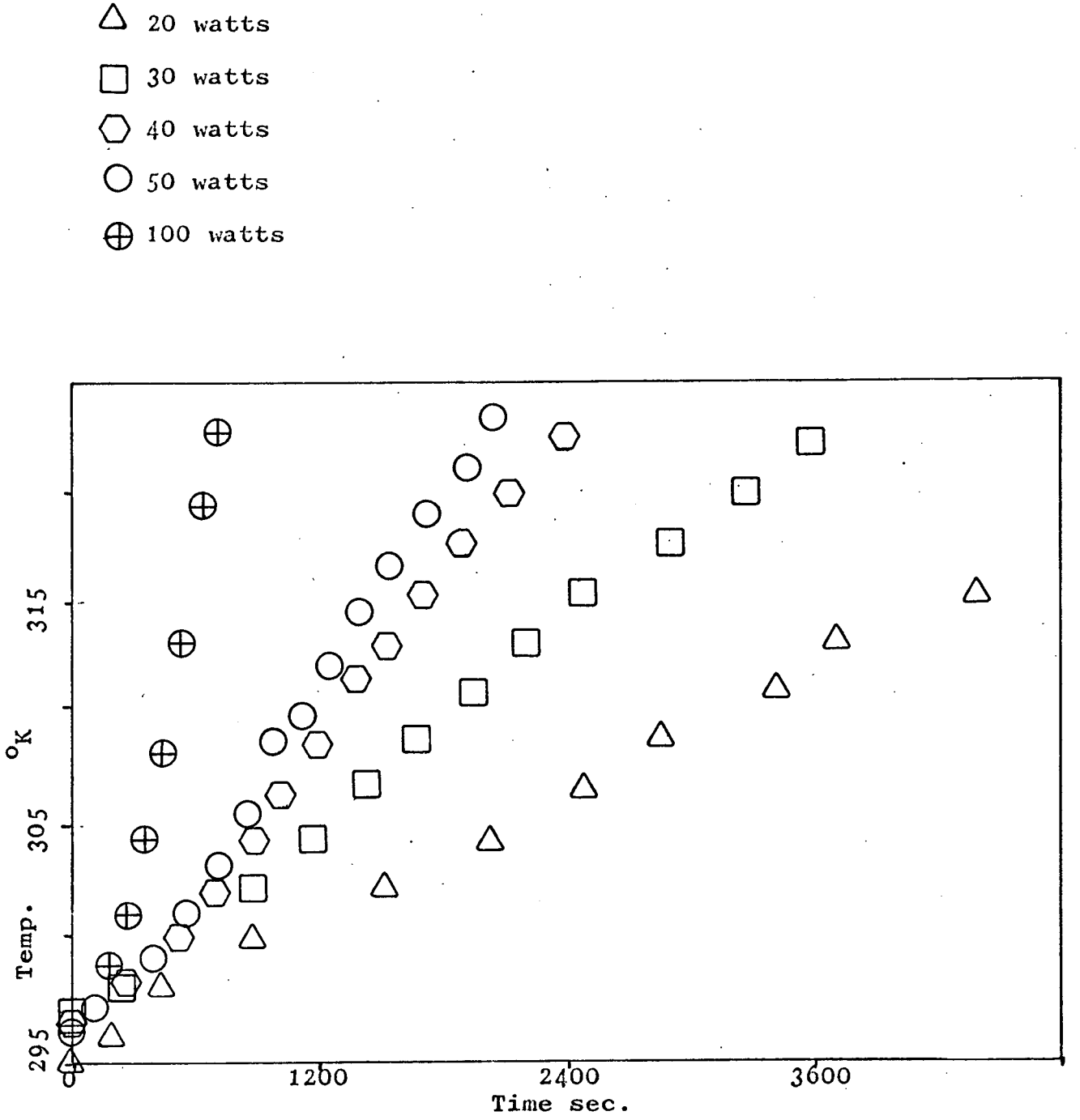

Figure 16

Hot Plate Temperature Profiles for the Pure N-Octdecane Runs

Figure 17

Experimential and theoretical temperature profiles at 20 watts for filler no. 1

Figure

17a 0.635 cm from the heating plate

17b 1.27 cm from the heating plate

17c 1.905 cm from the heating plate

17d 2.54 cm from the heating plate

Legend

△ F1-20-1

○ F1-20-2

—— Theoretical

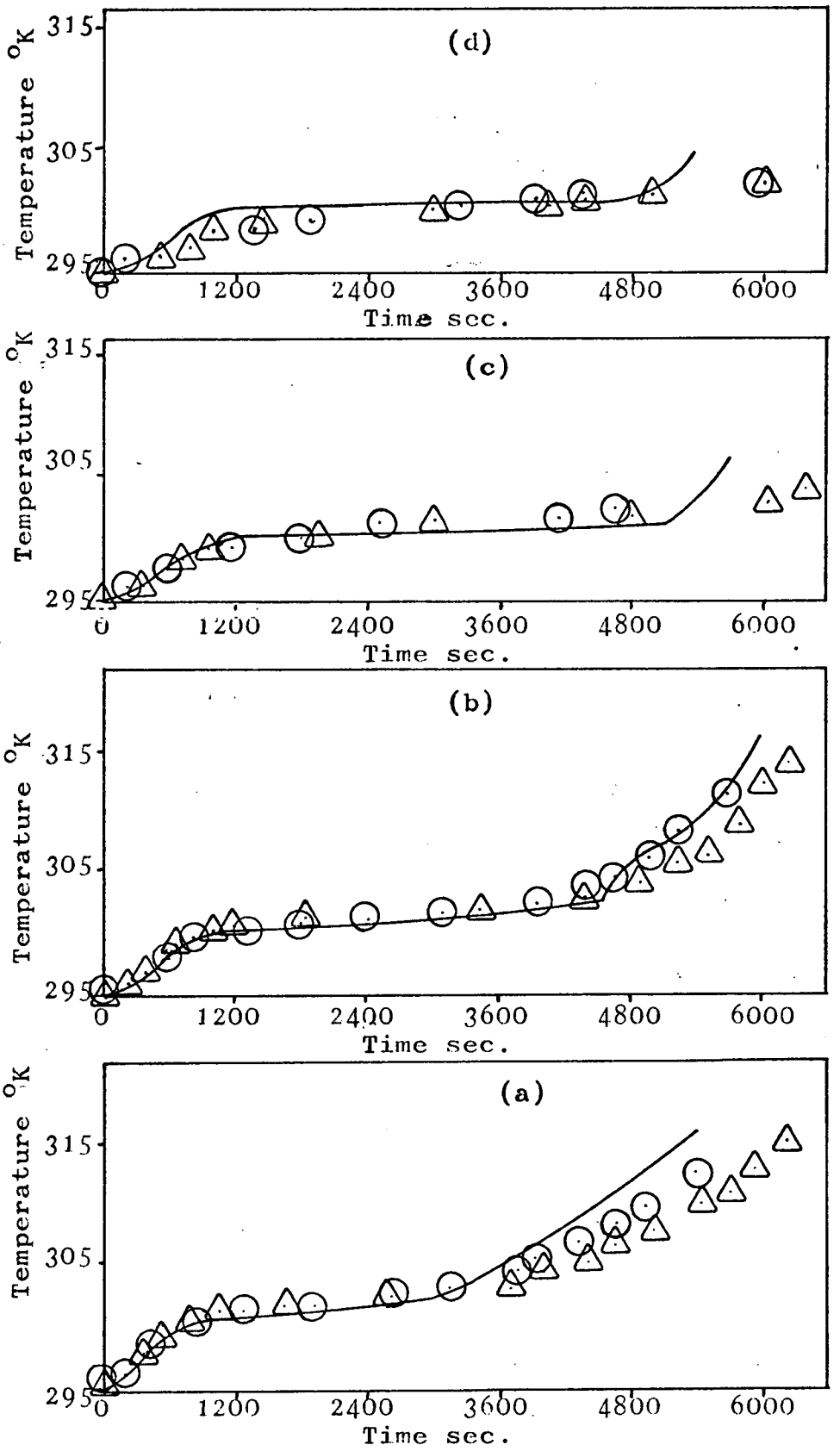
(d)
Temperature °K
315
305
295
0
1200
2400
3600
4800
6000
Time sec.
(c)
Temperature °K
315
305
295
0
1200
2400
3600
4800
6000
Time sec.
(b)
Temperature °K
315
305
295
0
1200
2400
3600
4800
6000
Time sec.
(a)
Temperature °K
315
305
295
0
1200
2400
3600
4800
6000
Time sec.

Figure 18

Experimental and theoretical temperature profiles at 30 watts for filler no. 1

Figure

18a 0.635 cm from the heating plate

18b 1.27 cm from the heating plate

18c 1.905 cm from the heating plate

18d 2.54 cm from the heating plate

Legend

△ F1-30-1

○ F1-30-2

——— Theoretical

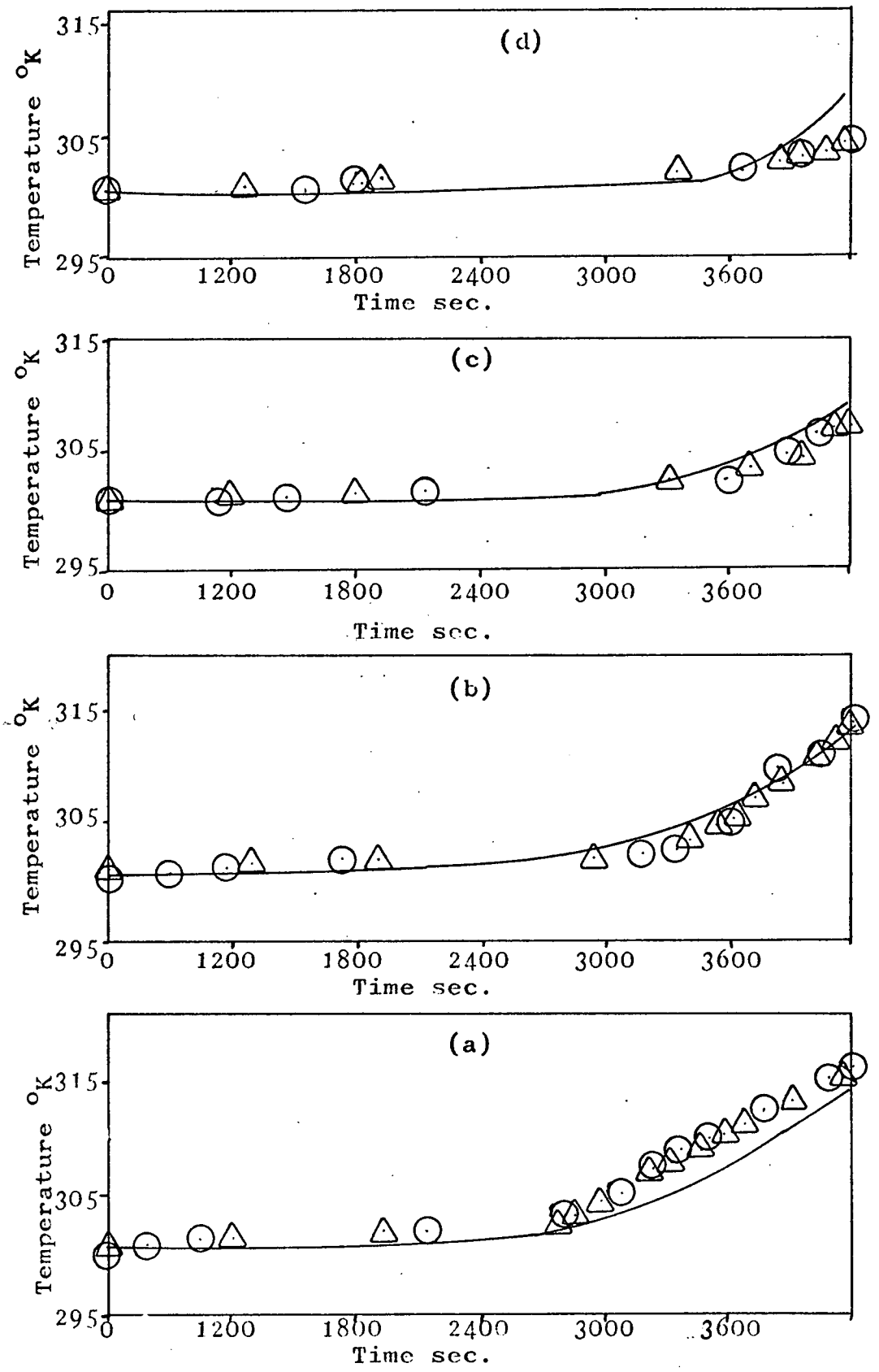
(d)
Temperature °K
315
305
295
0
1200
1800
2400
3000
3600
Time sec.
(c)
Temperature °K
315
305
295
0
1200
1800
2400
3000
3600
Time sec.
(b)
Temperature °K
315
305
295
0
1200
1800
2400
3000
3600
Time sec.
(a)
Temperature °K
315
305
295
0
1200
1800
2400
3000
3600
Time sec.

Figure 19

Experimental and theoretical temperature profiles at 40 watts for filler no. 1

Figure

19a 0.635 cm from the heating plate

19b 1.27 cm from the heating plate

19c 1.905 cm from the heating plate

19d 2.54 cm from the heating plate

Legend

△ F1-40-1

○ F1-40-2

—— Theoretical

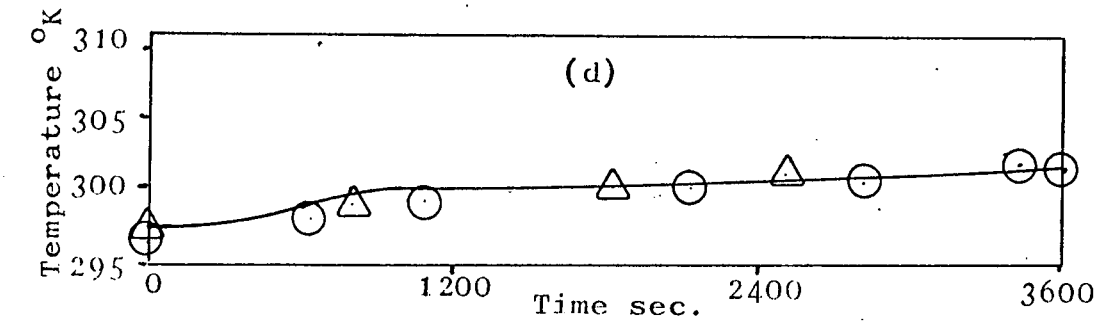
(d)
Temperature °K
310
305
300
295
0
1200
2400
3600
Time sec.

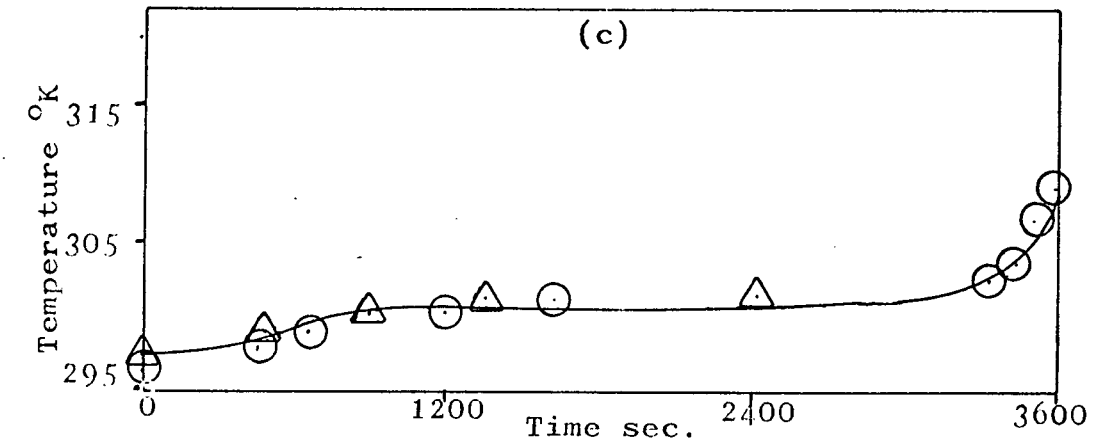
(c)
Temperature °K
315
305
295
0
1200
2400
3600
Time sec.

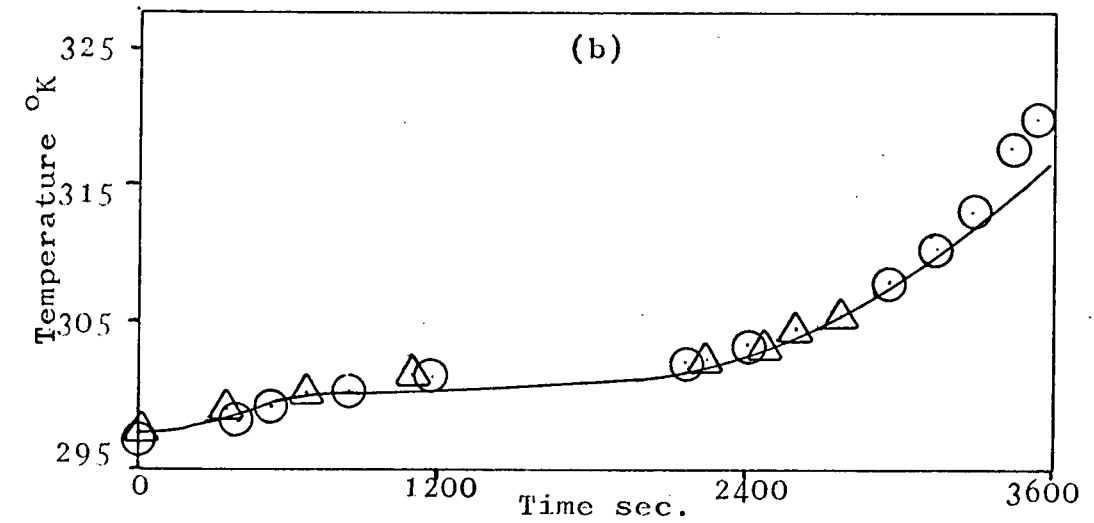
(b)
Temperature °K
325
315
305
295
0
1200
2400
3600
Time sec.

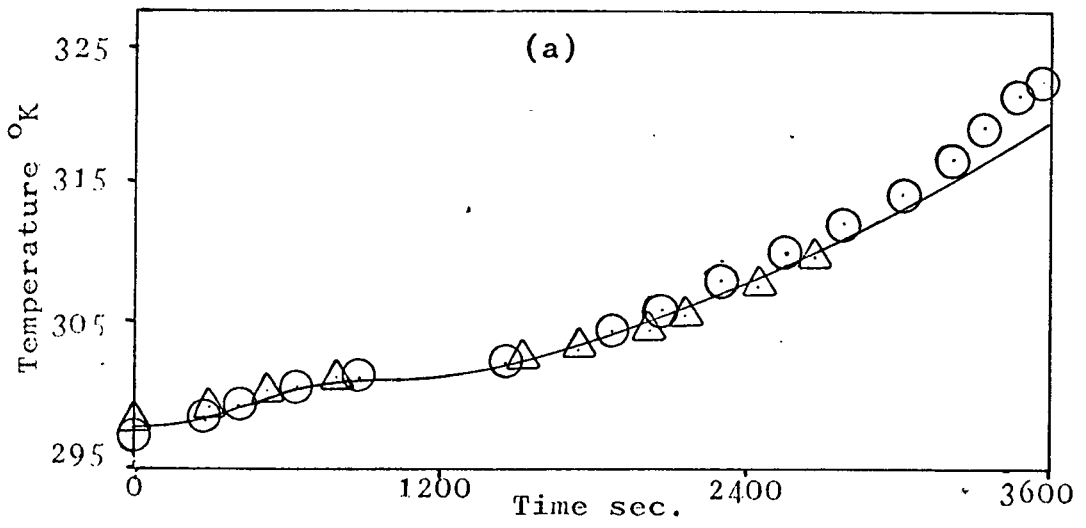
(a)
Temperature °K
325
315
305
295
0
1200
2400
3600
Time sec.

Figure 20

Experimental and theoretical temperature profiles at 50 watts for filler no. 1

Figure

20a 0.635 cm from the heating plate

20b 1.27 cm from the heating plate

20c 1.905 cm from the heating plate

20d 2.54 cm from the heating plate

Legend

△ F1-50-1

○ F1-50-2

—— Theoretical

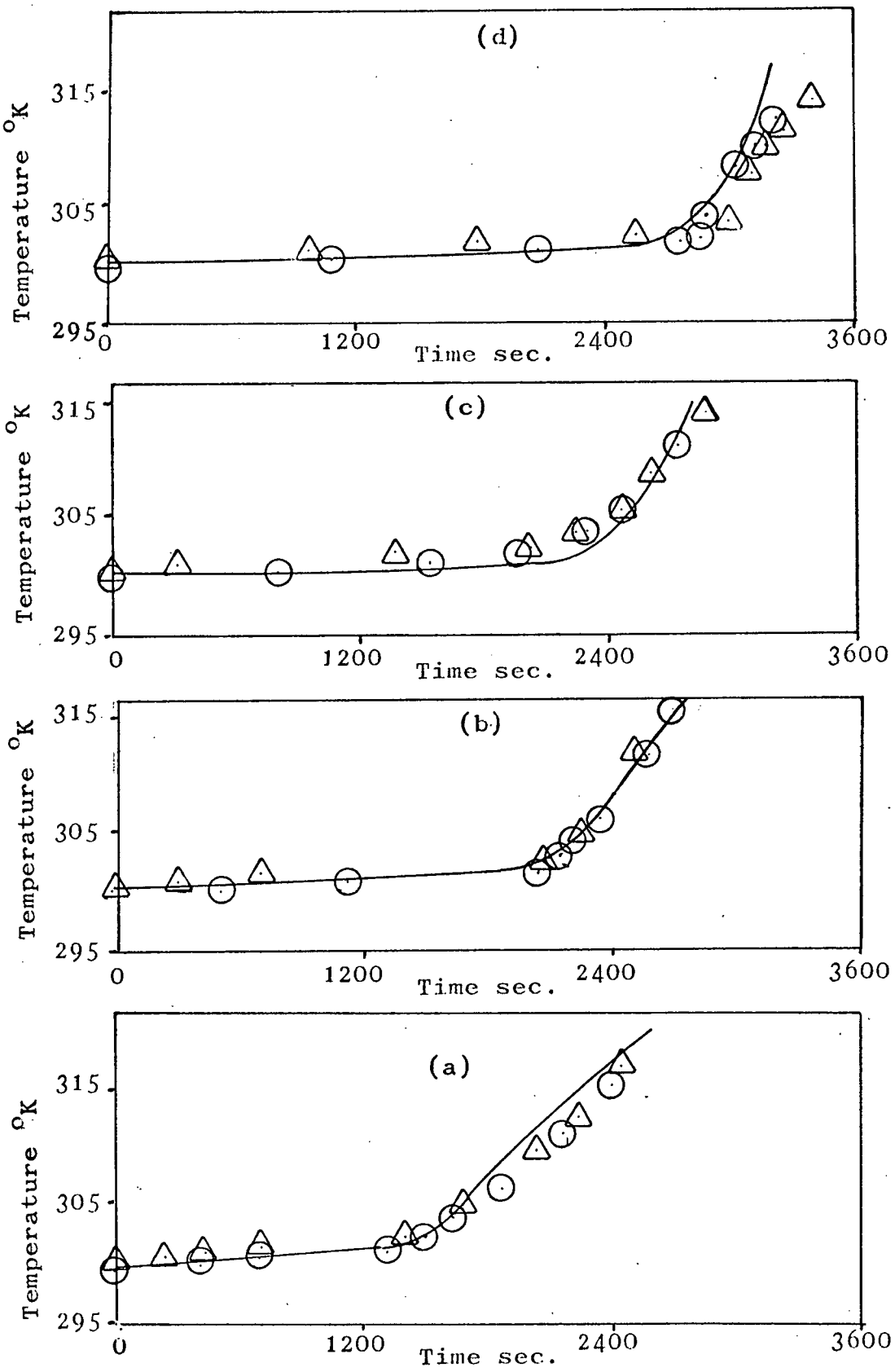
(d)
Temperature °K
315
305
295
0
1200
2400
3600
Time sec.
(c)
Temperature °K
315
305
295
0
1200
2400
3600
Time sec.
(b)
Temperature °K
315
305
295
0
1200
2400
3600
Time sec.
(a)
Temperature °K
315
305
295
0
1200
2400
3600
Time sec.

Figure 21

Experimental and theoretical temperature profiles at 100 watts for filler no. 1

Figure

21a 0.635 cm from the heating plate

21b 1.27 cm from the heating plate

21c 1.905 cm from the heating plate

21d 2.54 cm from the heating plate

Legend

△ F1-100-1

○ F1-100-2

—— Theoretical

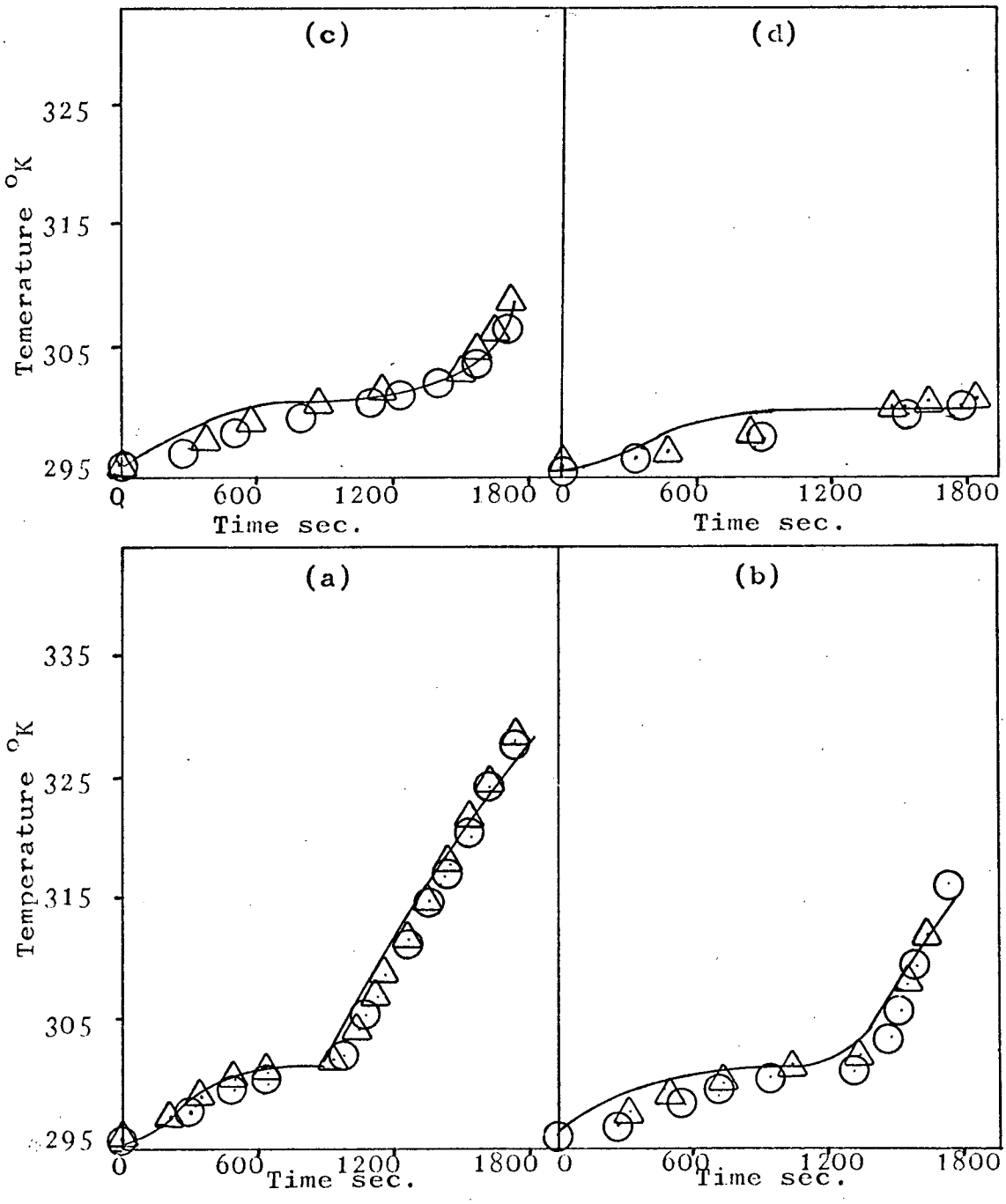
(c)
(d)
(a)
(b)
Temerature °K
Temperature °K
325
315
305
295
335
0
600
1200
1800
Time sec.

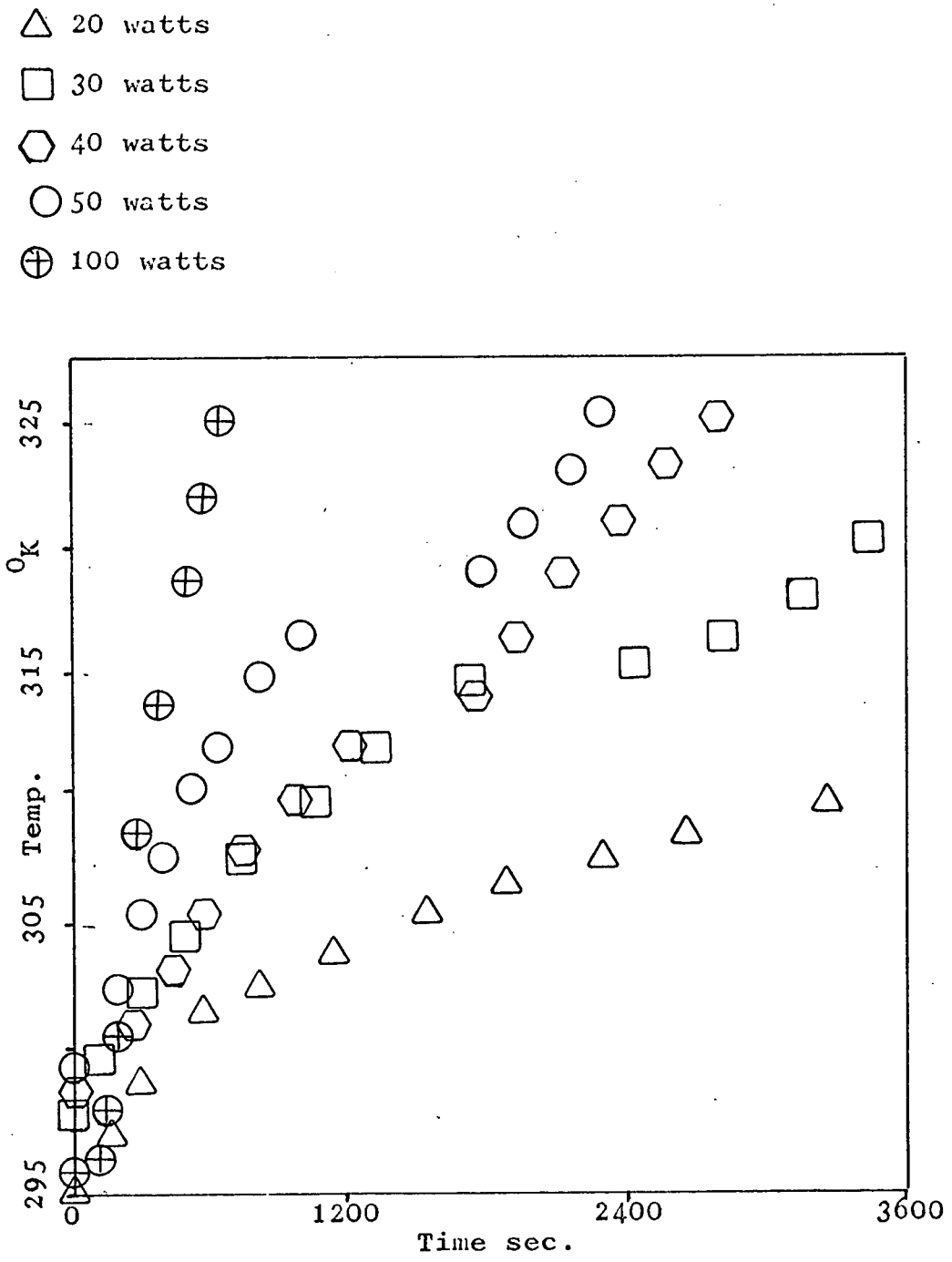

Figure 22

Hot Plate Temperatire Profiles for Filler No. 1

melted compared to the pure paraffin runs. The theoretical curves in all cases predict the solid-phase temperature profiles exactly, while there is some variation in the liquid phase. The liquid phase deviations are always on the high side. If the theoretical analysis had considered the heat losses, the theoretical temperature profiles could possibly have been brought down in line with the experimental data. The phase change times are all predicted. The theoretical profiles that curve up smoothly through the melt point are nodes closer to the aluminum filler, figure 17, while those that jump sharply after the phase-change are nodes farther away from the filler, figure 17b. The hot plate temperature profiles for filler number 1 are shown in figure 22.

Figures 23 to 28 show the experimental and theoretical results for filler number 2. The same statements that were made for filler number 1 can be made for filler number 2.

The results from filler number 3 are plotted in figures 29 to 32. Note that the theoretical temperature profiles deviate sharply from the experimental profiles at the 1.27 cm level. In this case the filler is only 1.27 cm deep, and when all of the n-octadecane has melted in the theoretical analysis, the whole cell will heat up rapidly as shown in figures 29b, 29d, 30b, 30d and 31b.

Figure 23

Experimental and theoretical temperature profiles at 20 watts for filler no. 2

Figure

23a 0.635 cm from the heating plate

23b 1.27 cm from the heating plate

23c 1.905 cm from the heating plate

23d 2.54 cm from the heating plate

Legend

△ F2-20-1

○ F2-20-2

—— Theoretical

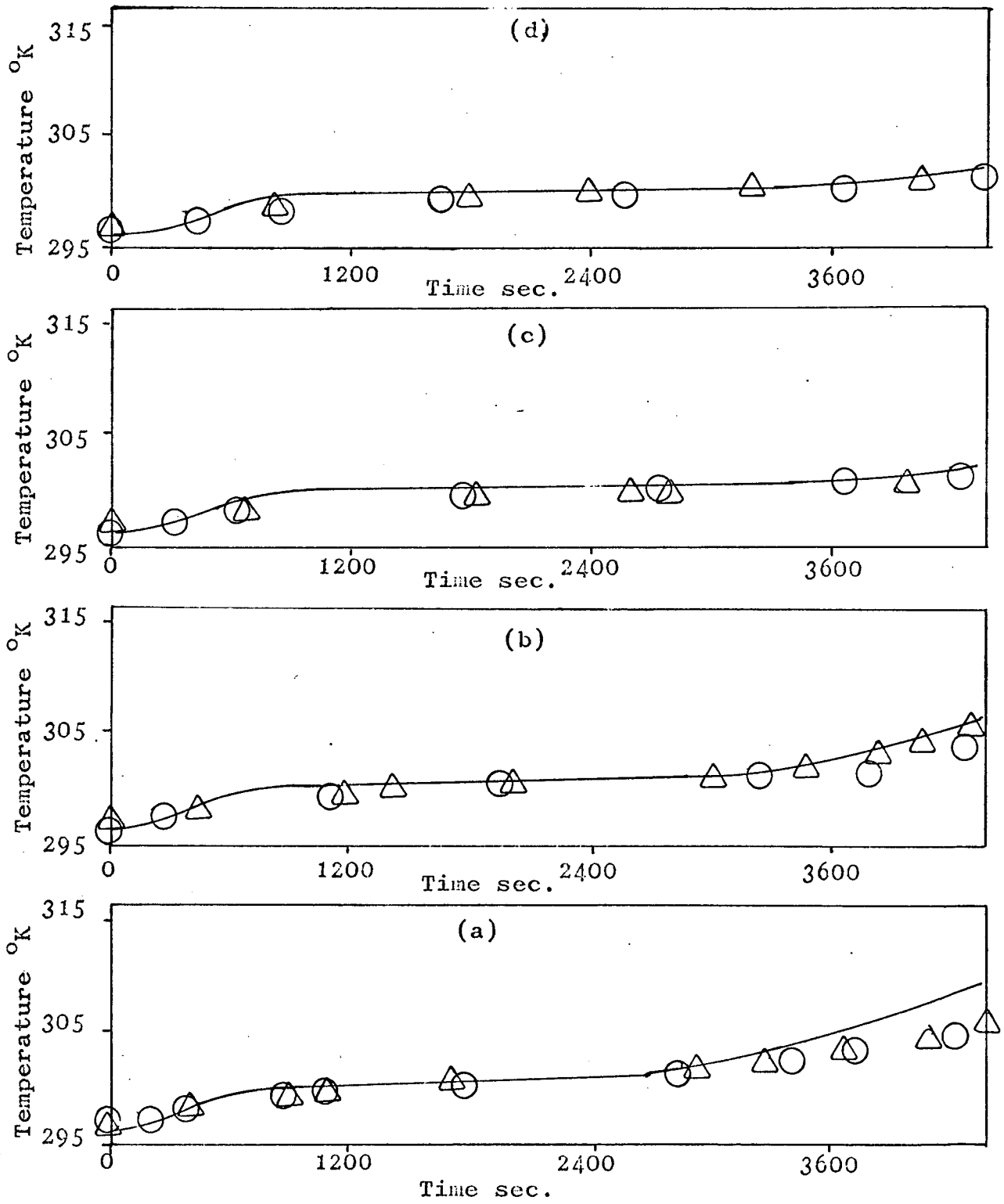
(d)
(c)
(b)
(a)
Temperature °K
315
305
295
0
1200
2400
3600
Time sec.

Figure 24

Experimental and theoretical temperature profiles at 30 watts for filler no. 2

Figure

24a 0.635 cm from the heating plate

24b 1.27 cm from the heating plate

24c 1.905 cm from the heating plate

24d 2.54 cm from the heating plate

Legend

△ F2-30-1

○ F2-30-2

—— Theoretical

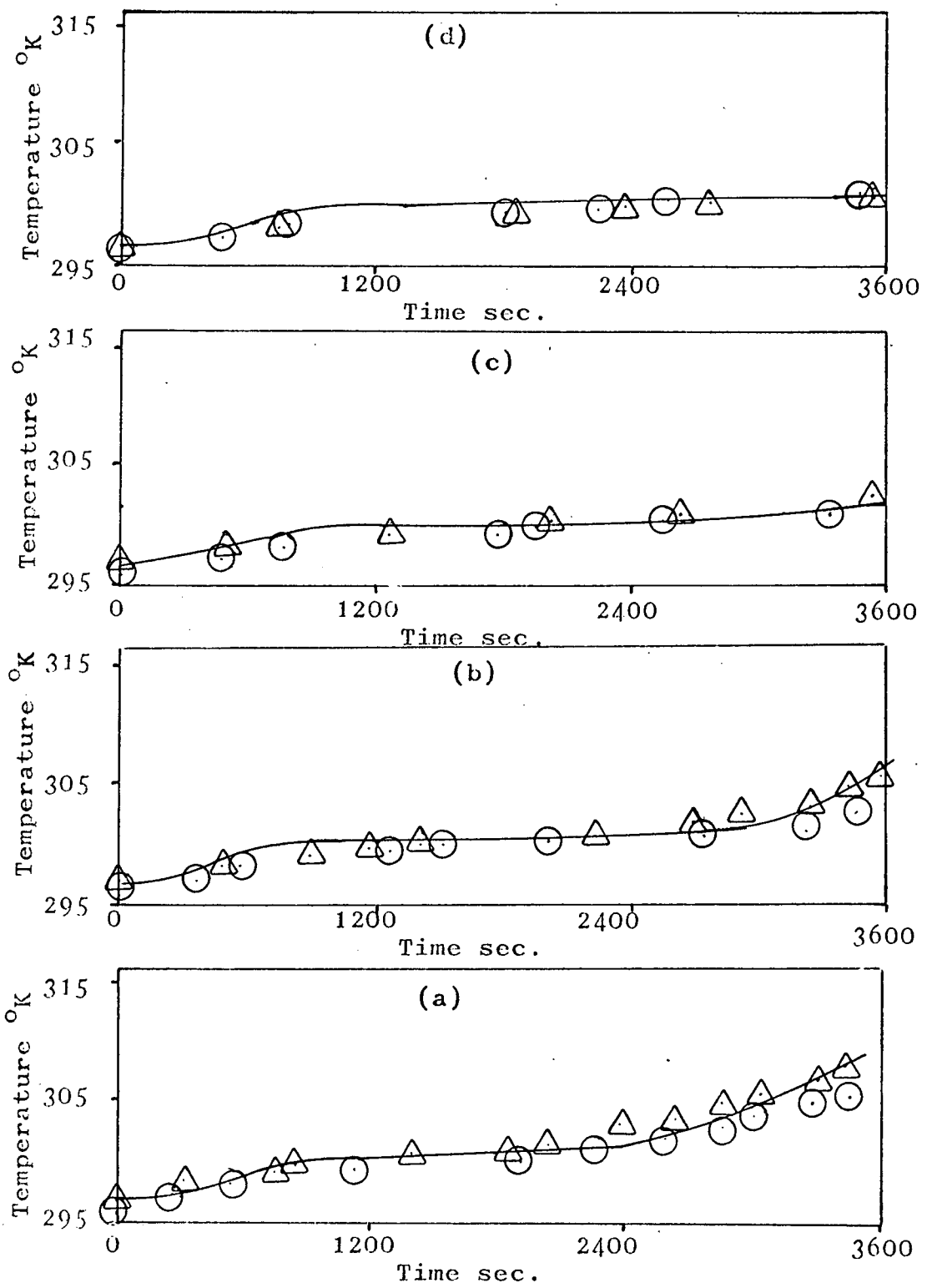
(d)
Temperature °K
315
305
295
0
1200
2400
3600
Time sec.
(c)
Temperature °K
315
305
295
0
1200
2400
3600
Time sec.
(b)
Temperature °K
315
305
295
0
1200
2400
3600
Time sec.
(a)
Temperature °K
315
305
295
0
1200
2400
3600
Time sec.

Figure 25

Experimental and theoretical temperature profiles at 40 watts for filler no. 2

Figure

25a 0.635 cm from the heating plate

25b 1.27 cm from the heating plate

25c 1.905 cm from the heating plate

25d 2.54 cm from the heating plate

Legend

△ F2-30-1

○ F2-30-2

—— Theoretical

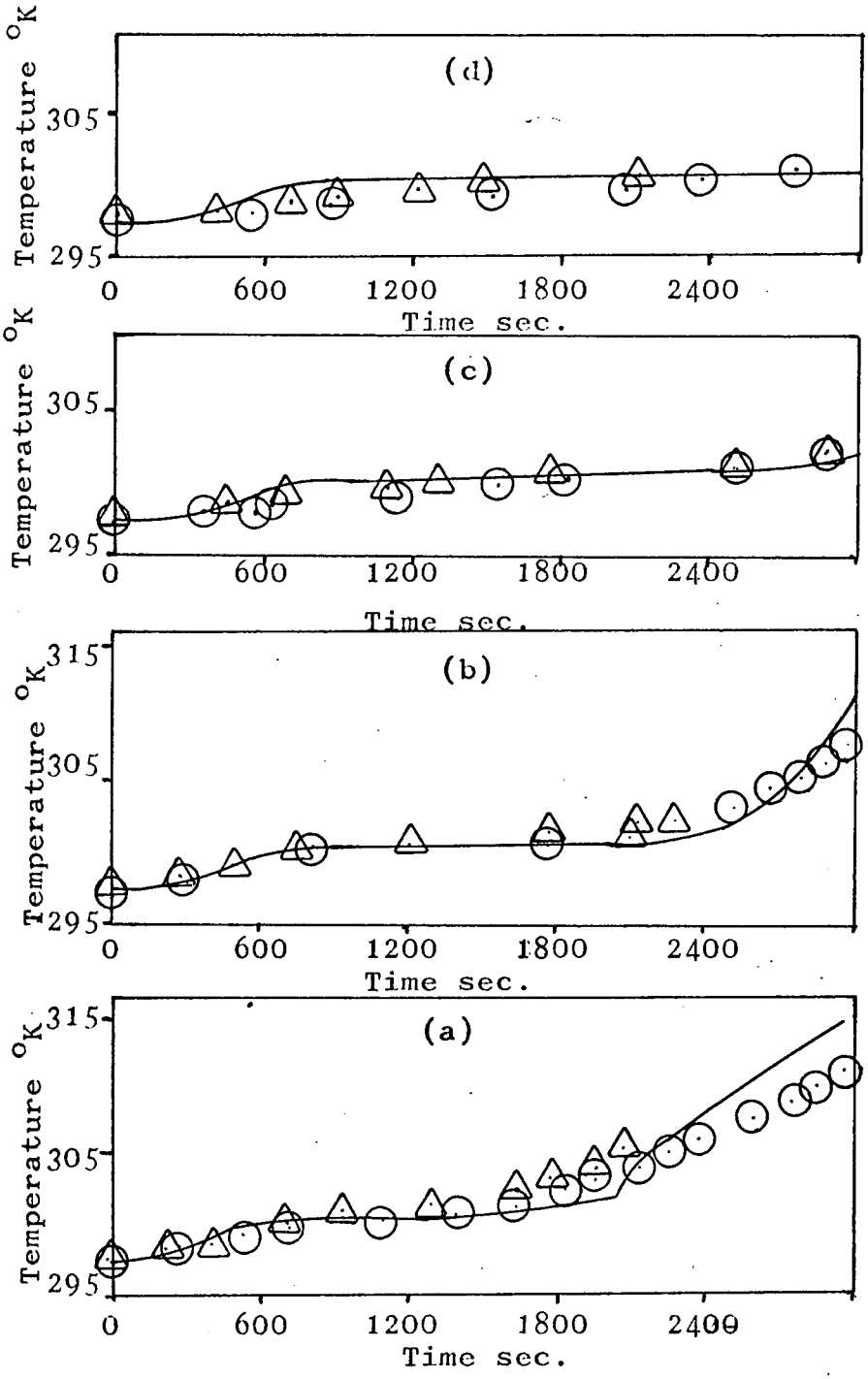
(d)
Temperature °K
305
295
0
600
1200
1800
2400
Time sec.
(c)
Temperature °K
305
295
0
600
1200
1800
2400
Time sec.
(b)
Temperature °K
315
305
295
0
600
1200
1800
2400
Time sec.
(a)
Temperature °K
315
305
295
0
600
1200
1800
2400
Time sec.

Figure 26

Experimental and theoretical temperature profiles at 50 watts for filler no. 2

Figure

26a 0.635 cm from the heating plate

26b 1.27 cm from the heating plate

26c 1.905 cm from the heating plate

26d 2.54 cm from the heating plate

Legend

△ F2-50-1

○ F2-50-2

—— Theoretical

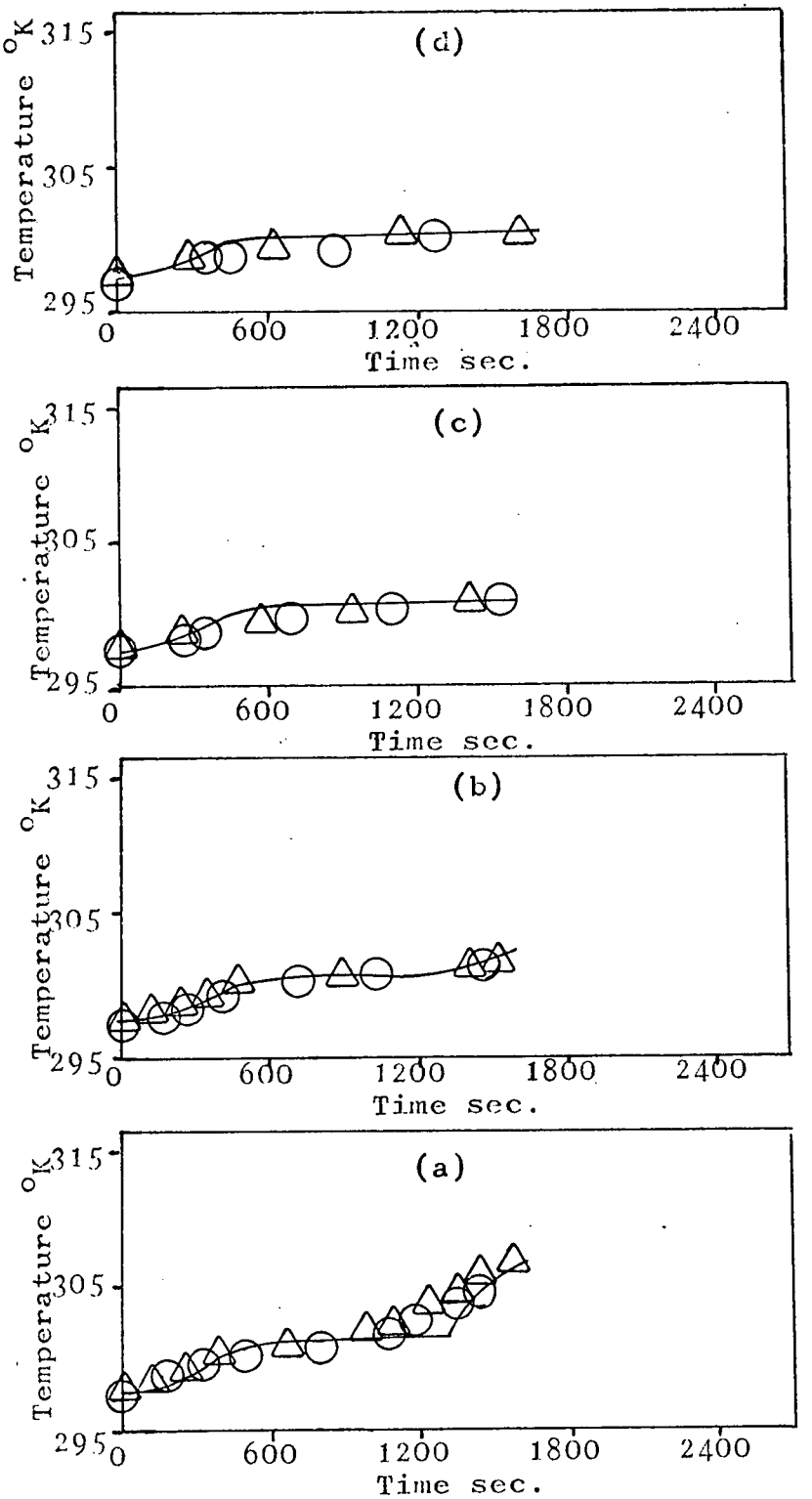
(d)
Temperature °K
315
305
295
0
600
1200
1800
2400
Time sec.
(c)
Temperature °K
315
305
295
0
600
1200
1800
2400
Time sec.
(b)
Temperature °K
315
305
295
0
600
1200
1800
2400
Time sec.
(a)
Temperature °K
315
305
295
0
600
1200
1800
2400
Time sec.

Figure 27

Experimental and theoretical temperature profiles at 100 watts for filler no. 2

Figure

27a 0.635 cm from the heating plate

27b 1.27 cm from the heating plate

27c 1.905 cm from the heating playe

27d 2.54 cm from the heating plate

Legend

△ F2-100-1

○ F2-100-2

—— Theoretical

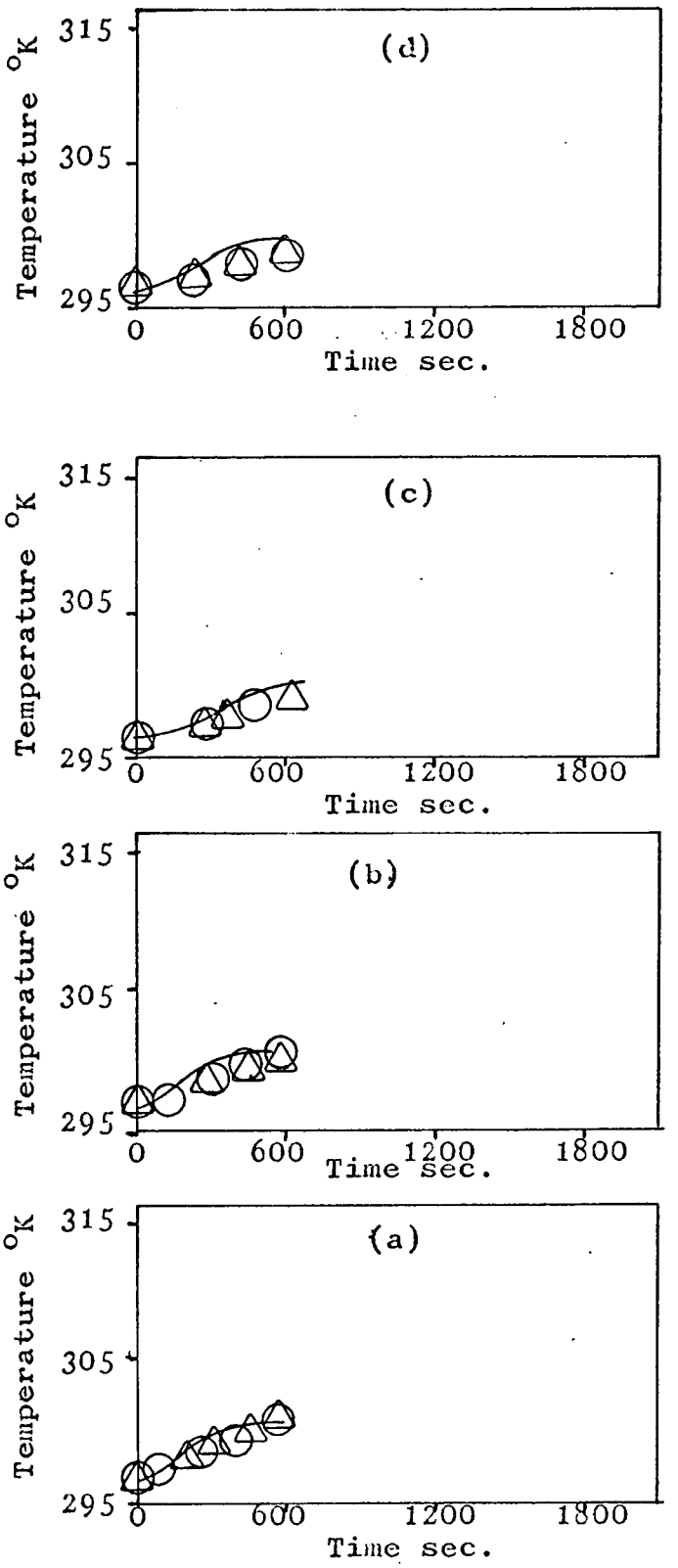
(d)
(c)
(b)
(a)
Temperature °K
315
305
295
0
600
1200
1800
Time sec.

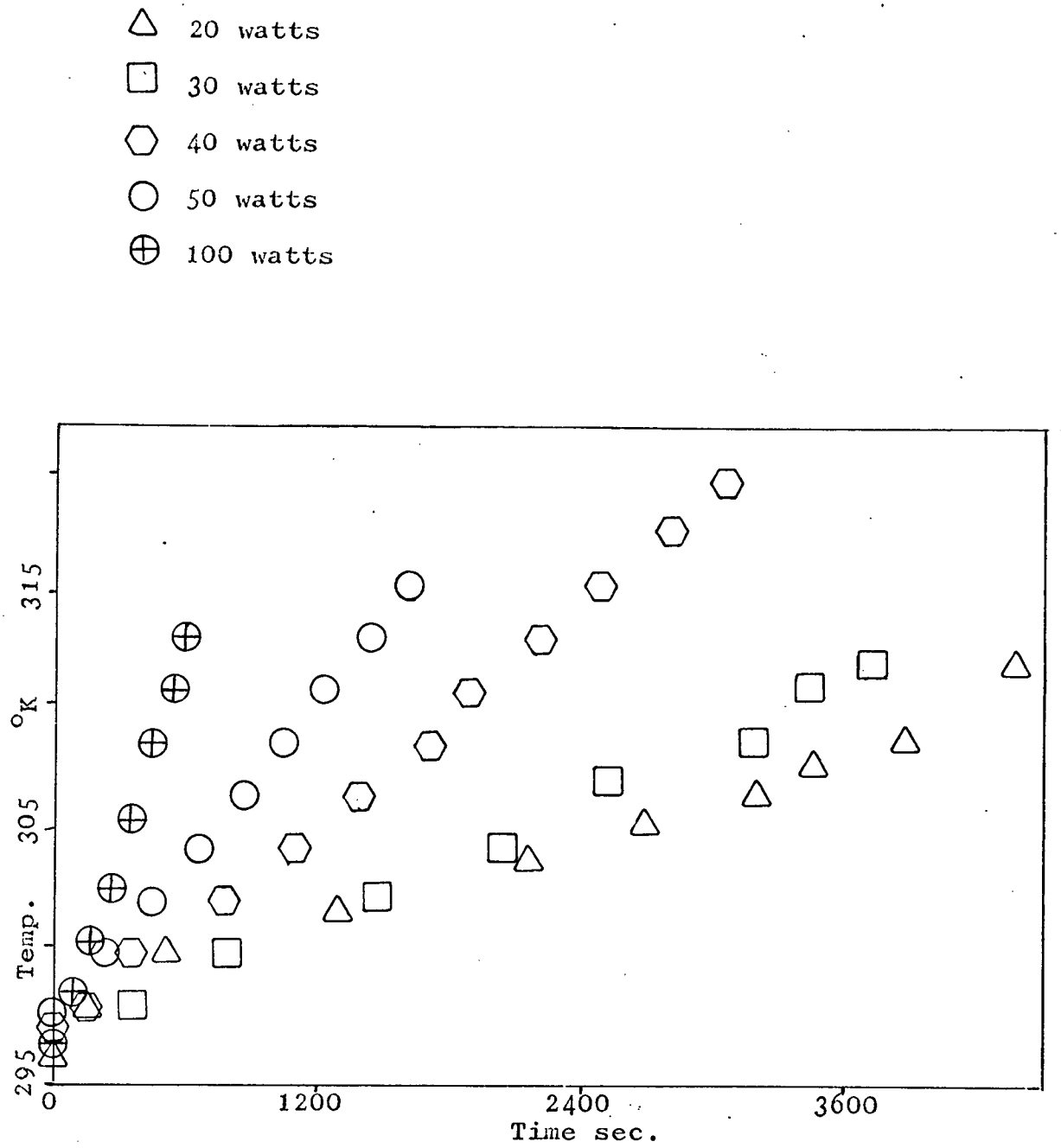

Figure 28

Hot Plate Temperature Profiles For Filler No. 2

This is due to the fact that the bottom is considered insulated and there is no more solid to change phase and thus absorb heat. In the experimental cell there is definately heat loss through the bottom, which could account for some of this deviation. Also the 2.54 cm deep cell was modified to test the 1.27 cm deep filler by inserting a 1.27 cm plexiglass plate. It was necessary to drill holes in this plate to accomodate the existing thermocouples. These holes filled with paraffin. With this extra n-octadecane around the cold plate or 1.27 cm thermocouples considerable more heat is absorbed, thus keeping the thermocouple temperature down. The hot plate temperature profiles for the third filler are shown in figure 32. It should be noted that the inflection in the hot plate temperature profiles are probably due to the presence of air bubbles.

Figures 33 through 37 demonstrate some of the theoretical studies that can be made with the mathematical model developed in this study. In figure 33 the temperature profiles from various filler wall thicknessess are plotted. It can be seen from these plots that as the filler thickness increases so does the heat-transfer rate. This is shown by the way in which the slope of the curve above the melt point increases as the wall thickness of the filler increases.

Figure 29

Experimental and theoretical temperature profiles at 20 and 30 watts for filler no. 3

Figure

29a 0.635 cm from the heating plate - 20 watts

29b 1.27 cm from the heating plate - 20 watts

Legend

△ F3-20-1

○ F3-20-2

—— Theoretical

Figure

29c 0.635 cm from the heating plate - 30 watts

29d 1.27 cm from the heating plate - 30 watts

Legend

△ F3-30-1

○ F3-30-2

—— Theoretical

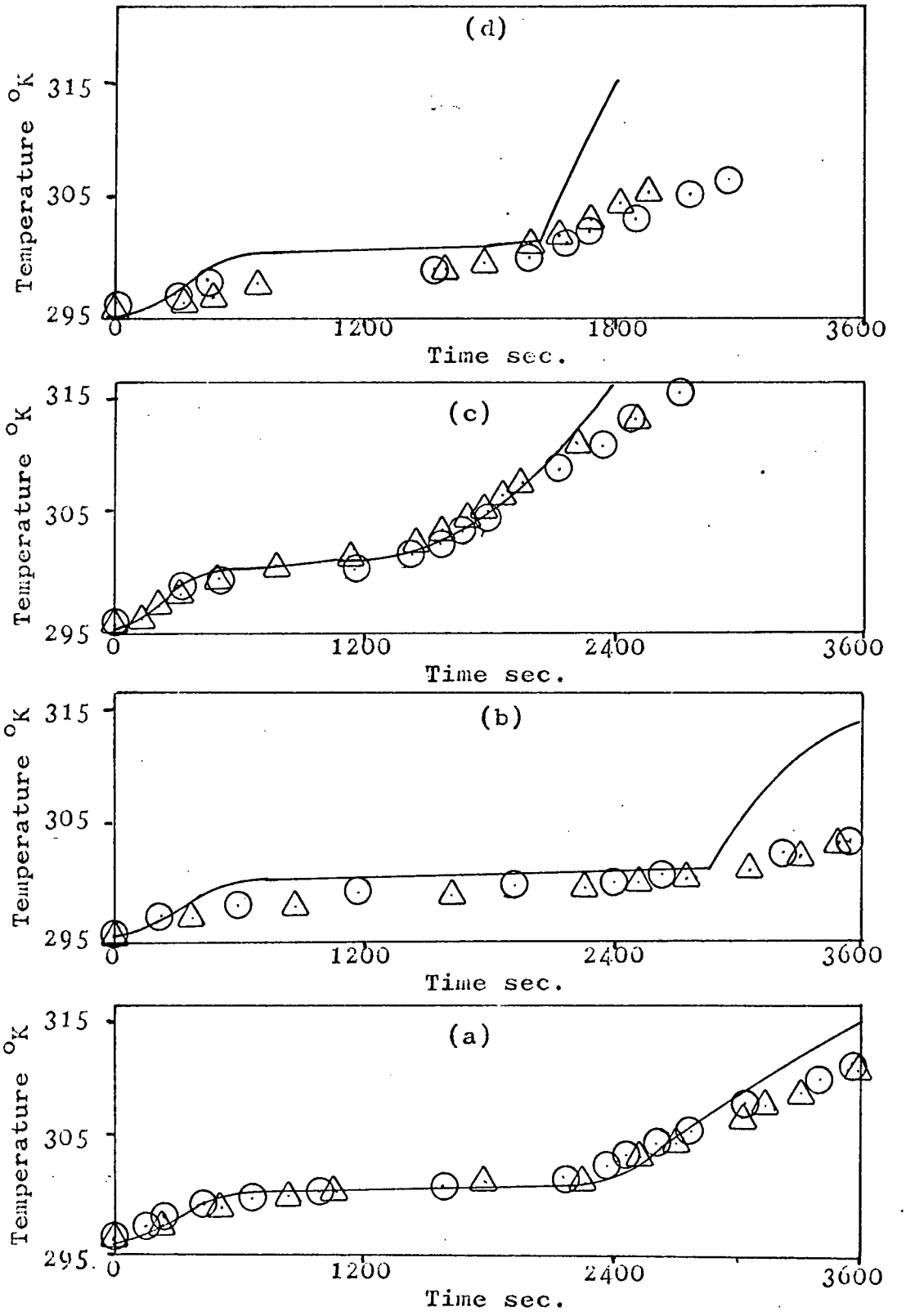
(d)
Temperature °K
315
305
295
0
1200
1800
3600
Time sec.
(c)
Temperature °K
315
305
295
0
1200
2400
3600
Time sec.
(b)
Temperature °K
315
305
295
0
1200
2400
3600
Time sec.
(a)
Temperature °K
315
305
295
0
1200
2400
3600
Time sec.

Figure 30

Experimental and theoretical temperature profiles at40 and 50 watts for filler no. 3

Figure

30a 0.635 cm from the heating plate - 40 watts

30b 1.27 cm from the heating plate - 40 watts

Legend

△ F3-40-1

○ F3-40-2

—— Theoretical

Figure

30c 0.635 cm fro the heating plate - 50 watts

30d 1.27 cm from the heating plate - 50 watts

Legend

△ F3-50-1

○ F3-50-1

—— Theoretical

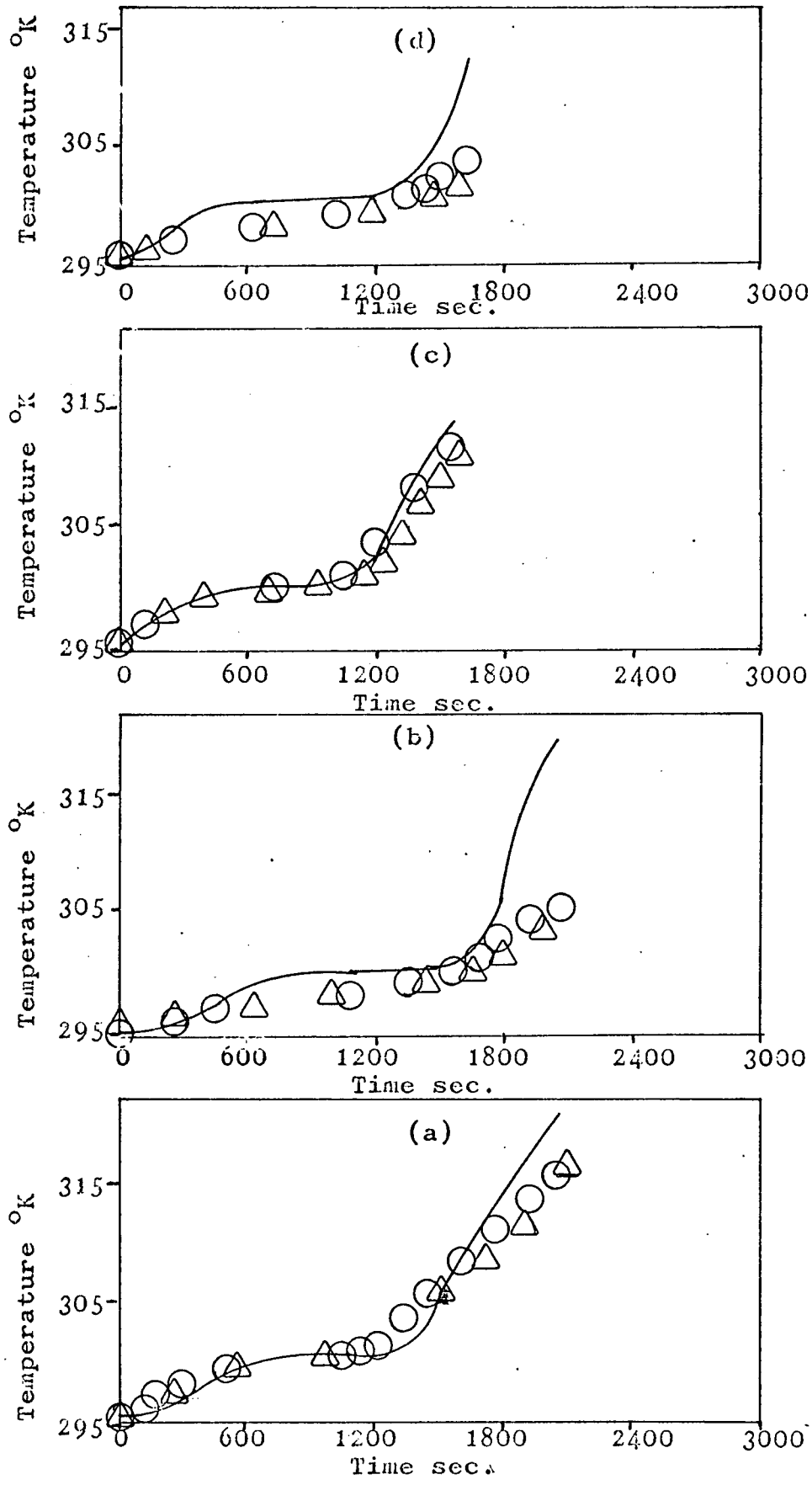
(d)
Temperature °K
315
305
295
0
600
1200
1800
2400
3000
Time sec.
(c)
Temperature °K
315
305
295
0
600
1200
1800
2400
3000
Time sec.
(b)
Temperature °K
315
305
295
0
600
1200
1800
2400
3000
Time sec.
(a)
Temperature °K
315
305
295
0
600
1200
1800
2400
3000
Time sec.

Figure 31

Experimental and theoretical temperature profiles at 100 watts for filler no. 3

Figure

30a 0.635 cm from the heating plate

30b 1.27 cm from the heating plate

Legend

△ F3-100-1

○ F3-100-2

—— Theoretical

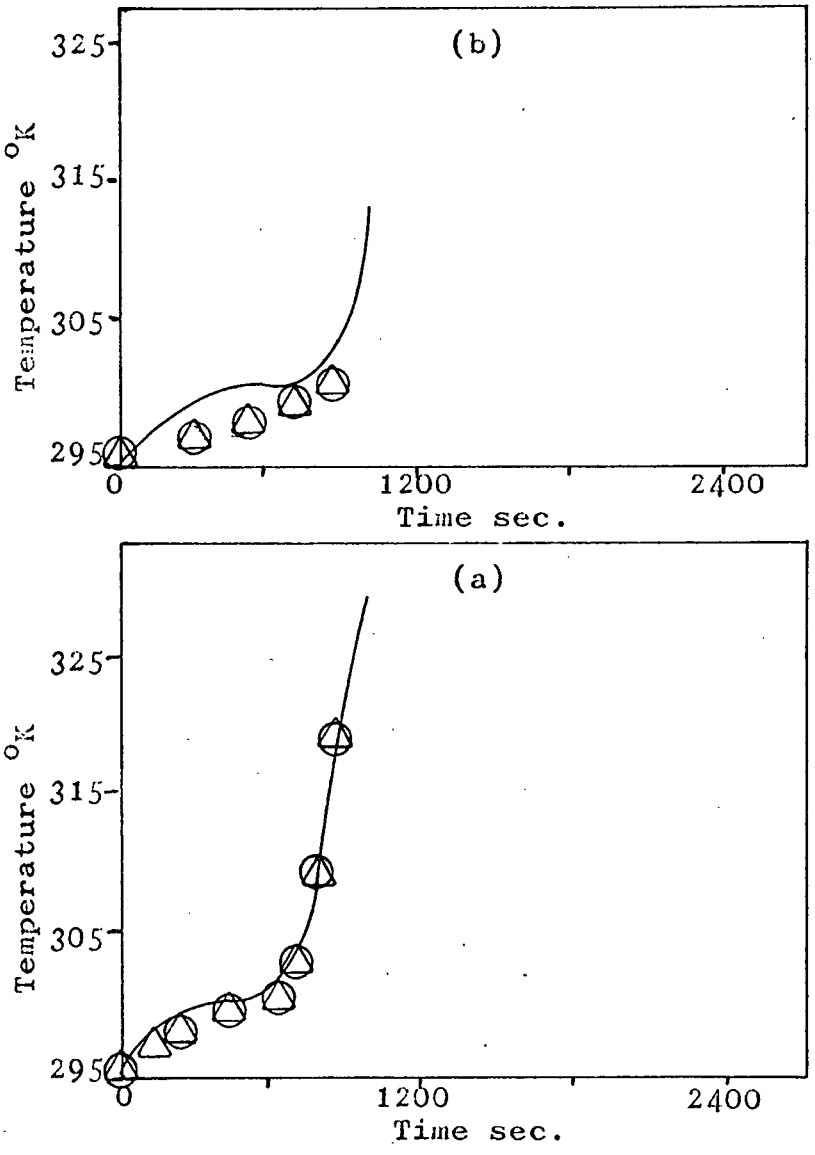
(b)
325
315
305
295
Temperature °K
0
1200
2400
Time sec.
(a)
325
315
305
295
Temperature °K
0
1200
2400
Time sec.

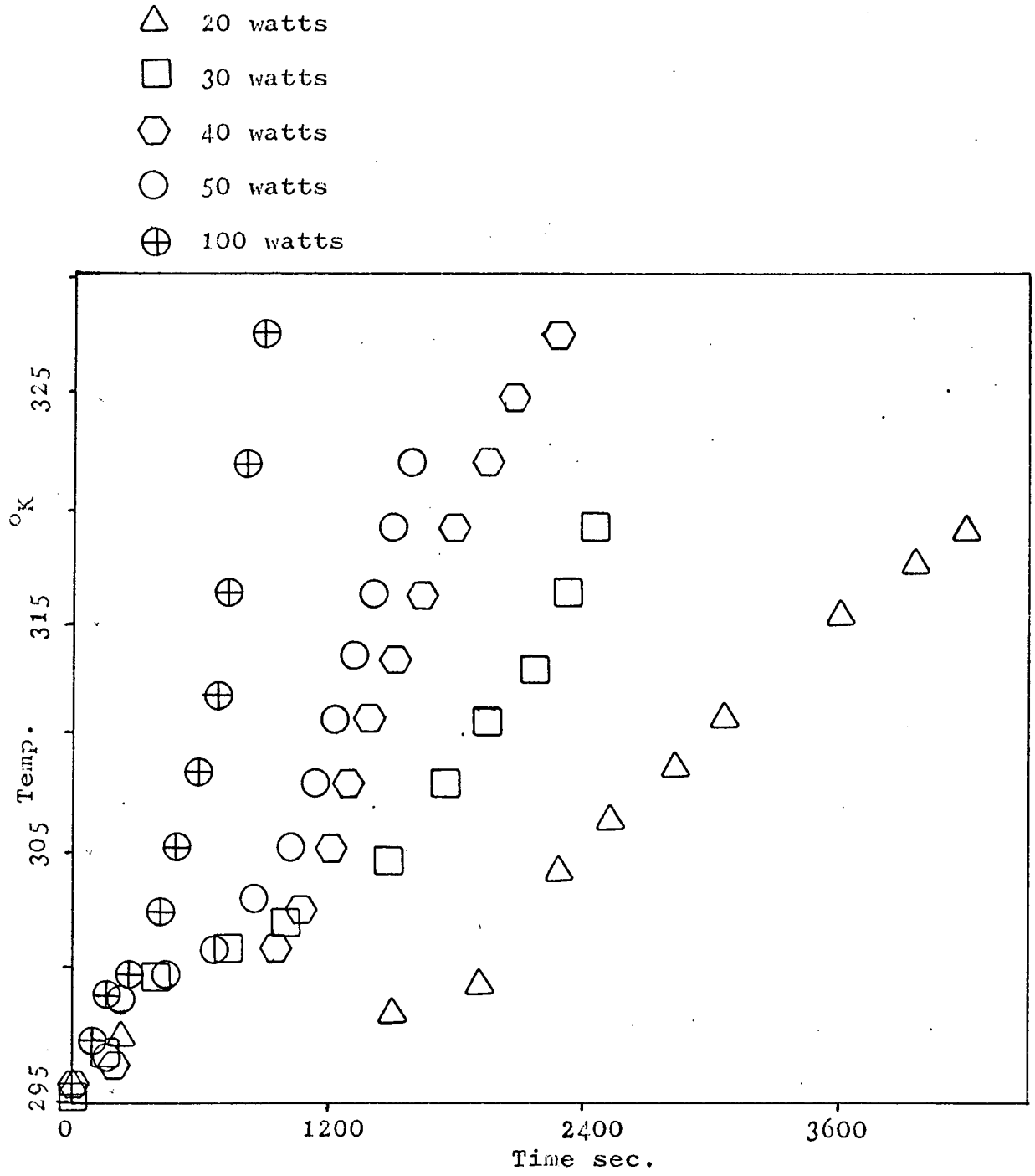

Figure 32

Hot Plate Temperature Profiles for Filler No. 3

Figures 34 through 37 are included to show the temperature profiles in the x-y plane. In figure 34, there is not much deviation in the x-y plane. This is intuitively correct since the graphs were made from data taken at a time early in the run. As time increased so does the temperature variation in the x-y plane. (Figures 35, 36 and 37) Note that the n-octadecane closer to the filler rises to a higher temperature than that farther away at any given time. This type of heating profile is exactly what is expected with a high thermally conductive metal matrix in a phase-change environment.

The experimental data in this section could be used for design providing that the design requirements fall within the experimental data and situation as presented in this study. The computer program written for this study can be used to predict the capabilities of other thermal-control devices by varying the physical properties of either the filler or phase-change material. If a different filler geometry is to be studied the subroutine which calculates the areas of the filler and phase-change material must be changed to accommodate the different geometry. If heat loss from the system is to be considered, the computer program can be modified as described in the theory section to provide for this. The computer program written for this study can also be

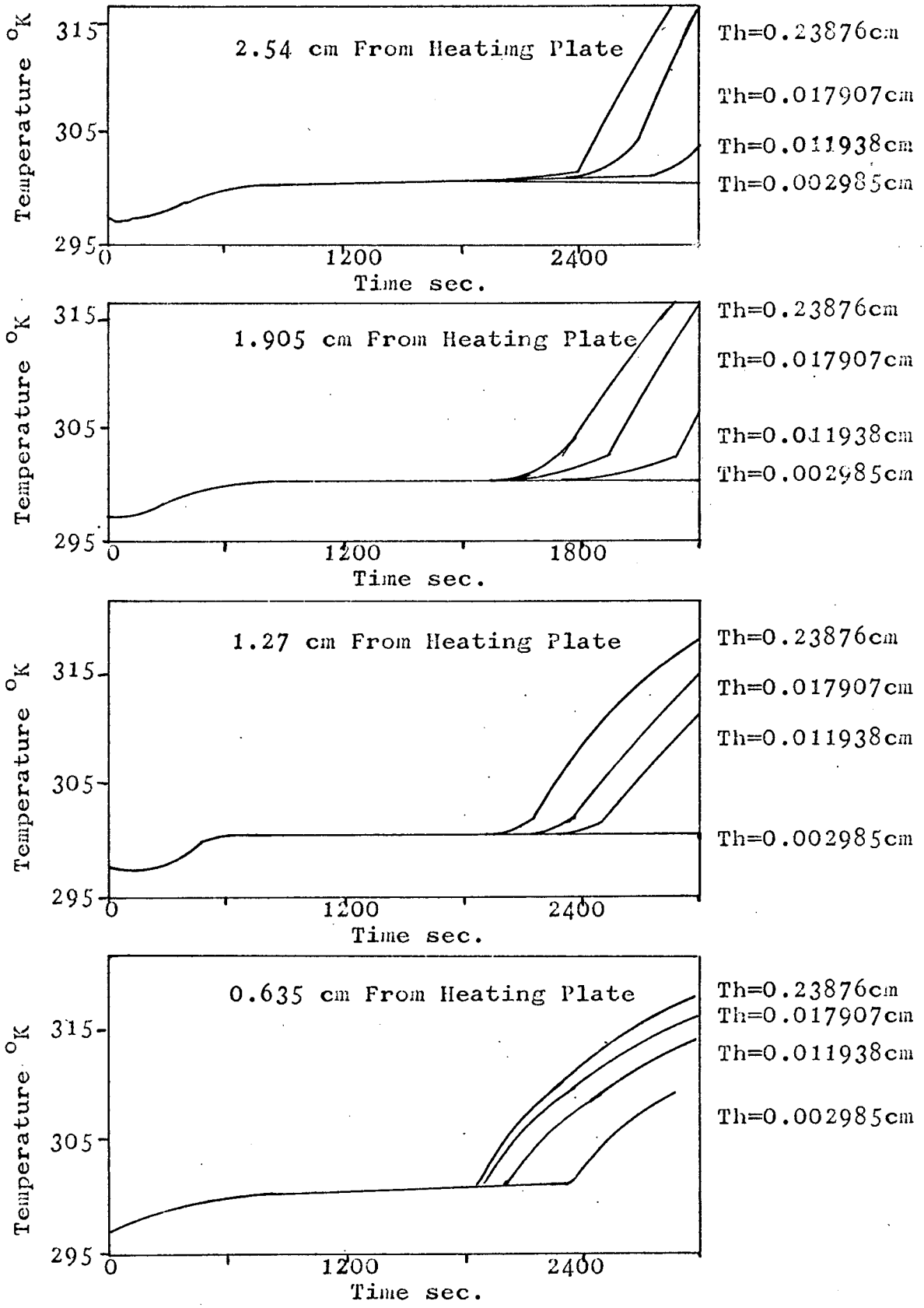

Figure 33
Theoretical Temperature Profiles for
Different filler Thicknessess

Figure 34

Theoretical temperature profiles in the x-y plane at t= 600 sec

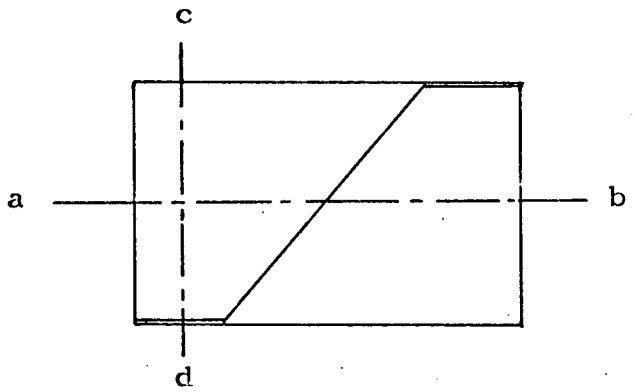

Figure	Temperature profile along line	z cm	Th cm
34-a	a-b	0.625	0.002985
34-b	a-b	0.625	0.011938
34-c	a-b	0.625	0.017907
34-d	a-b	0.625	0.23876
34-e	c-d	0.625	0.002985
34-f	c-d	0.625	0.011938
34-g	c-d	0.625	0.017907
34-h	c-d	0.625	0.23876
34-i	a-b	1.27	0.002985
34-j	a-b	1.27	0.011938
34-k	a-b	1.27	0.017907
34-l	a-b	1.27	0.23876
34-m	c-d	1.27	0.002985
34-n	c-d	1.27	0.011938
34-o	c-d	1.27	0.017907
34-p	c-d	1.27	0.23876
34-q	a-b	1.905	0.002985
34-r	a-b	1.905	0.011938
34-s	a-b	1.905	0.017907
34-t	a-b	1.905	0.23876
34-u	c-d	1.905	0.002985
34-v	c-d	1.905	0.011938
34-w	c-d	1.905	0.017907
34-x	c-d	1.905	0.23876

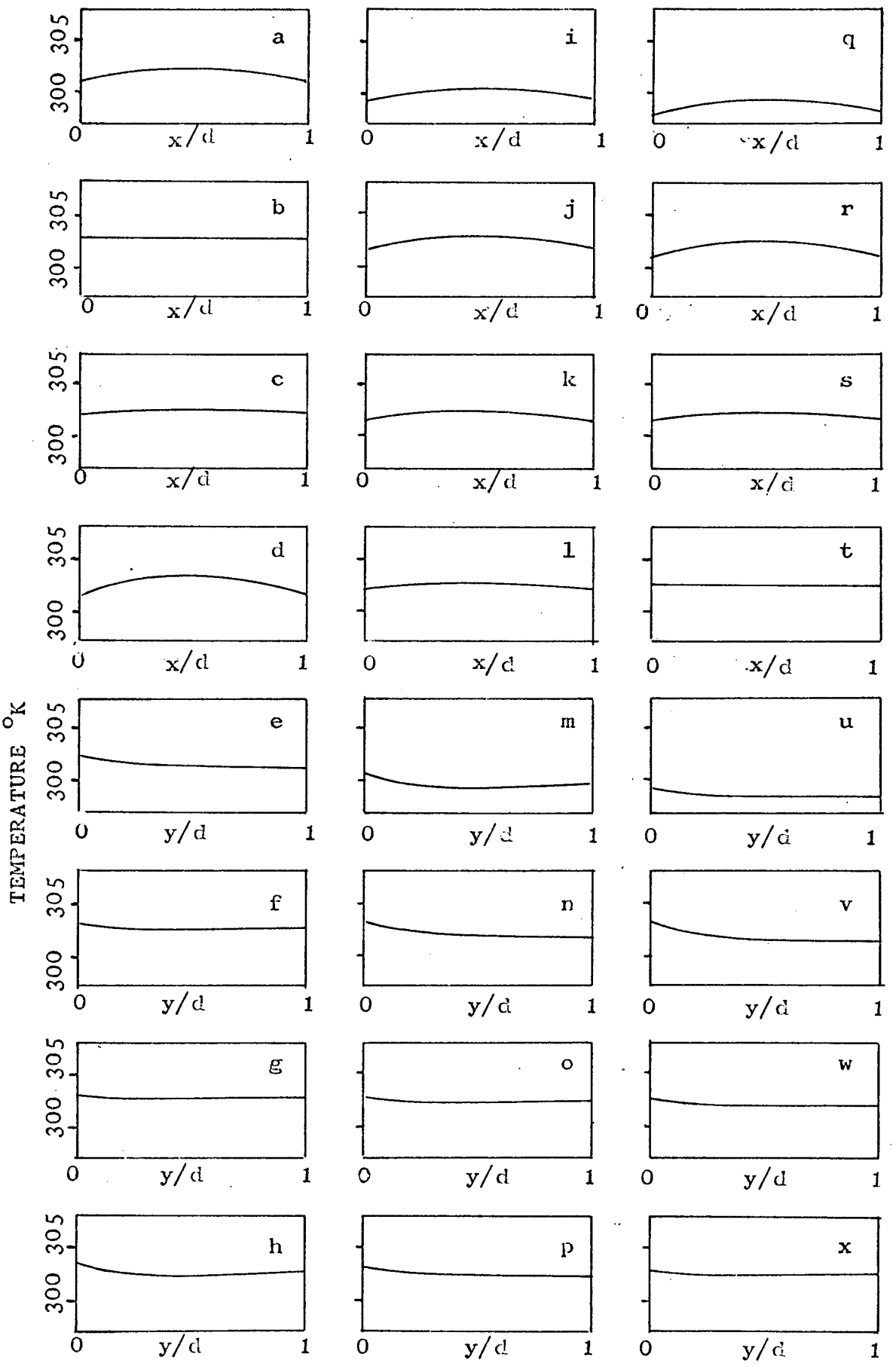
TEMPERATURE °K
300 305
a
b
c
d
e
f
g
h
i
j
k
l
m
n
o
p
q
r
s
t
u
v
w
x
0
x/d
y/d
1

Figure 35

Theoretical temperature profiles in the x-y plane at t= 1200 sec

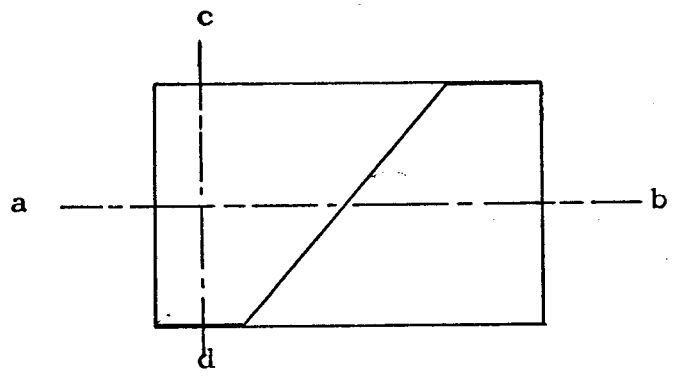

Figure	Temperature profile along line	z cm	Th cm
35-a	a-b	0.625	0.002985
35-b	a-b	0.625	0.011938
35-c	a-b	0.625	0.017907
35-d	a-b	0.625	0.23876
35-e	c-d	0.625	0.002985
35-f	c-d	0.625	0.011938
35-g	c-d	0.625	0.017907
35-h	c-d	0.625	0.23876
35-i	a-b	1.27	0.002985
35-j	a-b	1.27	0.011938
35-k	a-b	1.27	0.017907
35-l	a-b	1.27	0.23876
35-m	c-d	1.27	0.002985
35-n	c-d	1.27	0.011938
35-o	c-d	1.27	0.017907
35-p	c-d	1.27	0.23876
35-q	a-b	1.905	0.002985
35-r	a-b	1.905	0.011938
35-s	a-b	1.905	0.017907
35-t	a-b	1.905	0.23876
35-u	c-d	1.905	0.002985
35-v	c-d	1.905	0.011938
35-w	c-d	1.905	0.017907
35-x	c-d	1.905	0.23876

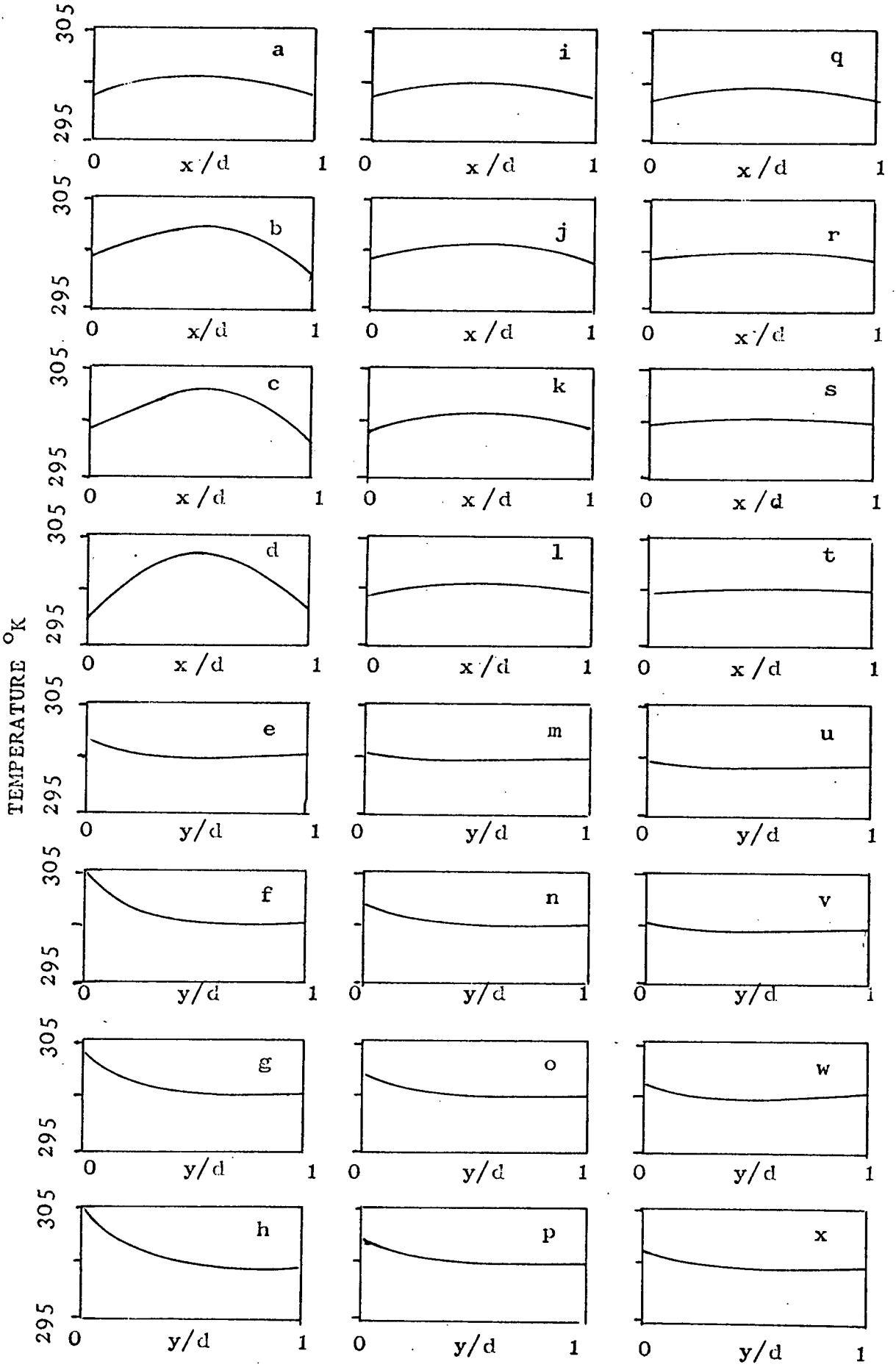
TEMPERATURE °K
305
295
a
b
c
d
e
f
g
h
i
j
k
l
m
n
o
p
q
r
s
t
u
v
w
x
0
x/d
y/d
1

Figure 36

Theoretical temperature profiles in the x-y plane at t= 1800 sec

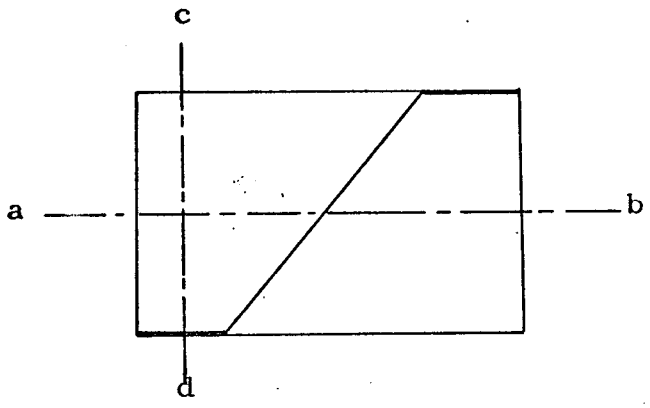

Figure	Temperature profile along line	z cm	Th cm
36-a	a-b	0.625	0.002985
36-b	a-b	0.625	0.011938
36-c	a-b	0.625	0.017907
36-d	a-b	0.625	0.23876
36-e	c-d	0.625	0.002985
36-f	c-d	0.625	0.011938
36-g	c-d	0.625	0.017907
36-h	c-d	0.625	0.23876
36-i	a-b	1.27	0.002985
36-j	a-b	1.27	0.011938
36-k	a-b	1.27	0.017907
36-l	a-b	1.27	0.23876
36-m	c-d	1.27	0.002985
36-n	c-d	1.27	0.011938
36-o	c-d	1.27	0.017907
36-p	c-d	1.27	0.23876
36-q	a-b	1.905	0.002985
36-r	a-b	1.905	0.011938
36-s	a-b	1.905	0.017907
36-t	a-b	1.905	0.23876
36-u	c-d	1.905	0.002985
36-v	c-d	1.905	0.011938
36-w	c-d	1.905	0.017907
36-x	c-d	1.905	0.23876

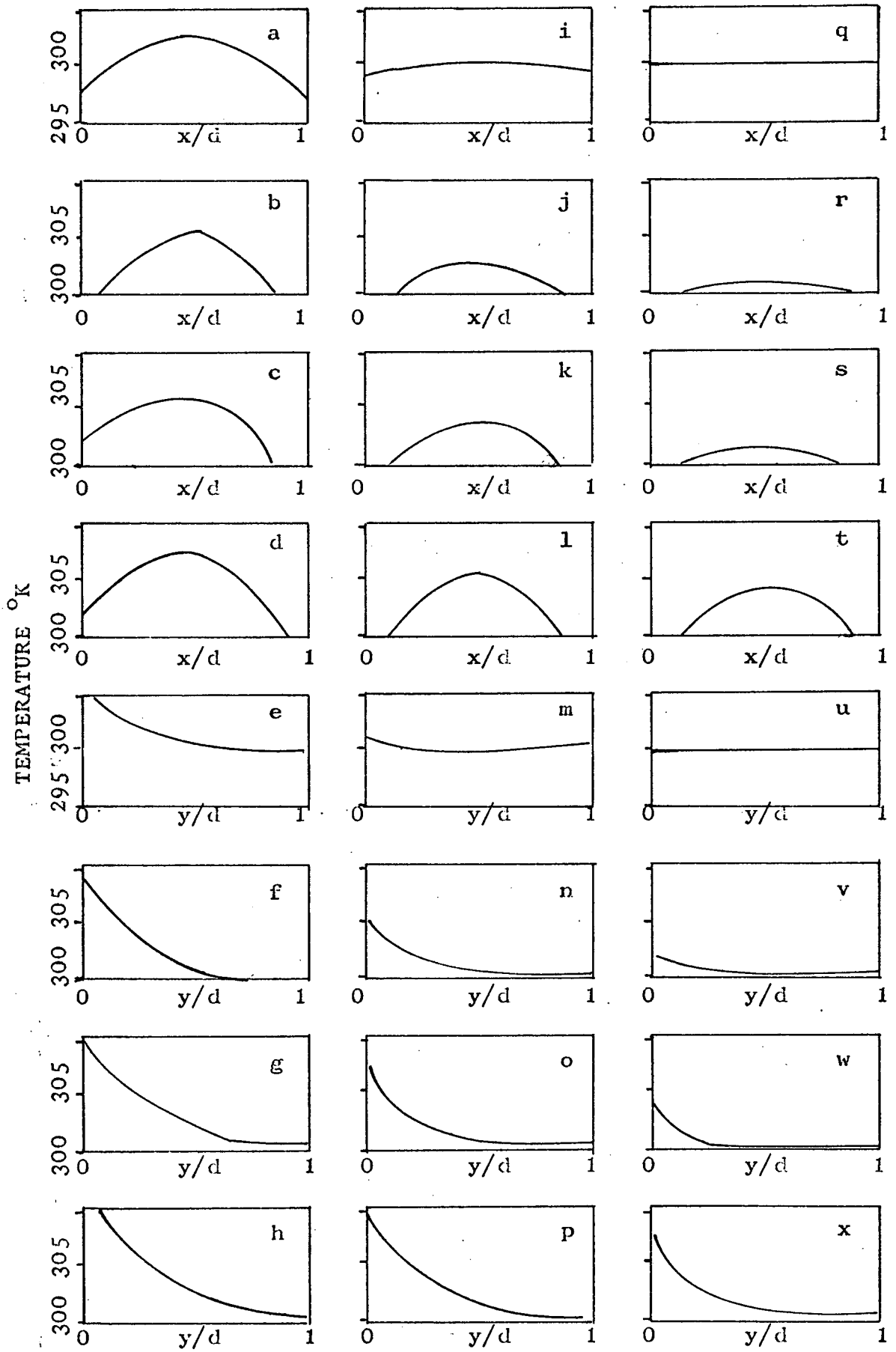
TEMPERATURE °K
a
b
c
d
e
f
g
h
i
j
k
l
m
n
o
p
q
r
s
t
u
v
w
x
295
300
305
0
x/d
y/d
1

Figure 37

Theoretical temperature profiles in the x-y plane at t= 2400 sec

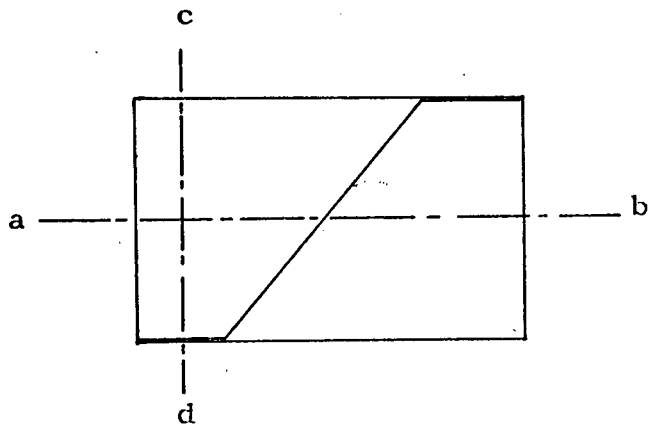

Figure	Temperature profile along line	z cm	Th cm
37-a	a-b	0.625	0.002985
37-b	a-b	0.625	0.011938
37-c	a-b	0.625	0.017907
37-d	a-b	0.625	0.23876
37-e	c-d	0.625	0.002985
37-f	c-d	0.625	0.011938
37-g	c-d	0.625	0.017907
37-h	c-d	0.625	0.23876
37-i	a-b	1.27	0.002985
37-j	a-b	1.27	0.011938
37-k	a-b	1.27	0.017907
37-l	a-b	1.27	0.23876
37-m	c-d	1.27	0.002985
37-n	c-d	1.27	0.011938
37-o	c-d	1.27	0.017907
37-p	c-d	1.27	0.23876
37-q	a-b	1.905	0.002985
37-r	a-b	1.905	0.011938
37-s	a-b	1.905	0.017907
37-t	a-b	1.905	0.23876
37-u	c-d	1.905	0.002985
37-v	c-d	1.905	0.011938
37-w	c-d	1.905	0.017907
37-x	c-d	1.905	0.23876

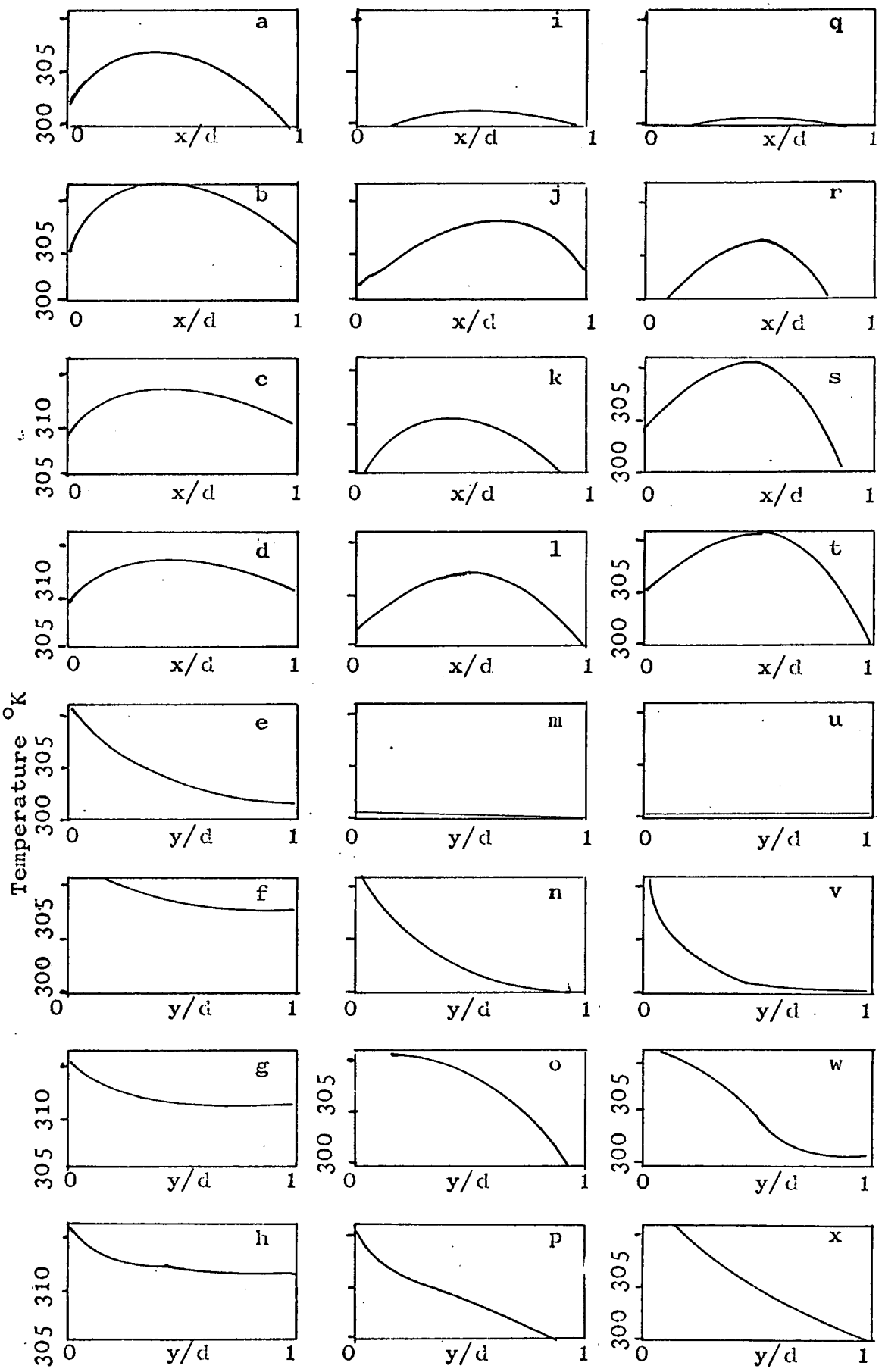
Temperature °K
a
b
c
d
e
f
g
h
i
j
k
l
m
n
o
p
q
r
s
t
u
v
w
x
x/d
y/d
0
1
300 305
305 310

used to predict the performance of thermal-control phase-change devices under different heat loads by modifing it to use a heat-flux boundary condition as described in the theory section.

RECOMMENDATIONS AND CONCLUSIONS

Conclusions

Based upon the results of this study, the following conclusions are presented.

1. As the weight of the filler material increases the heat-transfer rate of the thermal-control phase-change device increases.

2. The computer program written for this study predicts the experimental solid-phase-temperature profiles and the phase-change times correctly. While the maximum deviation between the theoretical and experimental solid-phase-temperature profiles is 2.8°K (5°F), there is essentially no deviation in most of the runs. There is as much as 14°K (25°F) deviation between the theoretical and experimental results in liquid phase. This deviation could possibly be corrected by changing the boundary condition along the bottom plate, in the computer program, to one in which heat loss is allowed.

3. The mathematical model presented in this study is general in terms of variable filler geometry, physical properties of the filler and phase-change material and the types of boundary conditions that can be placed on the theoretical model. The computer program written for this study is general in terms of variable physical properties

of the filler and phase-change material and sizes and shapes of the hexagonal filler. While the computer program is written for insulated boundaries along the bottom and four sides, it can be easily modified to allow for heat loss or gain along these boundaries. The computer program uses a temperature profile on the heating plate but this boundary, as discussed earlier, can also be changed to utilize a heat-flux boundary condition.

4. A three-dimensional analysis is needed to see the detailed temperature profiles in the x-y plane. As shown in the discussion of results section these theoretical temperature gradients can be as much as 11.1°K (20°F).

5. This study has shown that to correctly model the experimental system the heat losses must be known or predicted. If a heat-flux boundary condition is to be used in the theoretical model, the heat-flux into the test chamber must be accurately known.

Recommendations

The following recommendations are presented based on the results of this study.

1. The test chamber should be redesigned in such a way as to eliminate air bubbles.

2. Since the n-octadecane used in this study tended

to trap air in the solidification process, other phase-change materials should be considered. These other materials could include lithium nitrate trihydrate and acetamide.

3. Since the filler material adds weight to the phase-change thermal-control unit, and subtracts from its heat-absorbing capacity, other filler materials and geometries should be studied with the goal of optimizing the ratio of filler material to phase-change material.

LITERATURE CITED

1. Bentilla, E. W., Sterrett, K. F., and Karre, L. E., Thermal control by use of fusible materials: Final Report, Northrop Corporation, NSL65-16-1, Contract NAS8-11163, April 1966.

2. Hale, D. V., Hoover, M. J., and O'Neill, M. J., Phase change materials handbook: Lockheed Missiles and Space Company, Contract NASA CR-61363, Sept. 1971.

3. Carslaw, H. S. and Jaeger, J. C., Conduction of heat in solids: Oxford University Press, 1959.

4. Arpaci, V. S., Conduction heat transfer: Addison-Wesley Publishing Company, Reading, Massachusetts, 1966.

5. Pujado, P. R., Stermole, F. J., and Golden, J. O., Melting of a finite paraffin slab as applied to phase-change thermal control: Journal of Spacecraft and Rockets, V. 6, No. 3, March 1969, pp. 280-284.

6. Ukanawa, A. O., Stermole, F. J., and Golden, J.O., Phase change solidification dynamics: Journal of Spacecraft and Rockets, V. 8, Feb. 1971, pp. 193-196.

7. Shah, A. P., A microscopic and thermal study of the solidification of n-octadecane: Thesis No. T-1334, Colorado School of Mines, Golden, Colorado, 1970.

8. Dusinberre, G. M., Heat transfer calculation by finite differences: International Textbook Corporation, Scranton, Pennsylvania, 1961.

9. Bain, R. L., Stermole, F. J., and Golden, J. O., Gravity induced free convection effects in melting phenomena for thermal control: Journal of Spacecraft and Rockets, V. 8, No. 9, Sept. 1971, pp. 1000-1002.

B

10. Ukanawa, A. O., Thermal modeling of phase-change solidification in thermal control devices including natural convection effects: Thesis No. T-1422, Colorado School of Mines, Golden, Colorado, 1971.

11. Chi-Tien and Yin-Chao, Approximate solution of a melting problem with natural convection: Chemical Engineering Progress Symposium Series, V. 62, No. 64, pp. 77-85.

12. Goodman, T. R. and Shea, J. J., The melting of finite slabs: Journal Applied Mechanics, Transactions A.S.M.E., Feb. 1960, pp. 161-166.

13. Crank, J. and Nicholson, P., Proc. Cambridge Phil. Soc., 1947.

14. Douglas, Jim, Jr. and Rachford, H. H., Jr., Transactions Amer. Math. Soc., 1956.

15. Peaceman, D. W. and Rachford, H. H., Jr., Soc. Ind. Appl. Math., 1955.

16. Brian, P. L. T., A finite-difference method of high-order accuracy for the solution of three-dimensional transient heat conduction problems: A.I.C.H.E. Journal, Sept. 1961, pp. 367-370.

17. Grodzka, P. G., Space thermal control by freezing and melting: Lockheed Missiles and Space Company, Second Interim Report, Contract NAS8-21123, May 1969.

18. Shlosinger, A. P. and Bentilla, E. W., Interim Report: Contract NAS8-11163, Northrop Corporation, Feb. 1965.

19. Perry, J. H., Chemical engineers handbook: McGraw-Hill Book Company, New York, New York, 1950.

20. Pujado, P. R., Melting of a finite paraffin slab: Thesis No. T-1215, Colorado School of Mines, Golden, Colorado, 1968.

21. Bain, R. L., Stermole, F. J., and Golden, J. O., An experimental and theoretical investigation of the liquefaction dynamics of a phase-change material in a normal gravity environment: Annual Summary Report, Colorado School of Mines, Contract NAS8-30511, Mod. 2, January, 1972.

NOMENCLATURE

a,b,c	Coefficient of the unknown temperatures in the tridiagonal matrix
A	The cross sectional area perpendicular to the heat flux; cm^2
C_p	The heat capacity; watt-sec/gm/^oK
G	Amount of energy generated per unit volume; watt-sec/cc
h	The heat-transfer coefficient; watt/sec/cm^2
H_f	Enthalpy of liquefaction; watt-sec/gm
I	The last node in the x-direction in the nodal network
J	The last node in the y-direction in the nodal network
κ	The last node in the z-direction in the nodal network
K	Thermal conductivity; watt/cm/^oK
q	The heat flux; watt-sec/cm^2
T	Temperature; ^oK

T_e	The excess degrees; ^oK
Th	Wall thickness of the filler; cm
T_{mo}	The initial melting temperature; ^oK
T_m	The melting temperature; ^oK
t	Time; sec
Δt	Incremental time; sec
V'	The volume of the material that generates energy; cc
V	Volume; cc
ρ	Density; gm/cc
$(\rho C_p V)_{eff}$	The effective $(\rho C_p V)$ for a nonhomogeneous node; watt-sec/^oK
$(KA)_{eff}$	The effective (KA) for a nonhomogeneous node watt-cm/^oK

Subscripts

x	X-direction which is along an axis parallel to the 15.24 cm side of the test chamber
y	Y-direction which is along an axis parallel to the 7.62 cm side of the test chamber

z	Z-direction which is along an axis parallel to the 2.54 cm side of the test chamber
i	Indicates the x-direction in the finite difference formulation
j	Indicates the y-direction in the finite difference formulation
k	Indicates the z-direction in the finite difference formulation

APPENDIX I

Computer program to solve the nonhomogeneous phase-change problem.

This computer program was written in FORTRAN IV to solve the nonhomogeneous phase-change problem presented in this study. This program uses 14 cards of input data. The coefficients of the three straight-line fits for the hot plate temperature profiles are read on the first 3 cards. The physical properties of the filler and phase-change material are read on the next 9 cards. The filler geometry is specified by the last 2 cards. The following table specifies the exact variable to be read on each card.

VARIABLE	
Card 1	
A1	Coefficient of t in T = At + B; ^{o}F/min
B1	B in T = At + B; ^{o}F
TI1	The last time for which A1 and B1 hold; min
Card 2	
A2	Same as A1
B2	Same as B1
TI2	The last time for which A2 and B2 hold; min

VARIABLE	
Card 3	
A3	Same as A1
B3	Same as B1
Card 4	
DIF	The melting temperature range; ^{o}F
TM	The initial melting point; ^{o}F
TA	The initial temperature of the test cell; ^{o}F
Card 5	
CPM	The heat capacity of the melting paraffin; BTU/lb/^{o}F
HF	Enthalpy of liquefaction; BTU/lb
TS	The ending time of the run; min
Card 6	
ATI	The time for the first print out; min
XIC	The time increment between print outs; min
Card 7	
TH	The wall thickness of the filler; in
RF	Density of the filler; lb/cf
CPF	Heat capacity of the filler; BTU/lb/^{o}F
Card 8	
FK	Thermal conductivity of the filler; BTU/ft/hr/^{o}F
Card 9	
DX	Length of the node in the x-direction; in
DY	Length of the node in the y-direction; in
DZ	Length of the node in the z-direction; in

VARIABLE	
Card 10	
DT	Time increment; sec
PKS	Thermal conductivity of the solid phase-change material; BTU/ft/hr/^{o}F
PKL	Thermal conductivity of the liquid phase-change material; BTU/ft/hr/^{o}F
Card 11	
RPS	Density of the solid phase-change material; lb/cf
RPL	Density of the liquid phase-change material; lb/cf
CPS	Heat capacity of the solid phase-change material; BTU/lb/^{o}F
Card 12	
CPL	Heat capacity of the liquid phase-change material; BTU/lb/^{o}F
Card 13	
NX	The number of nodes in the x-direction plus 1
I1	The first node of the angular section of the filler
I2	The last node of the angular section of the filler
Card 14	
NY	The last node in the y-direction plus 1
N2	Set equal to 3
N4	The last node in the z-direction plus 2

```
      DIMENSION VP(7,7),VF(7,7)
      DIMENSION A(32),B(32),CC(32),D(32),T(32)
      DIMENSION APXI(7,7),AFXI(7,7)
      DIMENSION APYI(7,7),AFYI(7,7)
      DIMENSION T1(7,7,32),T2(7,7,32),T3(7,7,32)
      DIMENSION TE(7,7,32),KJ(7,7,32)
      DIMENSION APZ(7,7),AFZ(7,7)
      COMMON /S1/ N4,I,J,K
      COMMON /S2/ VP,VF
      COMMON /S3/ APXI,AFXI,NX
      COMMON /S4/ APYI,AFYI,NY
      COMMON /S5/ APZ,AFZ,NZ
      COMMON /S6/ A,B,CC,D
      COMMON /S7/ TM,HF,CPM,DIF,VT
      COMMON /S8/ A1,A2,A3,B1,B2,B3,TI1,TI2,TI
      COMMON /S9/ PKS,PKL
      COMMON /S10/ RPL,RPS,CPS,CPL
C.....N2 NODE THAT STARTS THE TEST MATERIAL
C.....N4= THE NO. OF NODES IN THE TEST MATERIAL
C.....VF=VOL OF FILLER * ROE(F)*CP(F)/DT
C.....VP=VOL OF PARA. * ROE(P)*CP(P)/DT
C.....NX= NO. OF NODES IN X DIR.
C.....NY= NO. OF NODES IN Y DIR.
C.....NZ= NO. OF NODES IN Z DIR.
C.....TM = MELT TEMP. OF PARA.
C.....HF= HEAT OF FUSSION OF THE PARA.
C.....CPM=HEAT CAPACITY OF THE PARA. AT THE MELT TEMP.
C.....CPP=HEAT CAPACITY OF PARA.
C.....CPF=HEAT CAPACITY OF FILLER
C.....RF=DENSITY OF FILLER
C.....PP=DENSITY OF PARA.
C.....PK=THERMAL COND. OF PARA.
C.....FK=THERMAL COND. OF FILLER
      READ(2,600) A1,B1,TI1,A2,B2,TI2,A3,B3
      READ(2,600) DIF,TM,TA,CPM,HF,TS,ATI,XIC
      READ(2,600) TH,RF,CPF,FK
      READ(2,600) DX,DY,DZ,DT,PKS,PKL
      READ(2,600) RPS,RPL,CPS,CPL
      READ(2,601) MX,I1,I2,MY,N2,N4
609   FORMAT(6I)
600   FORMAT(3F)
601   FORMAT(3I)
      WRITE(1,602) A1,B1,TI1,A2,B2,TI2,A3,B3
      WRITE(1,603) DIF,TM,TA,CPM,HF,TS,ATI,XIC
      WRITE(1,604) TH,RF,CPF,FK
      WRITE(1,605) DX,DY,DZ,DT,PKS,PKL
      WRITE(1,607) RPS,RPL,CPS,CPL
      WRITE(1,606) MX,I1,I2,MY,N2,N4
602   FORMAT(4X,'A1=',F8.4,' DEGF/MIN',7X,'B1=',F8.4,' DEGF',
     15X,'TI1=',F8.4,' MIN'/,4X,'A2=',F8.4,' DEGF/MIN'
     27X,'B2=',F8.4,' DEGF',5X,'TI2=',F8.4,' MIN'/,
     34X,'A3=',F8.4,' DEGF/MIN',7X,'B3=',F8.4,' DEGF')
603   FORMAT(3X,'DIF=',F8.4,' DEGF',11X,'TM=',F8.4,' DEGF',6X,'TA=',
     1F8.4,' DEGF',/3X,'CPM=',F8.4,' BTU/LB',9X,'HF=',F8.4,' BTU/LB',
     24X,'TS=',F8.4,' MIN',/,3X,'ATI=',F8.4,' MIN',11X,'XIC=',
     3F8.4,' MIN')
604   FORMAT(4X,'TH=',F8.4,' INCHES',9X,'RF=',F8.4,' LB/CF',4X,'CPF=',
     1F8.4,' BTU/LB/DEGF',/,4X,'FK=',F8.4,'BTU/FT/HR/DEGF')
605   FORMAT(4X,'DX=',F8.4,' INCHES',9X,'DY=',F8.4,' INCHES'
     1,4X,'DZ=',F8.4,' INCHES',/,4X,'DT=',F8.4,' SEC.',4X,'PKS=',F8.4,
```

```
     1'BTU/FT/HR/DEGF',3X,'PKL=',F8.4,' BTU/FT/HR/DEGF')
606      FORMAT(4X,'NX=',I3,21X,'I1=',I3,16X,'I2=',I3,/4X,'NY=',I3,
     121X,'N2=',I3,16X,'N4=',I3)
607      FORMAT(4X,'RPS=',F8.4,'LB/CF',3X,'RPL='F8.4,'LB/CF'
     13X,'CPS=',F8.4,' BTU/LB',/,4X,'CPL=',F8.4,' BTU/LB')
599      N3=N2+1
         NZZ=N4+1
         TI=0.
         NZ=N4
         DT=DT/60./60.
         NX=MX+1
         NY=MY+1
         DX=DX/12.
         DY=DY/12.
         DZ=DZ/12.
         VT=DX*DY*DZ
         TH=TH/12.
         CALL AREA(I1,I2,TH,DX,DY,DZ,DT,RF,CPF,FK)
         DO 5 K=2,NZ
         DO 5 J=2,NY
         DO 5 I=2,NX
         T1(I,J,K)=TA
         T2(I,J,K)=TA
         T3(I,J,K)=TA
         KJ(I,J,K)=1
5        CONTINUE
6        CALL TBN(TB1)
         TI=TI+2.*DT*60.
         CALL TBN(TB2)
         TB=(TB1+TB2)/2.
         DO 7 J=2,NY
         DO 7 I=2,NX
         T1(I,J,2)=TB
         T2(I,J,2)=TB
         T3(I,J,2)=TB
7        CONTINUE
C.......,SOLVING FOR T2
         DO 15 K=3,NZ
         KK=K+1
         DO 15 J=2,NY
         JJ=J+1
         DO 10 I=2,NX
         CALL KC(C,KJ(I,J,K))
         II=I+1
         CALL K1(C11,I,KJ(I,J,K))
         CALL K1(C12,II,KJ(I,J,K))
         CALL K2(C21,J,KJ(I,J,K))
         CALL K2(C22,JJ,KJ(I,J,K))
         CALL K3(C31,K,KJ(I,J,K))
         CALL K3(C32,KK,KJ(I,J,K))
621      FORMAT(' CS',3I2,4E)
610      FORMAT(' COE'3I2,5E)
         A(I)=-C11/C/DX
         B(I)=1.+(C11+C12)/C/DX
         CC(I)=-C12/C/DX
         D(I)=T1(I,J,K)
         Z1=(C21*T1(I,J-1,K)-(C21+C22)*T1(I,J,K)+C22*T1(I,J+1,K))/C/DY
         D(I)=D(I)+Z1
         Z2=(C31*T1(I,J,K-1)-(C31+C32)*T1(I,J,K)+C32*T1(I,J,K+1))/C/DZ
612      FORMAT(3X,4E)
```

```
      D(I)=D(I)+Z2
611   FORMAT(3E)
10    CONTINUE
      CALL SOLVE (T,2,NX)
      DO 12 KI=2,NX
12    T2(KI,J,K)=T(KI)
15    CONTINUE
C.....SOLVING FOR T3
      DO 25 I=2,NX
      II=I+1
      DO 25 K=3,NZ
      KK=K+1
      DO 20 J=2,NY
      CALL KC(C,KJ(I,J,K))
      JJ=J+1
      CALL K2(C21,J,KJ(I,J,K))
      CALL K2(C22,JJ,KJ(I,J,K))
      A(J)=-C21/C/DY
      B(J)=1.+(C21+C22)/C/DY
      CC(J)=-C22/C/DY
      Z=(C21+C22)*T1(I,J,K)-C21*T1(I,J-1,K)-C22*T1(I,J+1,K)
      Z=Z/C/DY
      D(J)=T2(I,J,K)+Z
20    CONTINUE
      CALL SOLVE (T,2,NY)
      DO 22 KI=2,NY
      T3(I,KI,K)=T(KI)
22    CONTINUE
25    CONTINUE
      DO 28 K=2,NZ
      DO 28 J=2,NY
      DO 28 I=2,NX
      T2(I,J,K)=T1(I,J,K)
28    CONTINUE
C.....SOLVING FOR T1
      DO 35 J=2,NY
      JJ=J+1
      DO 35 I=2,NX
      II=I+1
      DO 30 K=3,NZ
      CALL KC(C,KJ(I,J,K))
      KK=K+1
      CALL K3(C31,K,KJ(I,J,K))
      CALL K3(C32,KK,KJ(I,J,K))
      C33=C31
      EC=0.
      IF(K.GT.3) GO TO 29
      EC=T2(I,J,K-1)*C31/C/DZ
      C33=0.
29    A(K)=-C33/C/DZ
      B(K)=1.+(C31+C32)/C/DZ
      CC(K)=-C32/C/DZ
      D(K)=2.*T3(I,J,K)-T2(I,J,K)
      Z=(C31+C32)*T2(I,J,K)-C31*T2(I,J,K-1)-C32*T2(I,J,K+1)
      Z=Z/C/DZ
      D(K)=D(K)+Z+EC
30    CONTINUE
      CALL SOLVE (T,3,NZ)
      DO 32 KI=3,NZ
      T1(I,J,KI)=T(KI)
```

```
32      CONTINUE
35      CONTINUE
        DO 37 K=N2,NZ
        DO 37 J=2,NY
        DO 37 I=2,NX
        CALL PHASE(T1(I,J,K),KJ(I,J,K),TE(I,J,K),VP(I,J),T2(I,J,K),DT)
37      CONTINUE
38      IF(TI.LT.ATI) GO TO 6
        WRITE(1,42) TI,TB
        DO 40 K=2,NZZ,4
        L1=K-1
        L2=K+1
        WRITE(1,41) L1,(T1(I,2,L1),I=2,NX)
        WRITE(1,41) L1,(T1(I,3,L1),I=2,NX)
        WRITE(1,41) K,(T1(I,2,K),I=2,NX)
        WRITE(1,41) K,(T1(I,3,K),I=2,NX)
        WRITE(1,41) L2,(T1(I,2,L2),I=2,NX)
        WRITE(1,41) L2,(T1(I,3,L2),I=2,NX)
        WRITE(1,444)
40      CONTINUE
444     FORMAT(//)
45      FORMAT(4(3X,3I2,F6.1))
41      FORMAT(3X,I3,4(3X,F6.1))
42      FORMAT(//3X,'TIME=',F8.3,' MIN.',3X,'TB=',F6.1,/)
43      FORMAT(11X,12(2I2,5X))
        ATI=ATI+XIC
        IF(TI.GT.TS) GO TO 999
        GO TO 6
999     STOP
        END
        SUBROUTINE AREA(I1,I2,TH,DX,DY,DZ,DT,RF,CPF,FK)
        DIMENSION VP(7,7),VF(7,7)
        DIMENSION APXI(7,7),AFXI(7,7)
        DIMENSION APYI(7,7),AFYI(7,7)
        DIMENSION APZ(7,7),AFZ(7,7)
        COMMON /S2/ VP,VF
        COMMON /S3/ APXI,AFXI,NX
        COMMON /S4/ APYI,AFYI,NY
        COMMON /S5/ APZ,AFZ,NZ
C.....DX>DY/(TAN(AA=90,DEG.)
C.....WHERE]
C.....AA= THE ANGLE THE FILLER MAKES WITH THE HORIZONTAL
C.....II=NO. OF NODES IN THE X DIR.
C.....JJ=NO. OF NODES IN THE Y DIR.
C.....I1= NO. OF NODES TO THE ANGLE PART OF THE FILLER
C.....I2= NO. OF NODES IN THE ANGLE PART OF THE FILLER
C.....I1 & I2 MUST BE INTERGERS
C.....TH=FILLER THICKNESS
C.....DX=DELTA X
C.....DY=DELTA Y
C.....DZ=DELTA Z
C.....THIS SUBROUTINE WILL PRODUCE THE FOLLOWING ARAYS]
C.....APXI=AREA OF PARA. IN NODE I,J IN THE X DIR.
C.....AFXI=AREA OF FILLER IN NODE I,J IN THE X DIR.
C.....APYI=AREA OF PARA. IN NODE I,J IN THE Y DIR.
C.....AFYI=AREA OF FILLER IN NODE I,J IN THE Y DIR.
C.....APZ=AREA OF PARA IN THE Z DIR. IN NODE I,J
C.....AFZ= AREA OF FILLER IN THE Z DIR. IN NODE I,J
C.....VP=VOL. OF PARA IN NODE I,J
C.....VF=VOL. OF FILLER IN NODE I,J
```

```
      IU=NX-1
      JU=NY-1
      IL=1
      JL=1
      TA=FLOAT(I2-I1)/FLOAT(JU-JL+1)
      AA=ATAN(TA)
      R=FLOAT(I2-I1)*DX+FLOAT(I1)*DX
      DO 50 J=JL,JU
      YL=FLOAT(JU-J+1)*DY
      YU=FLOAT(JU-J)*DY
      XL=R-TA*YL
      XU=R-TA*YU
      DO 50 I=IL,IU
      IF(I.LE.I1) GO TO 10
      IF(I.LE.I2) GO TO 20
      IF(I.LE.IU) GO TO 33
10    IF(J.GT.JL) GO TO 14
11    APXI(I,J)=DZ*(DY-TH/2.)
      APYI(I,J)=0.
      AFZ(I,J)=DX*TH/2.
      AFXI(I,J)=DZ*TH/2.
      AFYI(I,J)=0.
      IF(I.EQ.IL) GO TO 12
      IF(J.EQ.JU) GO TO 34
      GO TO 52
12    APXI(I,J)=0.
      AFXI(I,J)=0.
      GO TO 52
14    APXI(I,J)=DY*DZ
      APYI(I,J)=DX*DZ
      AFXI(I,J)=0.
      AFYI(I,J)=0.
      AFZ(I,J)=0.
      IF(XBL.EQ.XL) GO TO 18
      IF(XBL-DX.EQ.XU) GO TO 19
16    IF(I.EQ.IL) APXI(I,J)=0.
      IF(J.EQ.JL) APYI(I,J)=0.
      GO TO 52
18    APYI(I,J)=DZ*(DX-TH/4.)
      AFYI(I,J)=DX*TH/4.
      GO TO 16
19    APXI(I,J)=DZ*(DY-TH/4.)
      AFXI(I,J)=DZ*TH/4.
      GO TO 16
20    XBL=FLOAT(I)*DX
      IF(XBL.LE.XL) GO TO 14
      IF(XBL-DX.GE.XU) GO TO 14
      X1=XBL-XL
      IF(X1.GT.DX) GO TO 28
      IF(XU.LT.XBL) X1=XU-XL
      H1=X1/SIN(AA)
      Y1=X1/TA
      APXI(I,J)=DZ*DY
      APYI(I,J)=DZ*(DX-TH)
      AFZ(I,J)=H1*TH
      AFXI(I,J)=0.
      AFYI(I,J)=DZ*TH
21    IF(XBL-DX.EQ.XL) GO TO 31
22    IF(I-1.EQ.I1.AND.J.EQ.JL) GO TO 26
23    IF(J.EQ.JL) GO TO 25
```

```
            GO TO 52
 25         APYI(I,J)=0.
            AFYI(I,J)=0.
            GO TO 52
 26         APXI(I,J)=DZ*(DY-TH/2.)
            AFXI(I,J)=DZ*TH/2.
            GO TO 23
 28         Y2=DY-Y1
            H1=Y2/COS(AA)
            APXI(I,J)=DZ*(DY-TH)
            APYI(I,J)=DX*DZ
            AFZ(I,J)=TH*H1
            AFXI(I,J)=DZ*TH
            AFYI(I,J)=0.
            GO TO 21
 31         APXI(I,J)=DZ*(DY-TH/4.)
            AFXI(I,J)=DZ*TH/4.
            APYI(I,J)=DZ*(DX-TH/4.)
            AFYI(I,J)=AFXI(I,J)
            GO TO 22
 33         IF(J.EQ.JU) GO TO 11
            GO TO 14
 34         APYI(I,J)=DZ*DX
            GO TO 52
 52         APZ(I,J)=DX*DY-AFZ(I,J)
            VP(I,J)=APZ(I,J)*DZ
            VF(I,J)=AFZ(I,J)*DZ
            APXI(IU+1,J)=0.
            APYI(I,JU+1)=0.
            AFXI(IU+1,J)=0.
            AFYI(I,JU+1)=0.
            XBL=0.
            X1=0.
            VF(I,J)=VF(I,J)*RF*CPF/DT
            VP(I,J)=VP(I,J)/DT
            AFXI(I,J)=AFXI(I,J)*FK
            AFYI(I,J)=AFYI(I,J)*FK
            AFZ(I,J)=AFZ(I,J)*FK
 50         CONTINUE
100         FORMAT(1X,2I2,4E)
101         FORMAT(1X,4E)
            APXI(IU+1,JU+1)=0.
            APYI(IU+1,JU+1)=0.
            AFXI(IU+1,JU+1)=0.
            AFYI(IU+1,JU+1)=0.
            DO 200 I=IU,IL,-1
            DO 200 J=JU,JL,-1
            APXI(I+1,J+1)=APXI(I,J)
            APYI(I+1,J+1)=APYI(I,J)
            AFXI(I+1,J+1)=AFXI(I,J)
            AFYI(I+1,J+1)=AFYI(I,J)
            APZ(I+1,J+1)=APZ(I,J)
            AFZ(I+1,J+1)=AFZ(I,J)
            VP(I+1,J+1)=VP(I,J)
            VF(I+1,J+1)=VF(I,J)
200         CONTINUE
            DO 210 I=1,IU
            APXI(I,JL)=0.
            AFXI(I,JL)=0.
            APYI(I,JL)=0.
```

```
      AFYI(I,JL)=0.
      APZ(I,JL)=0.
      AFZ(I,JL)=0.
      VP(I,JL)=0.
      VF(I,JL)=0.
210   CONTINUE
      DO 215 J=1,JU
      APXI(IL,J)=0.
      AFXI(IL,J)=0.
      APYI(IL,J)=0.
      AFYI(IL,J)=0.
      APZ(IL,J)=0.
      AFZ(IL,J)=0.
      VP(IL,J)=0.
      VF(IL,J)=0.
215   CONTINUE
501   FORMAT(2X,2I2,2F)
      RETURN
      END
      SUBROUTINE KC(C,KZ)
      DIMENSION VP(7,7),VF(7,7)
      COMMON /S1/ N4,I,J,K
      COMMON /S2/ VP,VF
      CALL HC(KZ,RP,CPP)
      V1=RP*CPP*VP(I,J)
      V2=VF(I,J)
      C=V1+V2
      IF(K.EQ.N4) C=C/2.
100   FORMAT(' SC',3E)
101   FORMAT(' SC',3I2,4E)
      RETURN
      END
      SUBROUTINE K1(C1,II,L)
      DIMENSION APXI(7,7),AFXI(7,7)
      COMMON /S1/ N4,I,J,K
      COMMON /S3/ APXI,AFXI,NX
      IF(II.EQ.NX+1) GO TO 60
      IF(II.EQ.2) GO TO 60
      CALL TH(L,PK)
      A1=APXI(II,J)*PK
      A2=AFXI(II,J)
      IF(K.EQ.N4) GO TO 40
C.....PARAFFIN AND FILLER NODES
      GO TO 65
40    A1=A1/2.
      A2=A2/2.
      GO TO 65
60    A1=0.
      A2=0.
65    C1=A1+A2
100   FORMAT(' SC1',3I2,2E)
101   FORMAT(4E)
      RETURN
      END
      SUBROUTINE K2(C2,JJ,L)
      DIMENSION APYI(7,7),AFYI(7,7)
      COMMON /S1/ N4,I,J,K
      COMMON /S4/ APYI,AFYI,NY
      IF(JJ.EQ.NY+1) GO TO 60
      IF(JJ.EQ.2) GO TO 60
```

```
      CALL TH(L,PK)
      A1=APYI(I,JJ)*PK
      A2=AFYI(I,JJ)
      IF(K.EQ.N4) GO TO 40
C.....PARAFFIN AND FILLER NODES
      GO TO 65
40    A1=A1/2.
      A2=A2/2.
      GO TO 65
60    A1=0.
      A2=0.
65    C2=A1+A2
100   FORMAT(' SC2',3I2,2E)
101   FORMAT(4E)
      RETURN
      END
      SUBROUTINE K3(C3,KK,L)
      DIMENSION APZ(7,7),AFZ(7,7)
      COMMON /S1/ N4,I,J,K
      COMMON /S5/ APZ,AFZ,NZ
      EC=0.
      IF(KK.EQ.NZ+1) GO TO 60
      CALL TH(L,PK)
      A1=APZ(I,J)*PK
      A2=AFZ(I,J)
C.....PARAFFIN AND FILLER NODES
      GO TO 65
60    A1=0.
      A2=0.
65    C3=A1+A2
100   FORMAT(' SC3',3I2,3E)
101   FORMAT(4E)
      RETURN
      END
      SUBROUTINE SOLVE (T,J1,J4)
      DIMENSION A(32),B(32),CC(32),D(32),T(32)
      DIMENSION W(32),G(32)
      COMMON /S6/ A,B,CC,D
      J2=J1+1
      J3=J4-1
      W(J1)=B(J1)
      G(J1)=D(J1)/W(J1)
      DO 20 I=J2,J4
      X=CC(I-1)/W(I-1)
      W(I)=B(I)-A(I)*X
      G(I)=(D(I)-A(I)*G(I-1))/W(I)
20    CONTINUE
      T(J4)=G(J4)
      DO 30 I=J3,J1,-1
      X=CC(I)/W(I)
30    T(I)=G(I)-X*T(I+1)
101   FORMAT(/)
100   FORMAT(5E)
      RETURN
      END
      SUBROUTINE PHASE(T,KZ,TX,V,TO,DT)
      COMMON /S7/ TM,HF,CPM,DIF,VT
      VP=V*DT
      IF(KZ.GT.1) GO TO 20
      IF(T.LT.TM) GO TO 20
```

```
      SUM=T-TO+TX
      IF(SUM*VT*CPM/VP.GE.HF) GO TO 12
      TX=SUM
      T=TM+DIF*SUM*CPM*VT/VP/HF
      GO TO 20
12    T=DIF+TM+(SUM*CPM*VT/VP-HF)/CPM
      KZ=2
20    RETURN
      END
      SUBROUTINE TH(L,PK)
      COMMON /S9/ PKS,PKL
      IF(L.GT.1) GO TO 10
      PK=PKS
      GO TO 20
10    PK=PKL
20    CONTINUE
      RETURN
      END
      SUBROUTINE HC(L,RP,CPP)
      COMMON /S10/ RPL,RPS,CPS,CPL
      IF(L.GT.1) GO TO 12
      CPP=CPS
      RP=RPS
      GO TO 14
12    RP=RPL
      CPP=CPL
14    RETURN
      END
      SUBROUTINE TBN(TB)
      COMMON /S8/ A1,A2,A3,B1,B2,B3,TI1,TI2,TI
      IF(TI.LE.TI1) GO TO 10
      IF(TI.LE.TI2) GO TO 20
      GO TO 30
10    TB=A1*TI+B1
      GO TO 40
20    TB=A2*TI+B2
      GO TO 40
30    TB=A3*TI+B3
40    CONTINUE
      RETURN
      END
```